The Effects of Composition and Heat Treatment on the Passivation of Steel Rebar in Concrete Simulated Environment

BY

MUHAMMAD FAIZAN

A Thesis Presented to the

DEANSHIP OF GRADUATE STUDIES

KING FAHD UNIVERSITY OF PETROLEUM & MINERALS

DHAHRAN, SAUDI ARABIA

In Partial Fulfillment of the
Requirements for the Degree of

MASTER OF SCIENCE

In

MATERIALS SCIENCE AND ENGINEERING

MAY 2017

KING FAHD UNIVERSITY OF PETROLEUM & MINERALS

DHAHRAN- 31261, SAUDI ARABIA

DEANSHIP OF GRADUATE STUDIES

This thesis, written by **MUHAMMAD FAIZAN** under the direction of his thesis advisor and approved by his thesis committee, has been presented and accepted by the Dean of Graduate Studies, in partial fulfillment of the requirements for the degree of **MASTER OF SCIENCE IN MATERIALS SCIENCE AND ENGINEERING.**

Dr. Zuhair Mattoug Gasem
(Advisor)

Dr. Zuhair Mattoug Gasem
Department Chairman

Dr. Zafarullah Khan
(Member)

Dr. Salam A. Zummo
Dean of Graduate Studies

Dr. Mohammad Maslehuddin
(Member)

21/8/17
Date

Dedicated To

My

Beloved Parents

ACKNOWLEDGMENTS

I would love to present my deep gratitude to my advisor Dr. Zuhair Mattoug Gasem for advising me during the ups and downs of my research work. He provided me technical guidance to deal with the problems during the experimental work but the way he assisted me during the technical discussion, it provided me a great experience to learn and write about the critical results. “Brief and To the Point” and “What We Write That Does Actually Means” is what I learnt from him. I believe that writing just few grateful words cannot wage the sincerity and effort of our teacher for building and repairing our hollow structure. Respect from heart and attitude should prevail over pretending!

I would like to thank also to my committee members Dr. Maslehuddin and Dr. Zafarullah Khan for providing me moral and ethical support. Of course, how can I forget the support provided by Dr. Madhan Kumar from research institutes who really helped me to understand the equipment for experimental work at initial stages!

I would also like to thank to the corrosion center of Research Institute, Mechanical Engineering department as well as the staff of the Materials Science and Corrosion Lab of King Fahd University of Petroleum and Minerals. Without their support, I could never be able to complete my research work.

Table of Contents

LIST OF FIGURES

LIST OF TABLES

LIST OF ABBREVIATIONS

GNP : Gross National Product

TMT : Thermo-Mechanical Treatment

QST : Quenched and self-Tempered

AE : Atmospheric Exposure

SCPS : Simulated Concrete Pore Solution

SEM : Scanning Electron Microscope

XRD : X-ray Diffraction

XPS : X-ray Photoelectron Spectroscopy

E_{corr} : Corrosion Potential (V)

I_{corr} : Corrosion Current Density (A/cm^2)

R_p : Polarization Resistance

AC : Alternating Current

WE : Working Electrode

RE : Reference Electrode

CE : Counter Electrode

SCE : Saturated Calomel Electrode

OCP : Open Circuit Potential

LPR : Linear Polarization Resistance

PDP : Potentiodynamic Polarization Resistance

EIS : Electrochemical Impedance Spectroscopy

M-1 : Carbon Steel without Copper

M-2 : Carbon steel with 0.2% Copper

R_s : Solution Resistance

R_f : Film Resistance

R_{ct} : Charge Transfer Resistance

T : Temperature

^0C : Degree Celsius

Fig. : Figure

ABSTRACT

Full Name : Muhammad Faizan

Thesis Title : The Effects of Composition and Heat Treatment on the Passivation of Steel Rebar in Concrete Simulated Environment

Major Field : Materials Science and Engineering

Date of Degree : May 2017

Corrosion resistance of steel rebars in concrete is strongly dependent on its ability to passivate and the stability of the passive film in the presence of chlorides and acidizing gases. This study investigates the effect of tempering temperature and copper content on the corrosion resistance of two commercial rebars exposed to concrete simulated alkaline solution. Electrochemical impedance spectroscopy (EIS), linear polarization resistance (LPR) and potentiodynamic polarization (PDP) tests were employed to examine the corrosion properties of M-1 rebar (no copper) and M-2 rebar (0.2% Cu) samples heat treated in the as quenched condition and at various tempering temperatures: 200°C, 300°C, 400°C, 500°C, and 600°C. Two alkaline solutions with Cl^-/OH^- ratios of 0 and 1 were used to examine the effect of introducing chloride ions in the pore solution. The chemistry of the oxide film was characterized by x-ray photoelectron spectroscopy (XPS).

LPR, EIS, and PDP results indicated that quenching and tempering (Q&T) of M-1 and M-2 rebars at 400^0C produced microstructures with highest corrosion resistance in simulated concrete pore environments (pH 13.5) with and without chlorides. LPR and EIS results of both grades consistently revealed that the polarization resistance of M-2 was higher than M-1 in alkaline solutions with and

without chloride. Q&T M-1 and M-2 rebars at 300°C showed the lowest corrosion resistance. M-1 rebar showed the lowest and highest passive current densities for samples Q&T at 400°C and 300°C, respectively. The passive current density of M-2 sample Q&T at 400°C was lower than that Q&T at 300°C. The effect of chloride on the PDP curves was characterized for both steels. The microstructures at 400°C for both steels comprised of tempered martensite and ferrite.

The effects of tempering temperature and copper content on the corrosion behavior of M-1 and M-2 rebars were related to the passive film composition and the underlying microstructure. XPS spectrum of rebar M-1 Q&T at 400°C was consistent with the formation of a double layer film structure comprised mainly of magnetite (Fe_3O_4) and Wüstite (FeO) as a mixed inner layer and an outer layer primarily composed of hematite (γ-Fe_2O_3). XPS spectrum for M-1 Q&T at 300°C indicated the presence of goethite (α-FeOOH) in the outer layer. It is argued that the formation of (α-FeOOH) in the outer layer might be responsible for the lower corrosion resistance owing to its defective nature. It is proposed that higher ratio of (α-FeOOH) to (γ-Fe_2O_3) in the outer layer could compromise the protective nature of the outer layer and lower rebar corrosion resistance.

ملخص الرسالة

الاسم الكامل: محمد فيزان

عنوان الرسالة: تأثيرالتركيب والمعالجة الحرارية على مقاومة التآكل لحديد التسليح الصلب في بيئة محاكاة خرسانية

التخصص: علم وهندسة المواد

تاريخ الدرجة العلمية: مايو 2017

مقاومة التآكل لحديدالصلب المسلح في الخرسانة تعتمد على قابلية الصلب لتكوين طبقة من الأكسيدات العازلة على السطح (passive films) وعلى استقرار الطبقة في وجود الكلوريدات والغازات الحمضية. تبحث هذه الدراسة عن تأثير درجة حرارة معالجة الصلب ومحتوى النحاس على مقاومة التآكل لنوعين من الصلب التجاري خلال تعريضهم لمحلول الخرسانة القلوي. تم استخدام اختبار الطيف الكهروكيميائي (EIS) ومقاومة الاستقطاب الخطي (LPR) واختبارات الاستقطاب الديناميكي (PDP) لفحص خصائص التآكل لحديد التسليح M-1 (بدون نحاس) وحديد التسليح M-2 (0.2٪ نحاس) بعد المعالجة الحرارية في درجات حرارة مختلفة: 200 ،300 ،400 ،500 ،و600 درجة مئوية. تم استخدام محاليل قلوية مع إضافة الكلورايد لدراسة تأثير أيونات الكلوريد على مقاومة التآكل للصلب في الخرسانة. تم دراسة التركيب الكيميائي لطبقة الأكسدة باستخدام الأشعة السينية الضوئية الطيفي (XPS).

أشارت النتائج المعملية LPR ، EIS ، و PDP إلى أن التبريد والتسخين (Q&T) لصلب M-1 و M-2 عند 400 درجة مئوية أنتجت أعلى مقاومة للتآكل في البيئة القلوية المحاكية لمسام الخرسانة (الرقم الهيدروجيني 13.5) مع وبدون الكلوريدات. نتائج LPR وEIS لكلا النوعين من الصلب دلت على أن مقاومة الاستقطاب لصلب M-2 أعلى من صلب M-1 في المحاليل القلوية مع وبدون الكلوريد ، بينما المعالجة عند 300 درجة مئوية درجة مئوية لكلا النوعين من الصلب أظهرت أقل مقاومة للتآكل. أظهر حديد التسليح M-1 أدنى وأعلى كثافة للتيارالطبقي (passive current density) في عينات Q&T عند 400 درجة مئوية و 300 درجة مئوية على التوالي. وكان كثافة التيارالطبقي لعينات M-2 Q&T عند 400 درجة مئوية أقل من Q&T عند 300 درجة مئوية. كان التركيب المجهري عند 400 درجة مئوية يتألف من الفرايت و المارتنزيت المخفف.

أقترحت الدراسة أن تأثير درجة الحرارة على سلوك التآكل للصلب M-1 و M-2 ربما يعود إلى التركيبة الكيمائية للطبقة الحامية. طيف XPS لحديد التسليح M-1 المعالج عند 400 درجة مئوية كان متسقا مع تشكيل طبقة مزدوجة تتألف أساسا من المغناطيسيت (Fe_3O_4) ووستيت (FeO) كطبقة داخلية مختلطة وطبقة خارجية تتألف أساسا من الهيماتيت (γ -Fe_2O_3). طيف XPS لحديد التسليح M-1 في 300 درجة مئوية أشار الى وجود غثيت (α-FeOOH) في الطبقة الخارجية. من المحتمل أن تكون (α-FeOOH) في الطبقة الخارجية هي المسؤولة عن هبوط مقاومة التآكل بسبب طبيعة هذا الأكسيد المعيبة. تقترح النتائج أن زيادة نسبة (α-FeOOH) إلى (γ-Fe_2O_3) في الطبقة الخارجية من الطبقة الواقية الخارجية ربما تقلل مقاومة التآكل للصلب المسلح في المحيط القلوي لمسام الخرسانة.

CHAPTER 1: Introduction

Carbon steel is the most demanding type of steel across the globe among steel family because of its enduring strength, toughness, ductility and cost. This is the only materials whose production is increasing day by day and it will not be wrong to claim that its production reflects the development and progress of a certain country. Steel rebar is extensively used as reinforcing material in concrete matrix for building infrastructures. The most serious issue concerned while using steel rebar in concrete is its corrosion issue which reduces the integrity and life of the structure. The losses are reported to be 22.1 billion $ per year in USA. In the gulf countries, the direct or indirect loss due to corrosion is more severe than the rest of the world because of the harsh environment. The amount is reported more than 1000 million dollars per year (NACE 2016).

It is estimated that nearly 15-20% losses due to corrosion can be controlled by corrosion preventing techniques. A significant amount of research has been directed to enhance the steel rebar resistance against corrosion by a number of techniques. The most common are;

(i) Hot dipped galvanizing

(ii) Changing the alloy composition

(iii) Developing organic/inorganic coatings (epoxies, paints etc.)

(iv) Heat treatment

(v) Cathodic protection

(vi) Inhibitors

Although all of the above mentioned protection techniques are being used but none of them is completely reliable and warrants continuation of extensive research in order to combat this problem. Steel rebar has the tendency to passivate especially in highly alkaline environment (pH>13) and the protective passive oxide layer prevents it from further corrosion and deterioration. But this passive layer degrades with time by the presence of chlorides, sulfides and carbon dioxide and thus does not offer the required long term protection against the corrosion [1-2]. This phenomenon leads to slow degradation of the structures.

Numerous studies [3-4] have shown that nitrites ions act as beneficial inhibitors in concrete matrix and reduce corrosion. It is reported that these ions react with ferrous ions and produce the Fe_2O_3 protective layer and ultimately reduce the corrosion rate by acting as anodic corrosion inhibitors [6-7]. However, addition of inappropriate amount of these inhibitors could lead to pitting if surface was already under passivation state [3,5,8]. In addition to this, when concrete is surrounded by marine environment or concrete matrix is prepared from the contaminated sand then chlorides can penetrate through the pores of concrete matrix and depassivate the oxide layer on steel surface. As steel is embedded in concrete, having high alkaline environment, so it develops the passive layer over it but this passive state is challenged by the presence of chloride ions and ultimately corrosion rate depends on the chlorides/hydroxyl ratio [9-10].

However, the electrochemical testing of steel in the solid concrete matrix is difficult study because of the presence of high resistivity, porosity and difficult cell design. Hence the alternate way to investigate the corrosion of steel rebar is to simulate the concrete pore solution. Many researchers have conducted studies in just $Ca(OH)_2$

solution and simulated it as concrete solution but the fact is that concrete simulated solution is much more complex [12,13] and a number of such solutions has been reported [9,14–18].

There is a consensus that passivation tendency of steel rebar can be enhanced by introducing it in highly alkaline solution simulating to the concrete environment. However, still it is questionable that what is the effect of both heat treatment and composition of copper on the passivation resistance of steel rebar when it is introduced in concrete simulated environment and no research has been proposed on this agenda so far. So, the objectives of the current research are to investigate the effect of heat treatment and copper composition on the resistance of passive layer developed in rebar/concrete environment to chloride induced corrosion.

CHAPTER 2: Literature Review

2.1. Steel Rebar Production

Steel rebar in this era is produced by a latest patent technology-THERMEX. The important feature of this technique is the rapid quenching of outer surface of steel rebar by water [19]. After passing through the last series of rollers, thermo-processed steel rebar is passed through predetermined pressurized water. The outer surface of steel rebar becomes harder because of the quenching mechanism and, subsequently, a thermal gradient exists (from high temperature to room temperature) inside the bar. That thermal gradient set the condition of tempering and hence the periphery, just after the hard quenched surface, provide different microstructural properties compared to outer quenched surface. Also because of the existence of this thermal gradient, the core temperature of steel rebar becomes higher and hence the cooling mechanism is too slow in that region which leads to totally different microstructural properties than the outer discussed regions. This mechanism results in a composite structure where a peripheral zone (a transition zone of perlite and bainite), on one side, is surrounded by an outer hard martensitic case and by a soft core (a mixture of perlite and ferrite) on the other side.

Due to the combined mechanism of quenching and self-tempering, the rebar produced by the THERMEX technology is also given the name of quenched and self-tempered (QST) rebar [20]. This kind of treatment is applied to those industrial steels in which the carbon content is less than 0.3% [20-22]. This is widely being used in construction of bridges, buildings and dams. This is the highly demanding material for

concrete because of its high strength (above 450MPa), ductility and earthquake shocks absorbability.

2.1.1. Production Mechanism

The THERMEX technology is installed in-line to the rolling milling process [21,24,25]. Once the rebar leaves the finishing rolling mill, its temperature is maintained to 1000^0C as can be seen in Fig.2.1. But as this rebar passes through the cooling THERMEX system (Fig.2.2), the rapid water spray quenches the outer surface below the martensitic M_s (start of martensite) temperature (Fig.2.3) [21,24]. This phase of the process creates a hardened martensite but the inner core of the material is still at higher temperature and as a result, it remains as austenite. This residual heat moves from inside of the core to the outer hard martensitic case and starts self-tempering mechanism in this region [20-24]. This tempering/equalization temperature is the maximum temperature which is attained by a rebar after the quenching mechanism. This tempering mechanism reduces the strength of supersaturated martensitic structure by phase transformation. By this, the hardness is reduced considerably. The temperature of the surface reaches approximately to 600-700^0C due to the flow of heat from inside to the outer surface. Finally it cools to ambient temperature as shown in Fig.2.3 and the structure gained by this mechanism is somewhat a composite rather than a single phase [20].

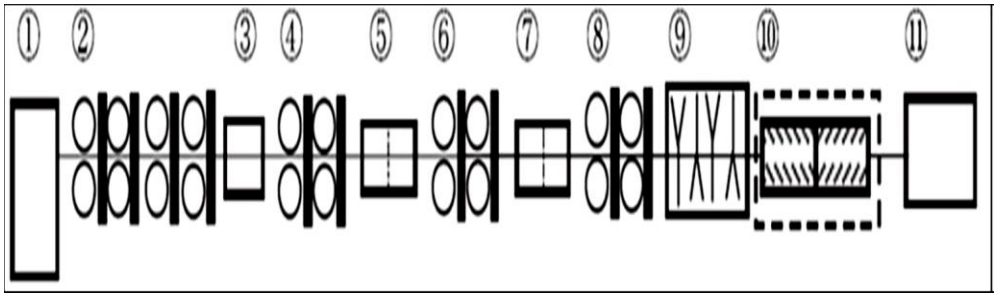

Figure 2.1: Layout of rolling mill and cooling zone in bar product line: (1) Reheating furnace, (2) Roughing mill, (3) Rough cooling zone, (4-6) Intermediate rolling Mill, (7) Intermediate cooling zone, (8) Finish rolling mill, (9) Finish rolling mill (SCFM), (10) Finish cooling zone, (11) Cooling bed [25]

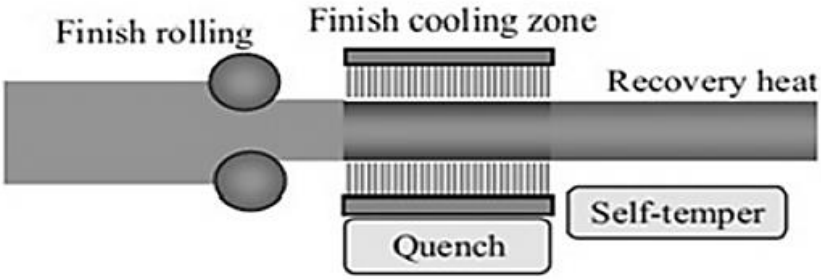

Figure 2.2: Rebar passes through the cooling THERMEX system **[20]**.

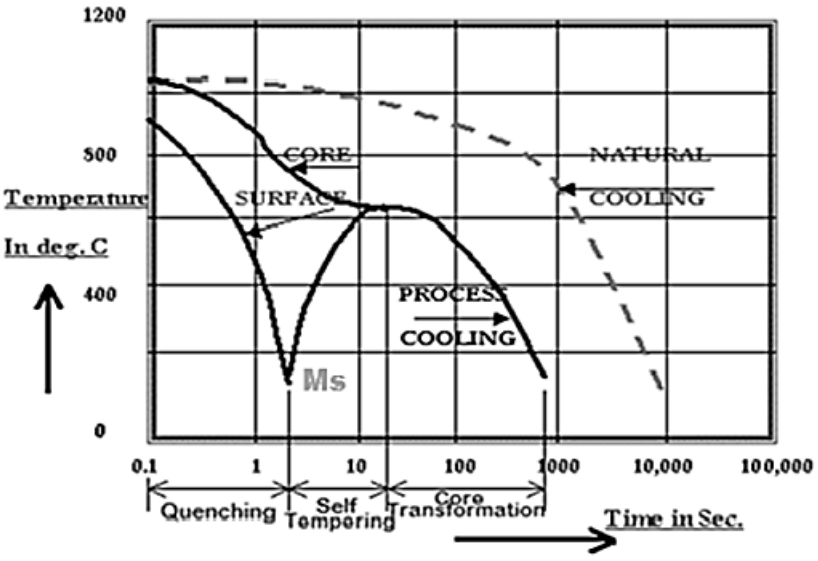

Figure 2.3: Cooling mechanism of steel rebar from outer quenched surface to core **[20]**.

2.2. Corrosion Process

Steel rebar is basically an alloy of iron, as a major constituent, and carbon, as a minor constituent. Iron is found in the nature as an oxide and most abundant ores of it are magnetite (Fe_3O_4) and hematite (Fe_2O_3) [26]. For getting the pure iron from its oxides to form a desired alloy, energy is provided from the external source as a combination of many physio-chemical processes. However the pure iron is always in its unstable from and it has tendency to form the oxides again to reduce its free energy. Typically for iron, the corrosion products are usually iron oxides and/or hydroxides.

Corrosion is an electrochemical process or it is also called physio-chemical process where the active part becomes an anode and release electrons due to the oxidation process while its counter part acts as a cathode which accepts an electron due to reduction phenomenon [27].

Reaction at the anode (Oxidation):

$$Fe = Fe^{2+} + 2e^{-} \qquad 2.1$$

Reaction at the cathode (Reduction):

$$H_2O + 1/2\ O_2 + 2e^{-} = 2OH^{-} \qquad 2.2$$

For the corrosion reaction to occur, dissolved oxygen is required in water to form the hydroxyl ions which in turns react with the iron ions and form the iron hydroxide.

Overall reaction:

$$Fe + H_2O + 1/2O_2 = Fe(OH)_2 \qquad 2.3$$

Iron hydroxide formed in reaction (2.3) undergoes to further oxidation reaction and forms iron oxides i.e. magnetite (Fe_3O_4) and hematite (Fe_2O_3).

2.2.1. Potential-pH Diagram (Pourbaix Diagram)

In an electrochemical process, the dissolution of hydrogen or oxygen affects the pH of the electrolyte. The chemical equilibrium condition in the presence of these substituents as well as the use of Nernst equation allow us to find the thermodynamic stability region in the presence of aqueous medium. Stability for both cathode and anode charge transfer reactions as well as of the pure chemical reaction can be a function of electrode potential, pH and the metal ions concentration in the electrolyte. Such diagram is known as Pourbaix diagram [28].

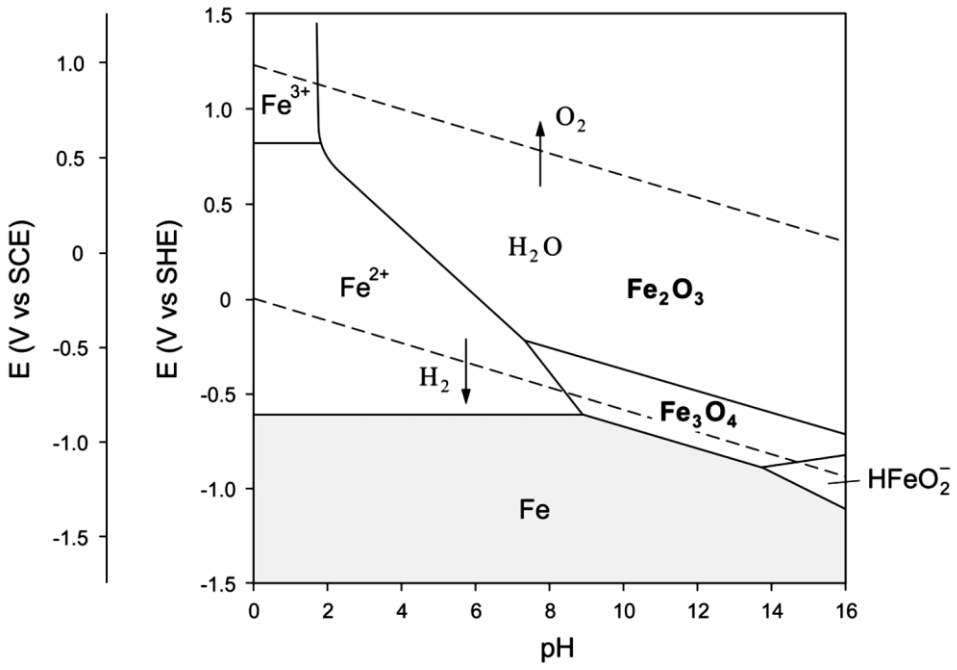

Figure 2.4: Pourbaix diagram for iron in water (for ion concentration 10–6 mol/l at 25°C). Only Fe, Fe_3O_4, Fe_2O_3 as solid products considered [28]

Figure (2.4) shows the stability regions of iron in the form of its oxides. The grey region defines immunity region because in this region for a specific potential-pH combination, iron remains stable [27].

The dotted lines in the diagram represent the hydrogen (lower) and oxygen (upper) evolution and in between these lines the water is stable. However, water dissociates into O_2 above the oxygen line and it dissociate in H_2 below the hydrogen line. In a neutral or alkaline environment, the O_2 evolution occurs according to reaction (2.3) but for H_2 evolution, the phenomenon is as following;

For lower pH (Acidic)

$$2H+ + 2e^- = H_2 \qquad 2.4$$

Neutral or alkaline:

$$2H_2O + 2e^- = H_2 + 2OH^- \qquad 2.5$$

2.2.2. Passivation

From the pourbaix diagram, it is clear that both iron and water are not stable simultaneously unless iron is provided more negative potential to bring it in immunity region or it is provided an highly alkaline environment (pH>13.5) where it can develop an oxide layer. In the later scenario, iron itself is not thermodynamically stable but a passive film of few nanometers thickness is developed over its surface. That passive layer is dense stable and transparent in its nature and stops further dissolution of iron and hence reduces the corrosion rate to a lower extent.

2.2.3. Pitting Corrosion

Usually halides, and particularly chlorides present in the environment breaks the protective passive layer of the iron and leads to localized corrosion [29-31]. Unlike the homogenous corrosion or general corrosion, chlorides damage the protective passive layer to a localized area. Once a localized pit is formed, the area inside the pit becomes depleted in oxygen and thus acts as an anode because of oxidation phenomenon. While the area adjacent to the pit is abundant it oxygen and hence reduction phenomenon takes place and this area acts as a cathode. As chloride enriched electrolyte is already inside the pit so the formation of localized cell keeps dissolving the iron under pitting area. The dissolved iron ions form hydroxide and acidification of the electrolyte occurs inside the pit [30]. The following chemical reaction occurs:

$$Fe + 2H_2O = Fe(OH)_2 + 2H^+ \quad 2.6$$

or by the electrochemical oxidation reactions [29]:

$$2Fe^{2+} + 3H_2O = Fe_2O_3 + 6H^+ + 2e^- \quad 2.7$$

$$3Fe^{2+} + 4H_2O = Fe_3O_4 + 8H^+ + 2e^- \quad 2.8$$

The schematic diagram of the pitting cell is shown Fig. 2.5

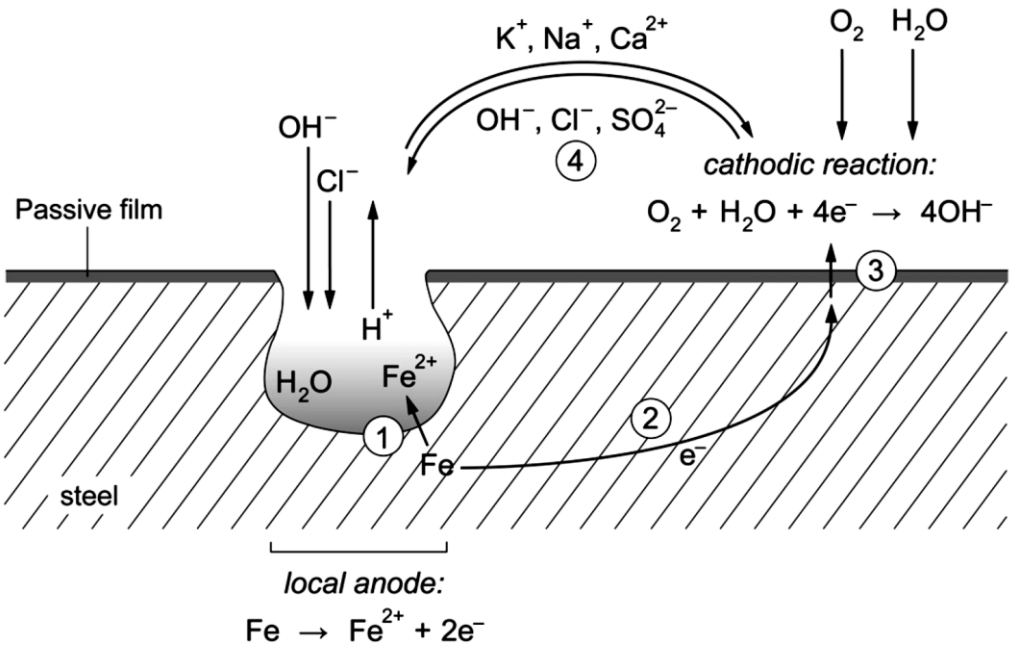

Figure 2.5: Schematic illustration of chloride induced pitting corrosion and reaction steps: 1. Anodic iron dissolution; 2. Flow of electrons through metal; 3. Cathodic reduction reaction; 4. Ionic current flow through the electrolyte [29-30]

2.3. Steel Rebar in Concrete

In this section, it will be discussed how steel rebar is affected in a special case when it is placed in the concrete environment.

2.3.1. Passivation in Alkaline Environment

Owing to the high moisture content in the pore structure of concrete as well as the presence of $Ca(OH)_2$, KOH and NaOH, the alkalinity of the concrete structure is increased with a pH ranging in between 13.5-13.7. This pH value agrees with the reported works in many literatures elsewhere [37-41].

Due to the highly alkaline environment, the steel rebar embedded in the concrete structure gets passiavted and corrosion rate is decreased to many folds. However, alkalinity of the concrete start to decrease as a result of carbonation when CO_2 and moisture from the atmosphere penetrate inside the concrete pore structure and form

carbonic acid there. As a result, from Potential-pH diagram, it is clear that the passivation state of the steel is maintained as long as the pH of the system is above 9. Due to carbonation, the pH is reduced from this critical limit and corrosion phenomenon gets severe.

2.3.2. Critical Chloride Content

Passive film of the steel in concrete under high alkaline environment suffers to localized corrosion by the presence of chlorides in the concrete structure. The minimum amount of chlorides required in the concrete to break the passive film of steel is termed critical chloride content or chloride threshold value. Chloride threshold value depends on many factors but the main factor is considered to be the pH of the system –more the pH, more will be the OH^- ions and hence more chloride ions will be needed to break the passive film [76-77].

Another factor, which affects the chloride critical value, is the quality of concrete/steel interface. Sometime the solid hydrates i.e. $Ca(OH)_2$, stick on the surface of steel and buffer the pH of the system. These hydrates create the resistance in the path of chloride ions to reach the passive layer and hence reduce the chances of localized corrosion [32-33]. It is a general consensus that this is the reason for having the high chloride threshold value in concrete [42-43]. The detailed study of this topic can be seen elsewhere [36].

2.4. Electrochemical Testing

2.4.1. Open Circuit Potential

Before conducting the electrochemical testing, the potential of working electrode is always measured with the help of reference electrode under the condition that no external current or voltage is applied to the working electrode. Once the system measures the open circuit potential of the working electrode, then it applies the desired working potential in addition to the open circuit potential which was already measured.

2.4.2. Electrochemical Impedance Spectroscopy (EIS)

Electrochemical impedance spectroscopy (EIS) is measured when a sinusoidal voltage (AC voltage) is applied to the working electrode at varying frequencies. Usually the frequency is ranged from MHz to μHz and the current is measured in response of applied voltage. From the applied voltages, the responded current readings and from their phase differences, many values of impedance (Z) can be recorded against each frequency. The relationship between the applied voltages, current and the shift of phase angles are shown in the below equation,

$$Z = \frac{E_t}{I_t} = \frac{E_0 \sin(\omega t)}{I_0 \sin(\omega t + \phi)} = Z_0 \frac{\sin(\omega t)}{\sin(\omega t + \phi)} \qquad 2.9$$

Where

E_t= Potential at time t, I_t = Current at time t

E_0= Amplitude of the signal, I_0= Current at time 0

$\omega = (2\pi f)$ = Radial frequency Φ = phase shift

However, in a linear system, the response signal, I_t is shifted in phase (Φ) and has a different amplitude than I_0 as it is shown in Fig. 2.6

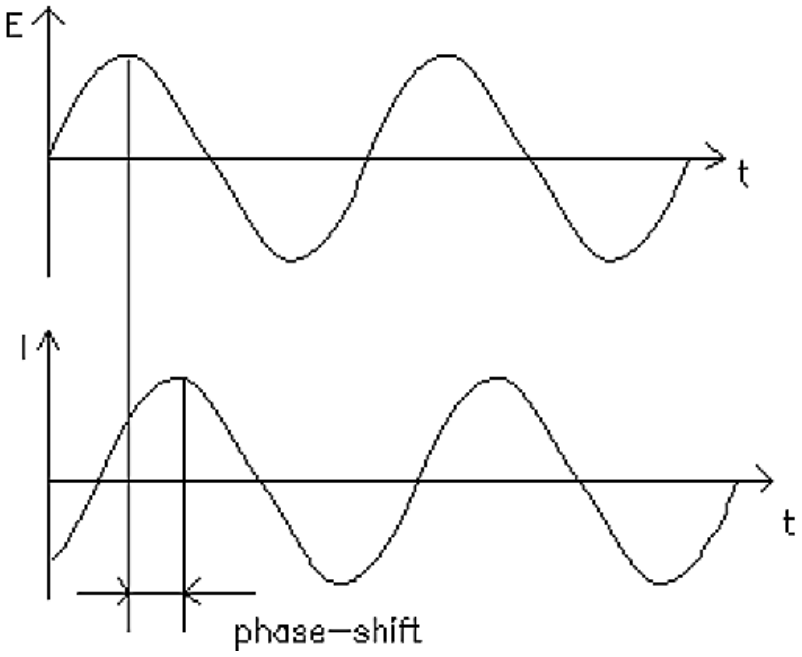

Figure 2.6: Sinusoidal current response in a linear system [46-49]

Let suppose, if a capacitors and a resistors are connected in a parallel way and at a very low applied frequency, the capacitor will act as an insulator and it will keep on charging. But once it will be fully charged, the current will be forced through the resistor. At this stage, the impedance of both the capacitors and resistors will be equal. But on the other hand, if the frequency of the applied voltage is too high, then the capacitor will be short circuited and there will be no impedance. However, if the applied frequency will be intermediate then both the capacitor and resistor will carry the AC current.

By using the equivalent circuit, the measurements can be calculated. By this equivalent circuit, the charge transfer resistance, double layer capacitance and ohmic resistance can be measured. This will provide information about corrosion rate and other important electrical properties of steel in concrete.

By utilizing complex natation, impedance is divided into a real, |Z|cos(Φ), and an imaginary parts, |Z|sin(Φ).When real impedance is plotted against imaginary impedance, the plot is obtained and is called Nyquist plot (Fig 2.7).

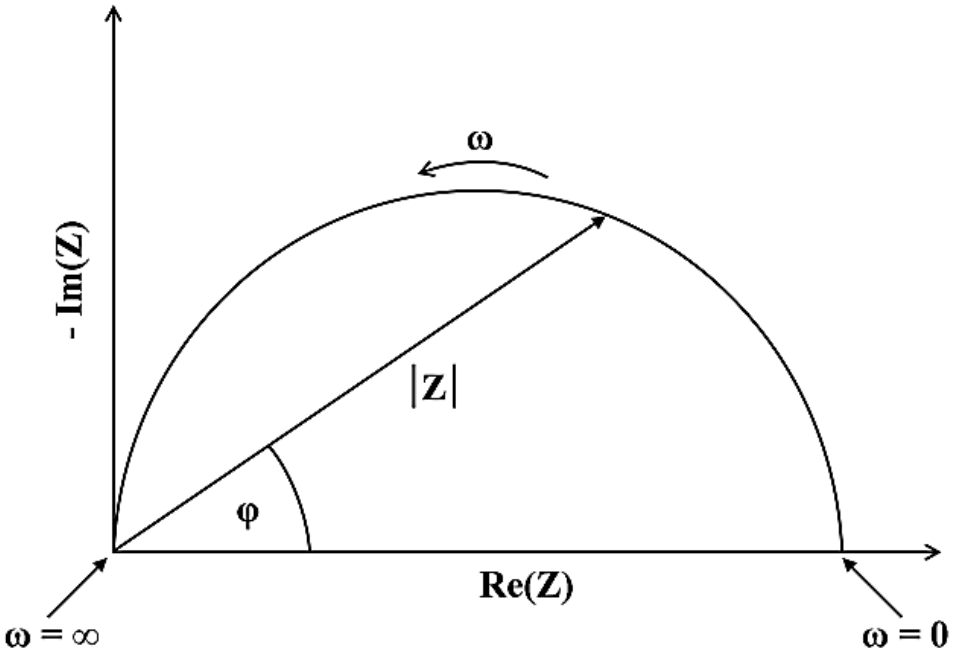

Figure 2.7: Schematic diagram of nyquist plot [46-49]

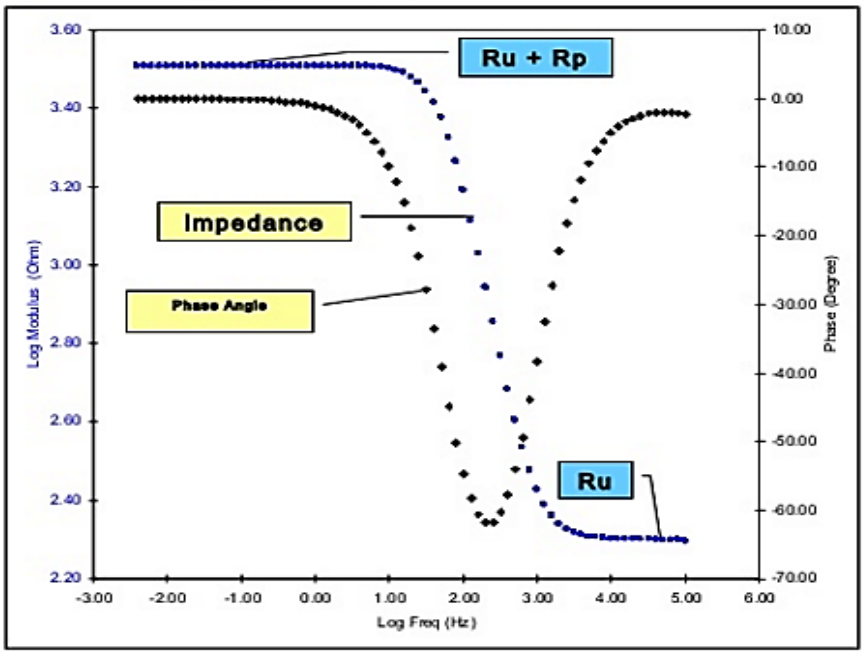

Figure 2.8: Schematic diagram of bode plot [46-49]

However, if the relation is plotted in between changing frequency and impedance/phase angle then the plot obtained is called as Bode plot. More detailed descriptions on theory and application of EIS for steel in concrete or to characterize concrete can be found elsewhere [46-49].

2.4.3. Linear Polarization Resistance (LPR)

LPR measurements are generally used to determine the instantaneous corrosion rate of an electrode. The technique is based on the observation that within a small potential range around E_{corr}, the E-I-relationship is approximately linear [44]. The linear polarization resistance is defined as the slope of this curve (R_p = dE/dI) at E_{corr}. It can experimentally be obtained in a conventional three-electrode configuration (WE, RE, CE) by polarizing the working electrode a few millivolts (typically 10 mV) into anodic and cathodic direction and recording the required current. The well-known Stern-Geary equation allows calculation of the corrosion current [44]

$$I_{corr} = \frac{B}{R_p} = \frac{\beta_a \cdot \beta_c}{2.3(\beta_a + \beta_c)} \cdot \frac{1}{R_p} \qquad 2.10$$

Constant *B* contains the anodic and cathodic Tafel slopes and is, in the case of reinforcement steel in concrete, usually assumed in the range 26 mV (corroding steel) or 52 mV (passive steel) [45].

If R_p is related to metal area, corrosion current density i_{corr} (mA/cm^2) instead of corrosion current I_{corr} (mA) is obtained. While in laboratory setups, the area of polarized steel is in general known, this is problematic in the case of field measurements where the reinforcement surface area is practically infinite. Moreover, calculation of corrosion rate from R_p is, strictly speaking, only correct for uniform corrosion; for localized corrosion

(chloride induced corrosion), the area of actively corroding metal is normally unknown. In fact, the anodically acting surface area is variable over time. This is only one example of reasons why the accuracy of corrosion rates (current densities) computed on the basis of R_p measurements is, in the case of localized corrosion, highly questionable.

2.4.4. Potentiodynamic Polarization (PDP)

Potentiodynamic anodic polarization is the characterization of a metal specimen by its current potential relationship. The specimen potential is scanned slowly in the positive direction and therefore acts as an anode such that it corrodes or forms an oxide coating. These measurements are used to determine corrosion characteristics of metal specimens in aqueous environments. A complete current-potential plot of a specimen can be measured in a few hours or, in some cases, a few minutes.

Investigations such as passivation tendencies and effects of inhibitors or oxidizers on specimens are easily performed with this technique. With this knowledge, the corrosion characteristics of different metals and alloys can be compared on a rational basis and compatible specimen-environment combinations secured for further long term testing.

When a metal specimen is immersed in a corrosive medium, both reduction and oxidation processes occur on its surface. Typically, the specimen oxidizes (corrodes) and the medium (solvent) is reduced. In acidic media, hydrogen ions are reduced. The specimen must function as both anode and cathode and both anodic and cathodic currents occur on the specimen surface. Any corrosion processes that occur are usually a result of anodic currents [52].

When a specimen is in contact with a corrosive liquid and the specimen is not connected to any instrumentation – as it would be "in service" – the specimen assumes a potential (relative to a reference electrode) termed the corrosion potential, E_{CORR}. A specimen at E_{CORR} has both anodic and cathodic currents present on its surface. However, these currents are exactly equal in magnitude so there is no net current to be measured. The specimen is at equilibrium with the environment (even though it may be visibly corroding). E_{corr} can be defined as the potential at which the rate of oxidation (anodic reaction) is exactly equal to the rate of reduction (cathodic reaction).

It is important to stress that when a specimen is at E_{corr} both polarities of current are present. If the specimen is polarized slightly more positive than E_{corr}, then the anodic current predominates at the expense of the cathodic current. As the specimen potential is driven further positive, the cathodic current component becomes negligible with respect to the anodic component. A mathematical relationship exists which relates anodic and cathodic currents to the magnitude of the polarization [50-51], but a discussion of this relationship is beyond the scope of this application note. Obviously, if the specimen is polarized in the negative direction, the cathodic current predominates and the anodic component becomes negligible [53].

Experimentally, one measures polarization characteristics by plotting the current response as a function of the applied potential. Since the measured current can vary over several orders of magnitude, usually the log current function is plotted vs. potential on a semi-log chart. This plot is termed a potentiodynamic polarization plot. Note that the use of a semi-log display prevents indication of polarity on such plots. Potentials negative

with respect to E_{CORR} give rise to cathodic currents, while potentials positive to E_{CORR} give rise to anodic currents.

Figure 2.9 shows the potentiodynamic anodic polarization plot of a sample of 430 stainless steel. The logarithm of the current is plotted (the abscissa) as a function of the applied potential (the ordinate). This plot is described in the following paragraphs [53].

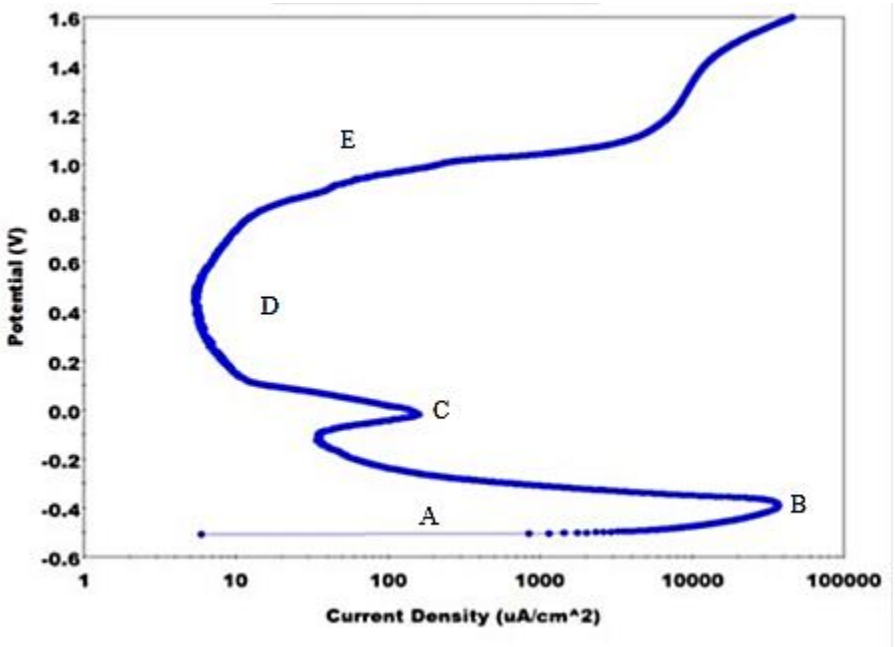

Figure 2.9: Standard potentiodynamic anodic polarization plot of 430 stainless steel. A = Active region; B = Primary passive potential (EPP); C = Onset of passivation D = Passivation region; E = Transpassive region [53].

Region A in Figure 2.9 is the active region, in which the metal specimen corrodes as the applied potential is made more positive. At B, further increase in the rate of corrosion (as measured by the current) ceases and the onset of passivation begins. The loss of chemical reactivity under certain environmental conditions, probably due to the formation of a film on the surface of the metal, is referred to as specimen passivation. This point is characterized by two coordinate values, the primary passive potential (EPP) and the critical current density (i_C). In region C, the current decreases rapidly as the passivating film forms on the specimen. A small secondary peak is observed followed by

region D, where there is little change in current as the potential is increased. The passivating film begins to break down in region E, the trans-passive region.

A potentiodynamic anodic polarization plot such as Figure 2.9 can yield important information such as:

1- The ability of the material to spontaneously passivate in the particular medium.

2- The potential region over which the specimen remains passive.

3- The corrosion rate in the passive region.

2.5. Recent Research Work

Carbon steel rebar is used extensively for construction of concrete structures [54]. Rebar normally is air-cooled after hot rolling. There is an increasing trend to cool rebar by water after hot rolling in order to improve its mechanical performance and reduce the costs of production [55-56]. However, rebar produced with water-cooling tends to rust during storage and transportation [57]. Therefore, it is important to keep the corrosion resistance of water-cooled rebar unaffected by the cooling process. Considerable research work has pointed out that the compositions and structure of the rebar scale, which are closely related to the manufacturing process, play a major role in the corrosion resistance of the rebar in service [54-57]. As it is well known, the scale of hot-rolled mild steel consists of oxide phases, including wustite (FeO), magnetite/maghemite (Fe_3O_4/g-Fe_2O_3) and hematite (α-Fe_2O_3) [58-60] and even fayalite ($2FeO.SiO_2$) [61]. Fe_2O_3 is the most compact among FeO, Fe_3O_4 and Fe_2O_3.Fe_3O_4 and has a compact inverse spinal structure, compared to the loose and porous structure of FeO. Thus, Fe_3O_4 and Fe_2O_3 are the two main factors contributing to the corrosion resistance of the scale. The methodology of producing a thick and compact scale has become the key to improve the corrosion resistance of water-cooled rebar, and a suitable cooling process could tackle this problem [62]. In addition to this, the passivation of reinforcing steel rebar achieved in highly alkaline environment has been reported in a number of studies to improve the corrosion resistance of low carbon steel [63-68].

In a recent study, a new type of low cost and non-toxic alkaline solution had been employed to quench the rebar after water-cooling to develop the discussed passive layer [69]. The results showed that the corrosion resistance of alkaline quenched rebar was

significantly better than of water-cooled rebar, and the alkaline quenching agent did not affect the phase constitution of atmospheric corrosion products. However, their relative content varied the protective ability index (PAI) of rust layers [70-71]. The value of PAI was about 0.23, 0.27 and 0.43 for water-cooled, air-cooled and alkaline-cooled rebar, respectively. Hence, the cooling process could generate relatively stable and compact rust layers that played a role in protecting the rebar from atmospheric corrosion. In order to investigate the influence of the cooling process on the corrosion resistance of the rebar scale, atmospheric exposure (AE) and wet/dry cyclic accelerated corrosion tests (CCTs), especially electrochemical tests, were carried out to evaluate the corrosion resistance of the rebar scale formed by water-cooling or alkaline-cooling. The compositions and structure of the rebar scale were analyzed using XRD, scanning electronic microscope (SEM) and FT-IR.

Bruna et al. [72] went through the passivation study of mild steel to investigate the effect of pH on corrosion rates and they showed that 10-13pH is the most favorable environment for the passivation of the low carbon steel. Similarly, Moreno et al. [73] studied the effect of carbonates and chlorides on passivation of low carbon steel and showed that in the presence of carbonates and bicarbonates, the corrosion resistance to general corrosion was enhanced.

Jiabin et al. [74] studied the spontaneous passivation effect on mild steel during scale formation in CO_2 concentrated sea water solution. They revealed that mild steel in highly alkaline solution develop a passive layer by which the corrosion potential was found to be shifted from negative to positive with low current density.

Subramanian et al. [75] studied the anodic polarization of low carbon steel in highly alkaline sodium hydroxide (NaOH) and sodium bicarbonate solution (Na_2CO_3) environment. They investigated the effect of molar concentration of both of the solution in addition to the temperature. They found that active-passive transition peak behavior in different environments and concluded that the passive nature of this peak's transition is attributed to the combination of optimum molar concentration and temperature.

Similarly, Valcarce et al. [76-77] went through the study on carbon steel passivity in alkaline environment and investigated the effect of chlorides and nitrites ions. They showed in their study that nitrite ions, in highly alkaline environment, acted as inhibitors and reduced the corrosion rate by not only protecting the passive film but also assisting the ferrous ion to form and maintain this layer.

Volpi et al. [78] recently carried out the electrochemical characterization of low carbon steel in different alkaline solutions simulating the concrete environment. They showed in their study that anodic polarization was achieved with the increase of embedding time of steel in alkaline solution and charge transfer resistance was enhanced on metal-solution interface.

It is inevitable that the industrial performance of a given metal will significantly decrease by exhibiting anodic dissolution, when an electrochemical reaction occurs [79]. The corrosion behavior of steels, which are the most widely used metallic materials, differs depending on their matrix and corrosive media [80-81]. Austenitic, ferritic, pearlitic, bainitic and martensitic steels, formed as a function of transformation conditions such as alloying and cooling rate, show different anodic dissolution in the

same media. Ferritic steels having a softer matrix can be easily and rapidly corroded by corrosion reactions depending on the time. On the other hand, hardness of the steel matrix provides good chemical and mechanical properties. Bainitic and martensitic steels having ceramic based hard precipitates, lath or plate shapes, are resistant to corrosion. Stainless steels are very resistant to corrosion due to high chromium alloying which results in the formation of a passive chromium oxide layer on the surface [82–88].

Many studies on the corrosion behavior of heat treated steels having different carbon and other alloying element contents concluded that both composition and heat treatment conditions in addition to corrosion media are very significant factor of their corrosion resistance [89–93].

Je-Kyoung et al. [94] investigated the corrosion resistance of Fe-0.4%Cu and found that there was significant improvement in the corrosion resistance by the addition of copper. On the other side, Jang et al. [95] proposed in their research that presence of copper in steel actually form the oxide of Cu_2O and $Cu(OH)_2$. These developed compounds hinder the attack of general corrosion on low carbon steel. Similarly, A. Aloya et al. [96] reported in their work that the presence of Cu ions in the alkaline solution promoted the passivation tendency of iron significantly.

On the other side, to notice the effect of heat treatment on the corrosion resistance of steel rebar, Lundberg [97] studied the effect of heat treatment on the corrosion resistance and reported that those steel which were quenched and followed by tempering were found in improved corrosion resistance than those which were produced by traditional method and left without any post heat treatment.

In another study, Atapeka et al. [98] investigated the effect of different tempering temperatures on the corrosion rate of low carbon steel in sea water solution. They also concluded that tempering had significant effect in improving the corrosion resistance.

CHAPTER 3: Proposed Work and Objectives

In concrete, steel rebar develops a protective passive layer over its surface due to strong alkaline environment (pH>13) which protects it from further deterioration by bringing it into the passive region according to Pourbiax diagram [99]. But steel rebar corrodes badly when the pH of the concrete starts to decrease due to carbonation which leads to general as well as localized corrosion. Chlorides also play a catastrophic role in enhancing the corrosion rate as they penetrate through this passive layer and cause localize attack [99-100]. From the literature review, it is cleared that alkaline exposure plays a significant beneficial role in developing the passive oxide layer to reduce the corrosion rate. Furthermore, many studies also revealed that both alloying addition, such as 0.1-0.4% copper, and heat treatment (tempered at different temperature) also have a significant effect on the corrosion resistance [89-93].

There is a consensus that passivation tendency of steel rebar can be enhanced by introducing it in highly alkaline solution simulating the concrete environment. However, still it is questionable that what is the effect of both heat treatment and composition of copper on the passivation resistance of steel rebar when it is introduced in concrete simulated environment and little research has been claimed out in this regard. The objectives of the current research are:

1- **To investigate the effect of heat treatment on the passive layer developed in rebar exposed to concrete environment containing chloride.**
2- **To investigate the effect of copper-containing commercial steel rebar on the passivation behavior in concrete pore simulated environment.**

CHAPTER 4: Experimental Work

4.1. Material Selection

Commercial steel rebar having two different compositions were utilized for carrying out this research work. Both steel grades had the same carbon but differed in copper content. The amount of copper was negligible (0.04%) in one grade while it was significant up to 0.2% in the second one. The compositions of both the grades were analyzed in the lab by spectrometry. Both the compositions are given acronyms to create easiness throughout the thesis.

Table 4.1: Two commercial rebars having different composition of copper

Composition Name	Copper Composition
M-1	Negligible (0.04%)
M-2	0.2%

4.2. Sample Preparation

Both the above mentioned steel rebars (M-1 and M-2) of 15mm diameter were used for sample preparation. For each composition of steel rebar, total six samples were cut by precise cutter and the height of each sample was fixed to 8mm.

4.3. Heat Treatment

4.3.1. Austenization and Quenching

Steel rebar samples from both of the grades were austenized by placing them inside the furnace at 870^0C for 5 minutes. Once all the samples were fully austenized, they were quenched in the water at room temperature to get martensitic structure.

4.3.2. Tempering

After quenching, tempering of quenched steel samples was done at different temperatures to study the effect of tempering.

For this purpose, every sample from each grade was tempered at different temperature. Tempering of the samples was done at 200^0C, 300^0C, 400^0C, 500^0C and 600^0C and the holding time of each sample in the furnace was fixed for 30 minutes. After completing the tempering, the samples were quenched again in the water at room temperature.

Fig. 4.1 represents the isothermal transformation diagram of 0.35% carbon steel and Fig. 4.2 represents the schematic diagram of adopted heat treatment.

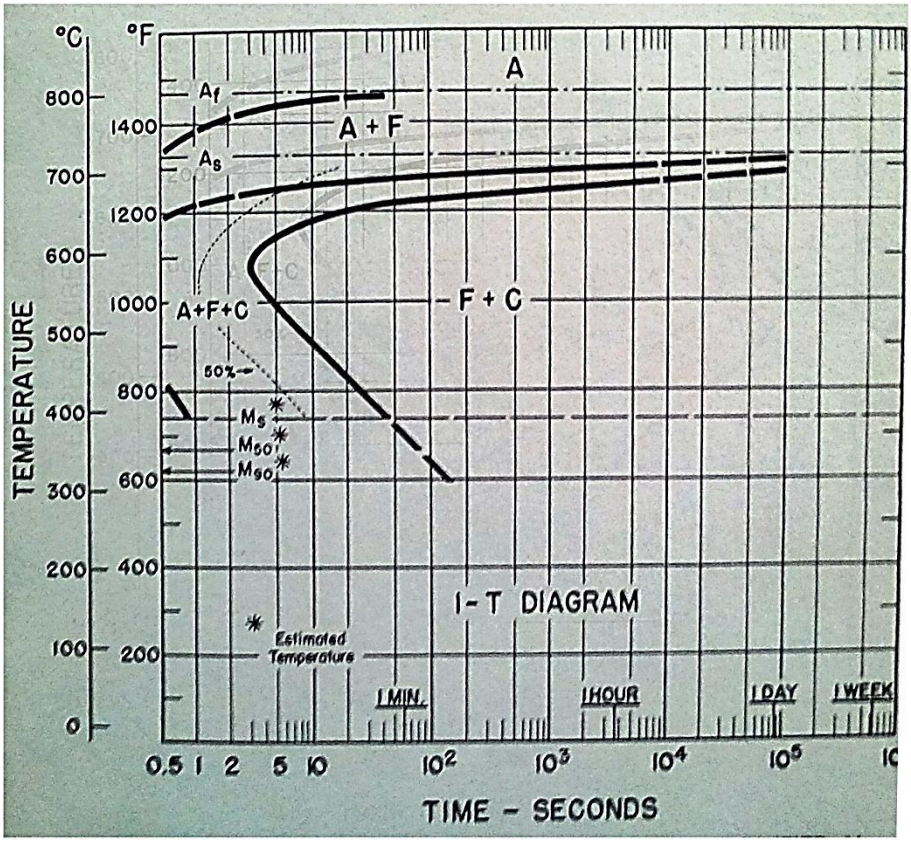

Figure 4.1: Isothermal transformation diagram for eutectoid steel

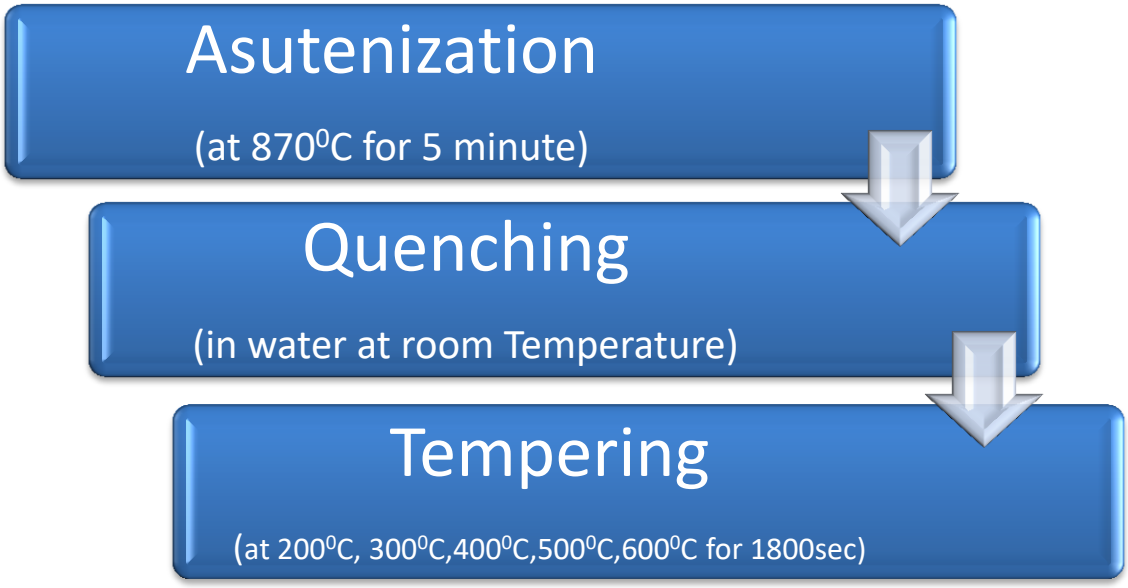

Figure 4.2: Schematic illustration for heat treatment

4.4. Metallography

After heat treatment, test samples were wet grinded with SiC grinding papers having grit size ranging from 240-1000. The grinding process was continued as long as all coarse scratches were removed. After that, grinded samples were wet polished with 0.3 micron alumina powder on rotating velvet cloth wheel. Finally the samples were ultrasonically degreased for 5 min in detergent containing water and rinsed thoroughly in distilled water and finally air dried.

4.5. Microhardness Testing

Microhardness testing of each sample, tempered at different temperature, was done by Vickers hardness tester (Bruker) under the applied load of 300g to evaluate the effect of heat treatment. Before moving towards tempering, each quenched sample was evaluated by measuring the Vickers hardness. The values obtained were compared by standard hardness values available already in the literature.

Once the transformation of austenite to martensite was confirmed then hardness was again evaluated for tempered samples.

4.6. Sample Preparation for Electrochemical Testing

After measuring the micro hardness, the next important step was to prepare the samples for electrochemical testing. For this, each sample was spot welded with a conducting wire by soldering. The welded samples were then cold mounted in epoxy resin and a hardener in such a way that only tested area was exposed in the electrolytic solution. Once all the samples were mounted, these were grinded up to 600 grit size. For electrochemical testing, no polishing was adopted to provide roughness as it is on steel rebar surface in real concrete environment.

4.7. Concrete Simulated Solution Preparation

It is not easy task to study the electrochemical behavior of steel rebar embedded in real solid concrete because of high resistivity and complexity involved in cell design. Although corrosion rate can be measured by making a cell through a real concrete but if there is a need of deep study to investigate the materials surface, i.e. passive layer, then scientist are agreed to make a concrete simulated solution. This solution should be the representative of actual concrete.

Table 4.2: Concrete simulated pore solution composition [76-77]

Compound	Molar Composition (mol/lit.)
KOH	0.6
NaOH	0.2
$Ca(OH)_2$	0.01

The composition of the concrete simulated solution, which is mentioned somewhere else [76-77], was considered for this study too. The composition of the solution is mentioned below in Table 4.3.

4.8. Sample Immersion in Concrete Solution

Sample coupons prepared for both electrochemical testing and surface analysis were firstly immersed inside the concrete simulated solution for 72 hours. This was done to allow the passive layer to be developed over the exposed surface of steel rabar. The pH of the solution was continuously monitored to maintain it above 13.5.

4.9. Electrochemical Testing

Electrochemical testing of the samples immersed in concrete simulated solution was conducted in two basic steps for both of the compositions of steel rebar. The two steps are categorized on the basis of electrolyte in which electrochemical testing was going to be conducted. The types of electrolyte used are:

i. Concrete Simulated Solution

ii. Concrete Simulated Solution + 0.8M NaCl

For each solution, three basic types of electrochemical testing were conducted for all the samples of both compositions. The conducted electrochemical tests are:

a. Electrochemical Impedance Spectroscopy (EIS)

b. Linear Polarization Resistance (LPR)

c. Potentiodynamic polarization (PDP)

4.9.1. Electrochemical Testing in Alkaline Solution

After alkaline immersion, study of electrochemical behavior of tempered sample for both grades (M-1 and M-2) was done by Gamry 3000 potentostat to evaluate the effect of copper composition and tempering temperature on the electrochemical properties of passive layer developed on steel surface in concrete solution free of chlorides. All the tests were performed by using saturated calomel electrode (SCE). The types of conducted experiments are:

i- Open Circuit potential (OCP)

ii- Electrochemical Impedance Spectroscopy (EIS)

iii- Linear Polarization Resistance (LPR)

iv- Potentiodynamic Polarization (PDP)

i- Open Circuit Potential (OCP)

First of all, open circuit potential of all the testing samples was measured for 30 minutes. After 30 minutes, when the open circuit potential was noted to be constant then electrochemical testing was started.

ii- Electrochemical Impedance Spectroscopy (EIS)

After measuring open circuit potential (OCP), electrochemical Impedance spectroscopy (EIS) was measured at first as this kind of technique is considered to be non-destructive. The applied AC voltage was set to ±10mV while the frequency range was set from 30 KHz to 10 mHz.

iii- Linear Polarization Resistance (LPR)

LPR testing was performed according to ASTM standard by applying ±15 mV of E_{corr} with a scan rate of 0.2 mV/s.

iv- Potentiodynamic Polarization (PDP)

After LPR, potentiodynamic polarization (PDP) was measured by setting the applied voltage from -0.8mV to +1.2mV with a scan rate 0.5 mV/s.

4.9.2. Electrochemical Testing in Alkaline Solution + 0.8M NaCl Solution

After completing the electrochemical testing within alkaline solution (representing concrete), the next set of experiments were repeated for the concrete simulated solution with the addition of 0.8M NaCl. The Cl^-/OH^- ratio of the electrolyte was set to 1.

4.10. Microscopy

The samples prepared by metallography were used for microscopy and surface analysis. Optical microscope of "Infinity" company and scanning electron microscope (JSM-6610LV) were used.

4.11. Surface Passive Film Analysis by XPS

The placement of the test coupons inside the concrete solution for 72 hours must had developed a passive layer on the surface of steel rebar in highly pH solution. So, X-ray photoelectron spectroscopy (XPS) technique was used to study the nature and chemistry of that developed passive layer.

CHAPTER 5: Results

5.1. Elemental Composition

The chemical compositions of the steel rebars were evaluated by spectrometer and the elemental compositions of both the grades are provided in Table 5.1

Table 5.1: Elemental compositions of steel rebar M-1 and M-2

Element	Composition (%)	
	M-1	**M-2**
C	0.294	0.308
Si	0.320	0.172
Mn	0.684	0.560
Co	0.0050	0.0106
Cr	0.0122	0.0708
Mo	0.0225	0.0441
Ni	0.0227	0.0110
Cu	0.0489	0.207
V	0.114	0.130
P	0.0027	0.0249
S	0.0061	0.0299
W	0.0627	0.0939
Al	<0.0010	<0.0010
Nb	<0.0020	<0.0020
Fe	Balance	Balance

5.2. Heat Treatment

Firstly, the steel samples were austenized at 870^0C for 5 minutes followed by quenching in water at room temperature. After that, each quenched sample was tempered at 200^0C, 300^0C, 400^0 C, 500^0C and 600^0C. After tempering, microhardness of each

sample was tested by a microhardness tester. Hardness variations with tempering temperature are shown in Table 5.2. The trends of hardness variation are provided graphically in Fig.5.1. Each reported hardness value is based on 5 measurements.

For M-1, it can be seen from the graph that the hardness of the quenched sample was found to be highest. The hardness began to decrease with the increase in tempering temperature and the lowest hardness was noted to be at 600^0C tempering temperature.

Table 5.2: Variation of hardness with tempering temperatures for rebar M-1 and M-2

Specimen	Hardness (Hv)	
	M-1	**M-2**
As Quenched	373	359
Tempered 200^0C	330	295
Tempered 300^0C	312	365
Tempered 400^0C	291	326
Tempered 500^0C	287	230
Tempered 600^0C	221	246

On the other side, for M-2, initially the hardness decreased from quenched to 200^0C tempering temperature and then increased sharply at 300^0C. The increase in hardness with the increase of tempering temperature from 200^0C to 300^0C can be attributed to the precipitation hardening due to the presence of copper as an alloying element in steel rebar. However, with the increase of tempering temperature from 400^0C to 600^0C, the hardness started to decrease and the lowest hardness was measured at 600^0C tempering temperature.

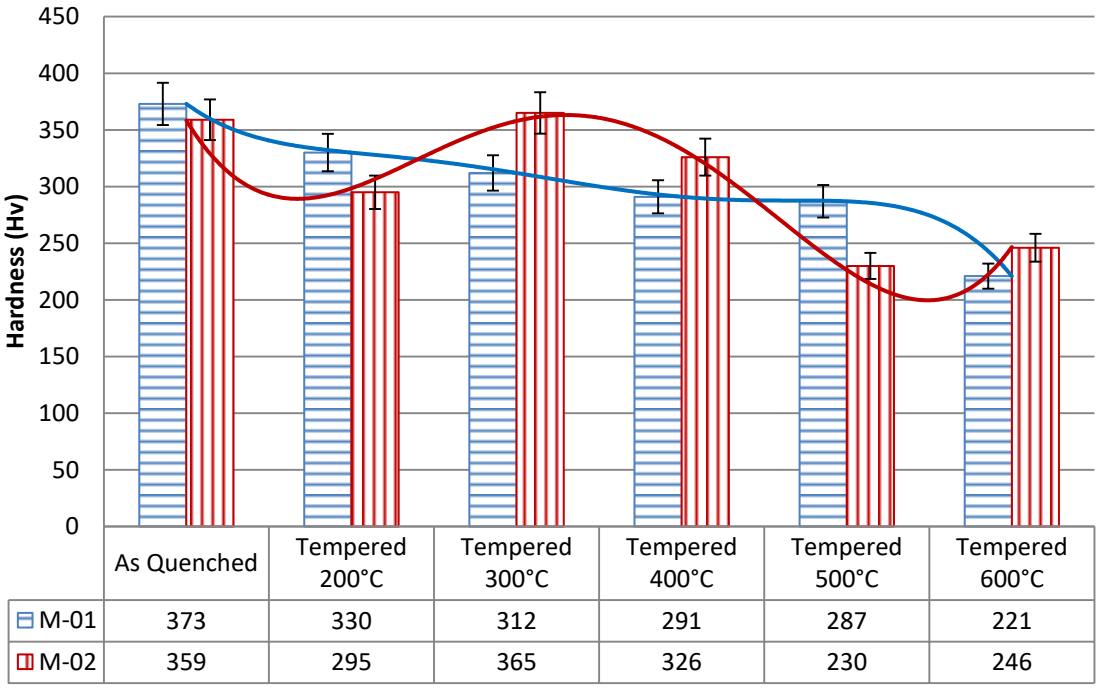

Figure 5.1: Variation of hardness with tempering temperature for steel rebar M-1 and M-2

5.3. Microstructures

5.3.1. Rebar M-1

Martensitic structure contains maximum amount of carbon which was restricted to be precipitated out of the solid solution due to the rapid cooling mechanism. So, the tempering mechanism changes the microstructure of carbon steel in three stages;

1- During the first stage, the excess carbon in the solid solution segregates at the defects or cluster inside the solid solution. It then precipitates out either as a cementite in low carbon steel or as transition iron carbide in high carbon steel.

2- With the increased time or tempering temperature, complete carbon precipitates out and transition iron carbide converts into stable cementite.

3- Increased tempering temperature coarsens the carbide particle size and ferrite recovery is achieved.

Optical micrographs of the samples tempered at different temperatures are provided in Fig.5.2 to 5.7. All the rebar samples were etched with nital (2%).

It can be seen in Fig. 5.2 that truly lath martensitic structure was achieved for as-quenched sample. There can be seen some of the retained austenite and ferrite in the microstructure. When tempering temperature was raised to 200^0C and 300^0C then tempered martensitic structure was obtained with some of the ferritic structure. It can be seen in Fig.5.3 and Fig.5.4 that with the increase of temperature, the laths became finer and hardness decreased. It reflects that increased tempering temperature reduced the carbon content inside the martensitic laths and carbon precipitated out at the lath interface. However, when tempering temperature was increased to 400^0C (Fig. 5.5), then in addition of getting tempered martensite, lower bainite is expected to form due to the transformation of retained austenite. Drop in hardness at 400^0C can be attributed due to the combined effect of ferrite, bainite and higher amount of precipitation of carbon at the laths interfaces. When tempering temperature was raised to 500^0C and 600^0C then further decrease in hardness was noted. This reduction in hardness can be because of the higher amount of carbon precipitation on the laths interfaces (Fig.5.6-5.7). In addition to this, the ferrite recovery and transformation of retained austenite either into upper bainite (at 500^0C) or into fine pearlite (at 600^0C) can be the reason for reduced hardness.

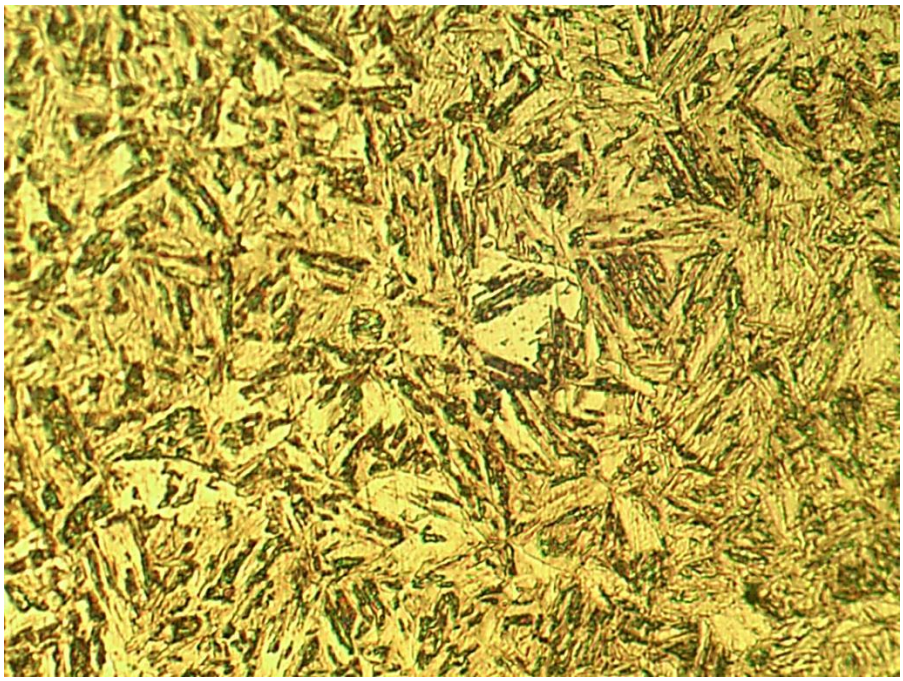

Figure 5.2: Optical microstructure of as-quenched martensite for steel rebar M-1 at 500x

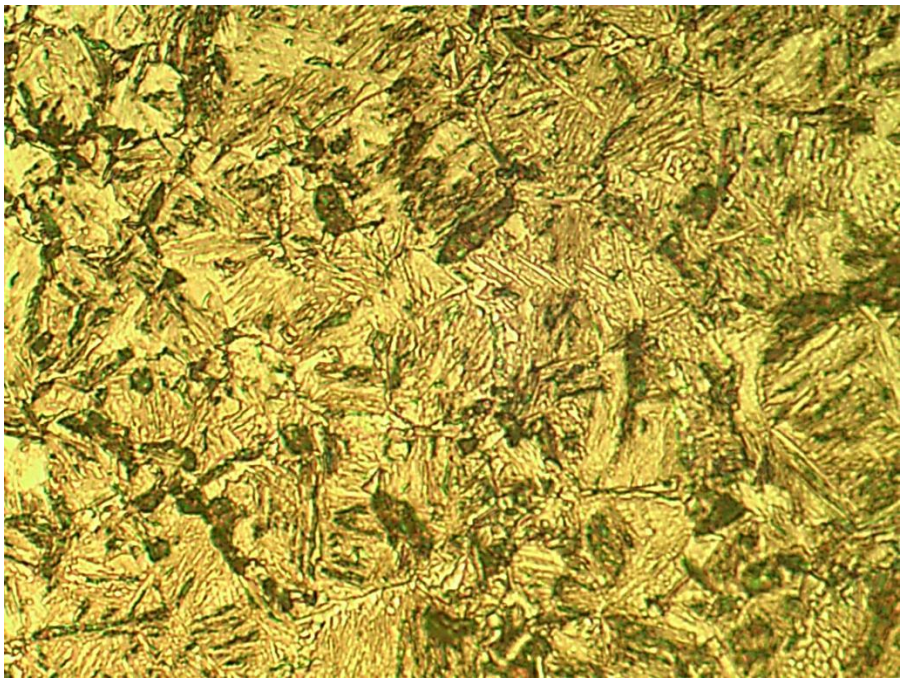

Figure 5.3: Optical microstructure of tempered-martensite at 200^0C for rebar M-1 at 500x

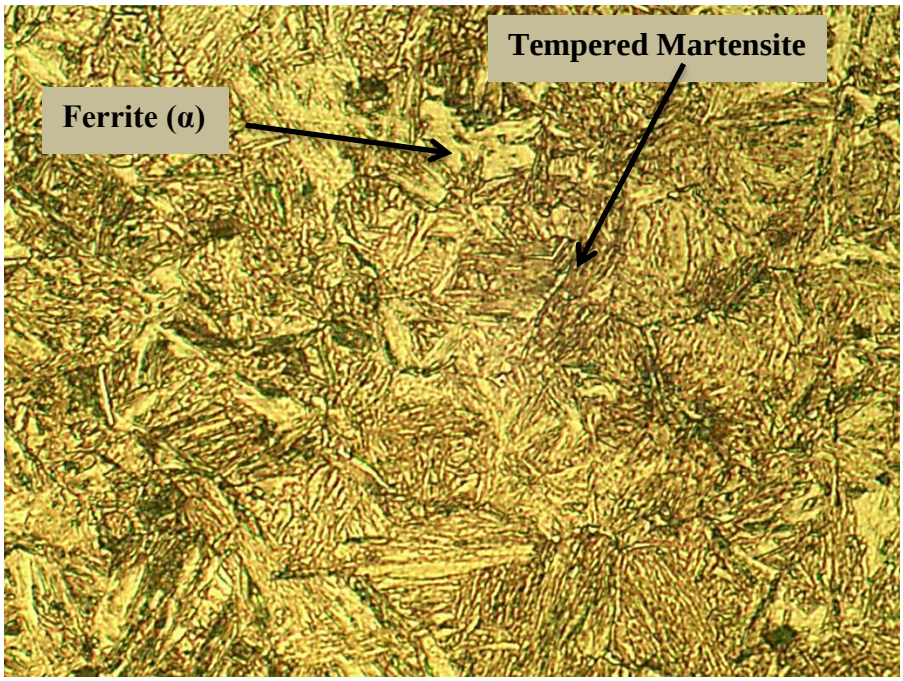

Figure 5.4: Optical microstructure of tempered-martensite at 300^0C for rebar M-1 at 500x

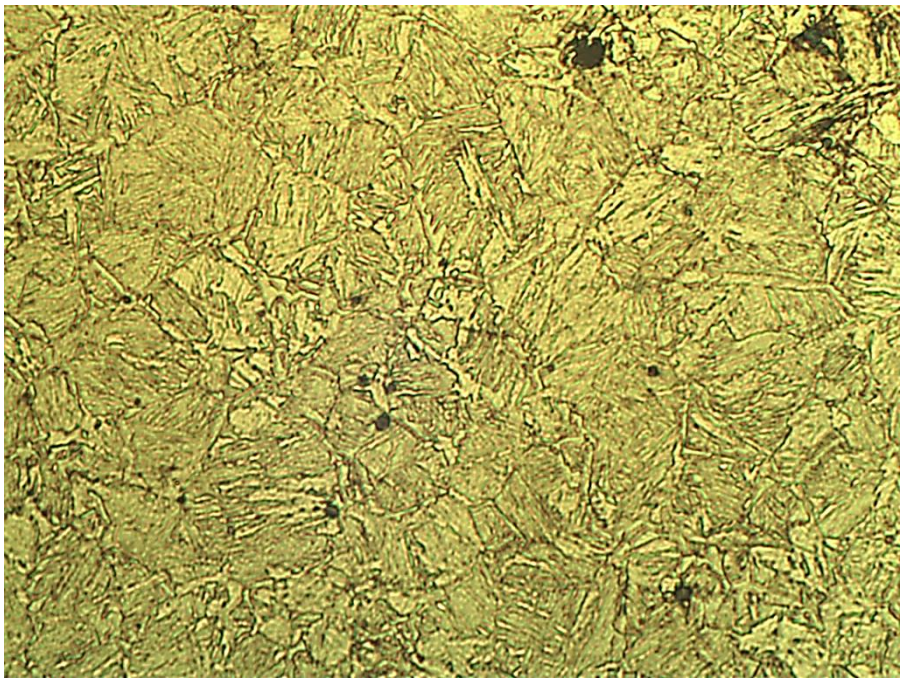

Figure 5.5: Optical microstructure of tempered-martensite at 400^0C for rebar M-1 at 500x

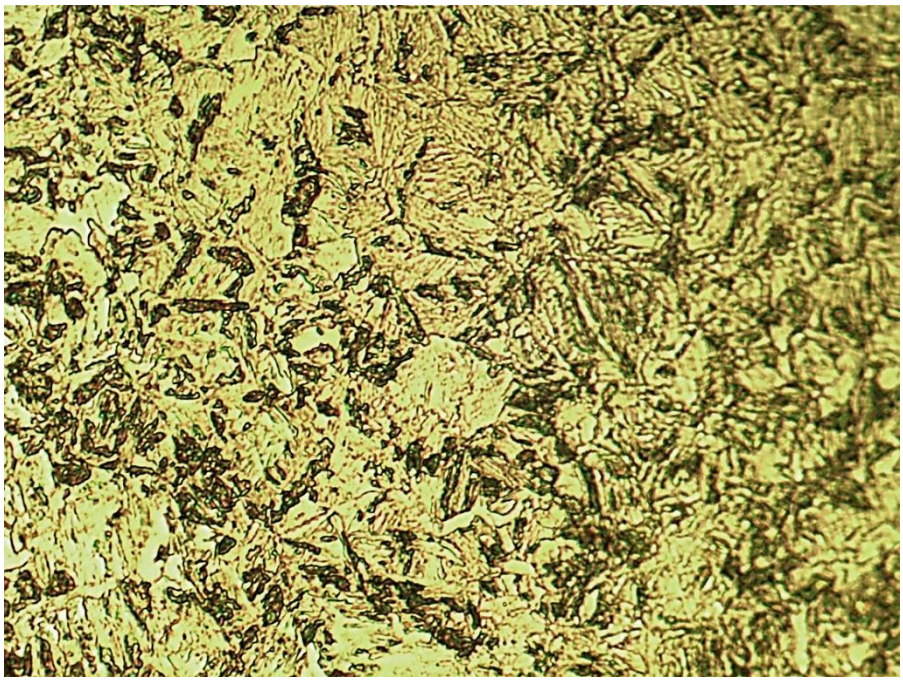

Figure 5.6: Optical microstructure of tempered-martensite at 500^0C for rebar M-1 at 500x

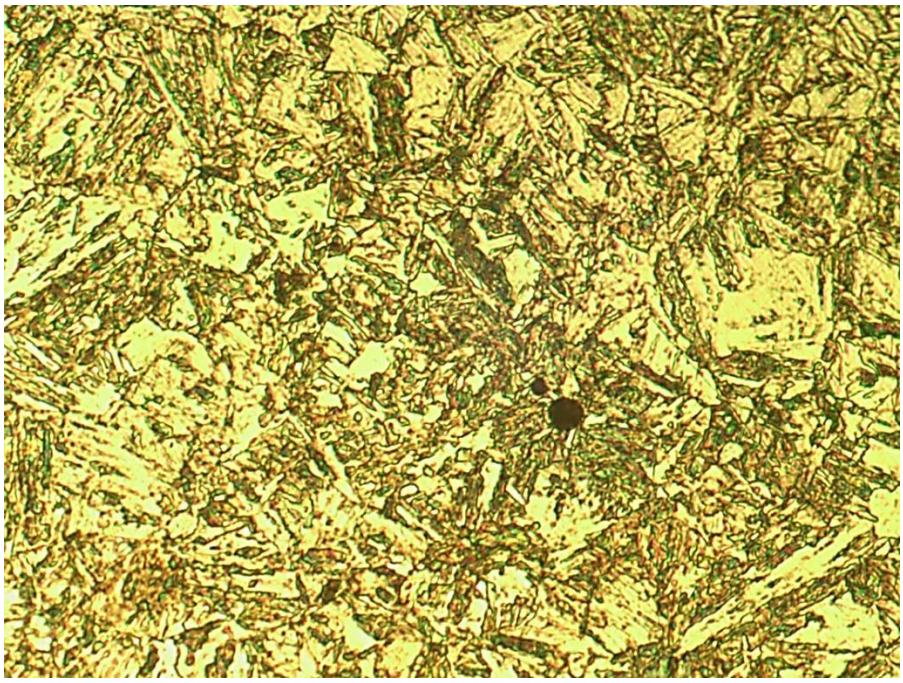

Figure 5.7: Optical microstructure of tempered-martensite at 600^0C for rebar M-1 at x500

5.3.2. Rebar M-2

Steel rebar M-2 provided the microstructure similar to rebar M-1 and can be seen from Fig.5.8-5.13 that no significant change was observed in the phases. However, it can be noted from the table 5.2 that tempered 300^0C provided highest hardness even than as-quenched sample. At 300^0C, a sudden and dramatical increase in hardness might be because of the participation hardening mechanism due to the presence of copper. For the current composition of steel rebar, 300^0C can be the optimum tempering temperature for precipitation hardening. Immense amount of researches have been reported so far in order to understand the precipitation hardening of copper and steel system [104-107].

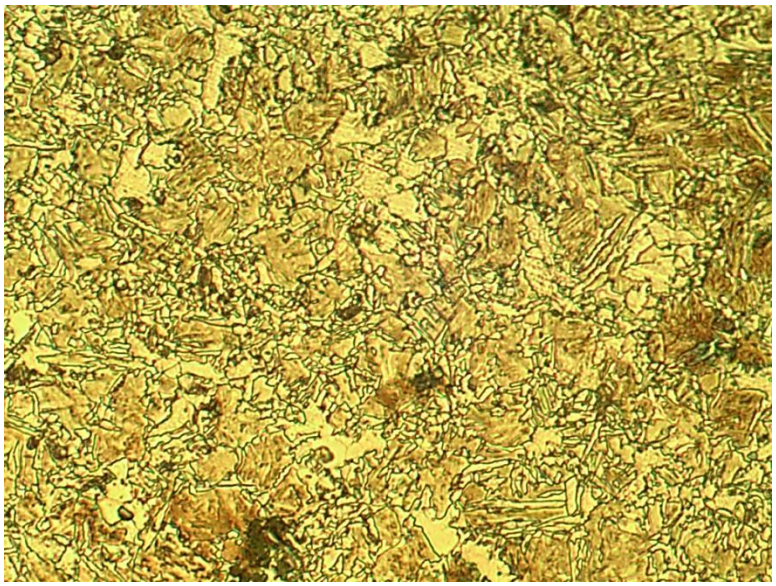

Figure 5.8: Optical microstructure of as-quenched martensite for rebar M-2 at 500x

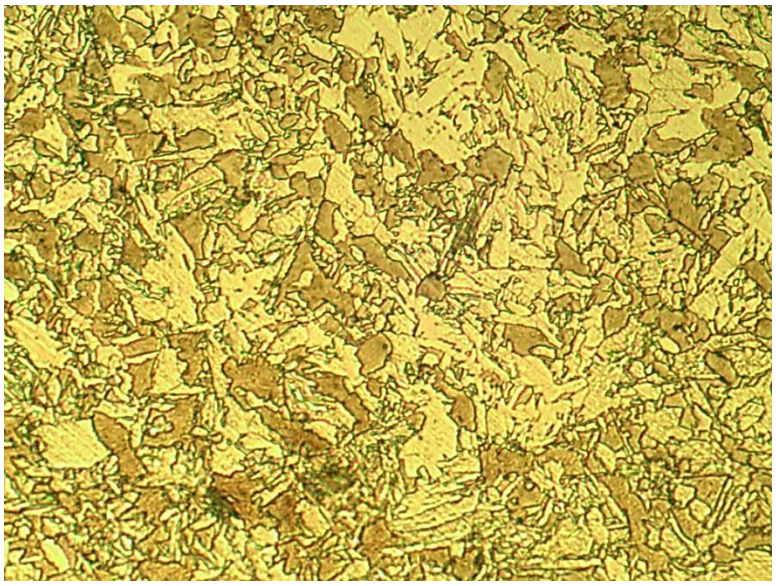

Figure 5.9: Optical microstructure of tempered-martensite at 200^0C for rebar M-2 at 500x

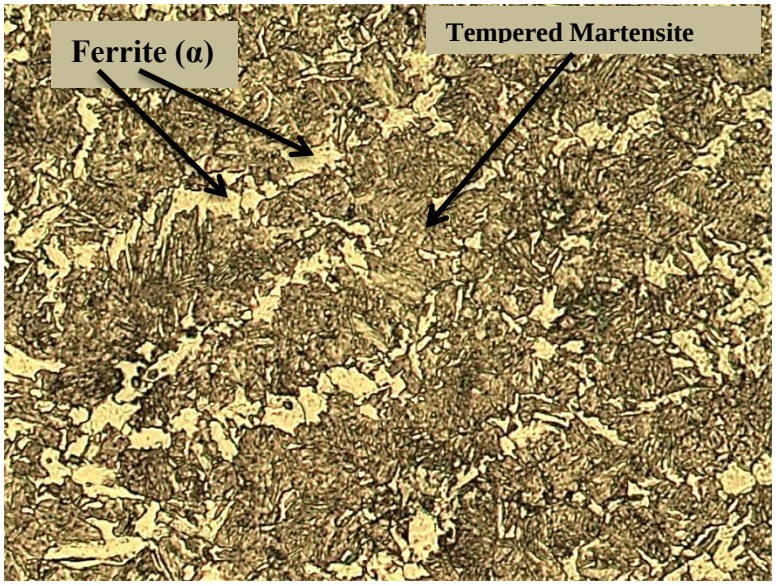

Figure 5.10: Optical microstructure of tempered-martensite at 300^0C for rebar M-2 at 500x

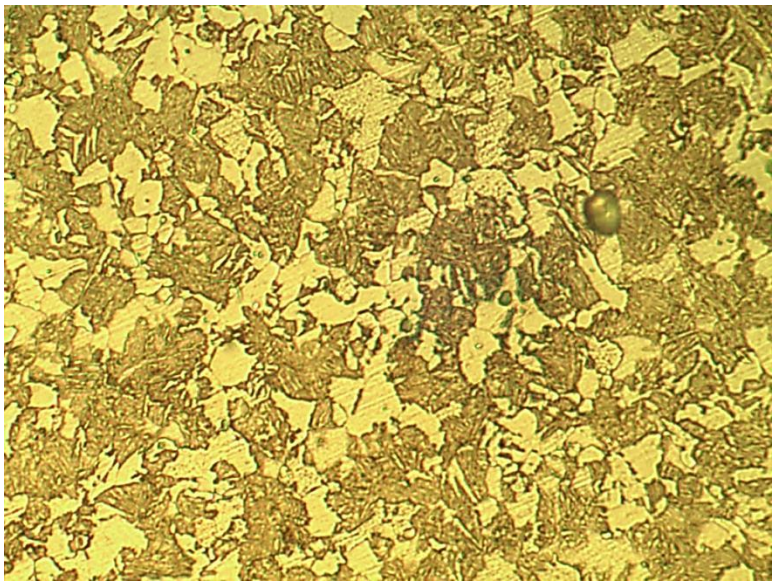

Figure 5.11: Optical microstructure of tempered-martensite at 400^0C for rebar M-2 at 500x

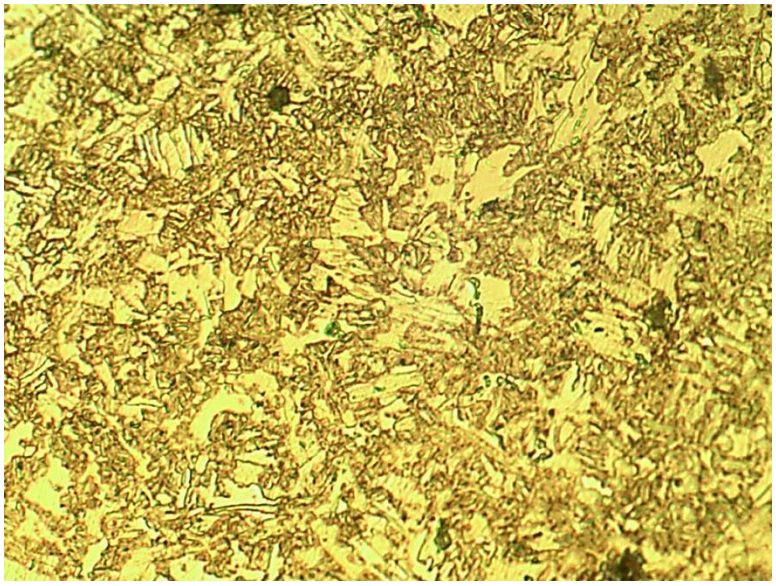

Figure 5.12: Optical microstructure of tempered-martensite at 500^0C for rebar M-2 at 500x

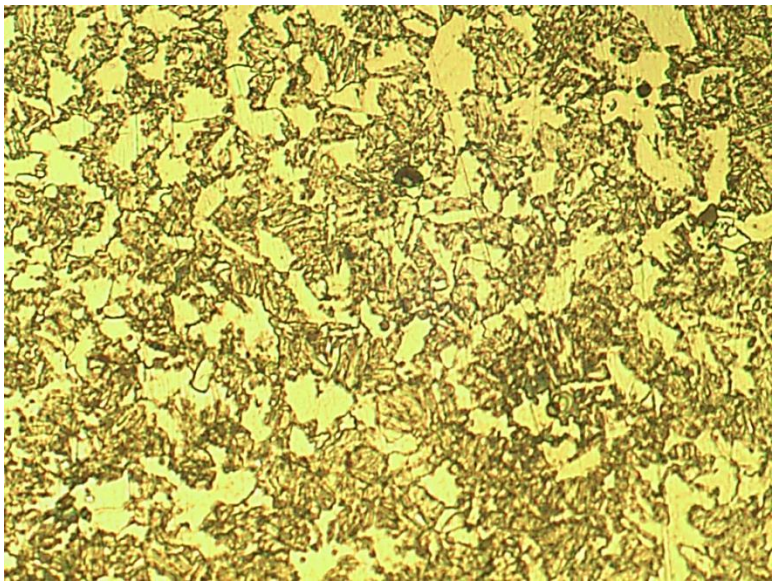

Figure 5.13: Optical microstructure of tempered-martensite at 600^0C for rebar M-2 at 500x

5.3.3. Scanning Electron Microscope

Scanning electron microscopic images of steel rebar M-1 and M-2 at different tempering temperatures can also be seen in Fig.5.14-5.18

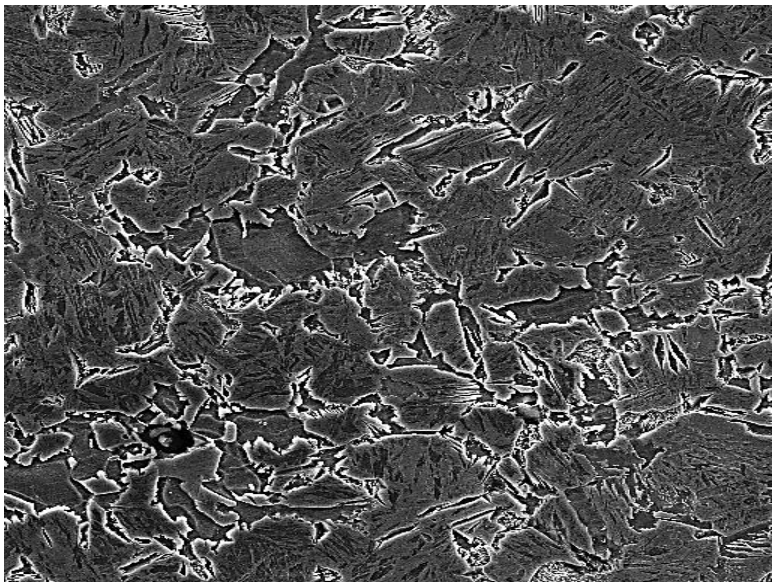

Figure 5.14: SEM image of as-quenched martensite for rebar M-1 at 1000x

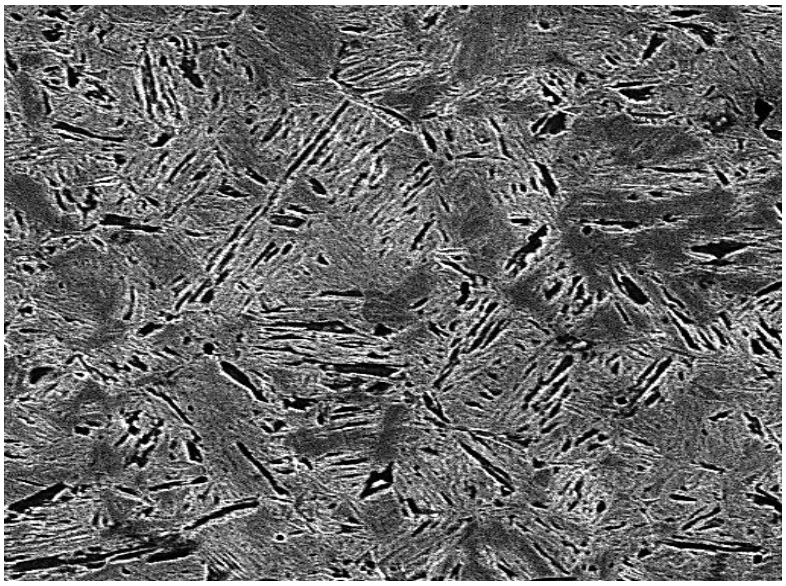

Figure 5.15: SEM image of tempered-martensite at 300^0C for rebar M-1 at 1000x

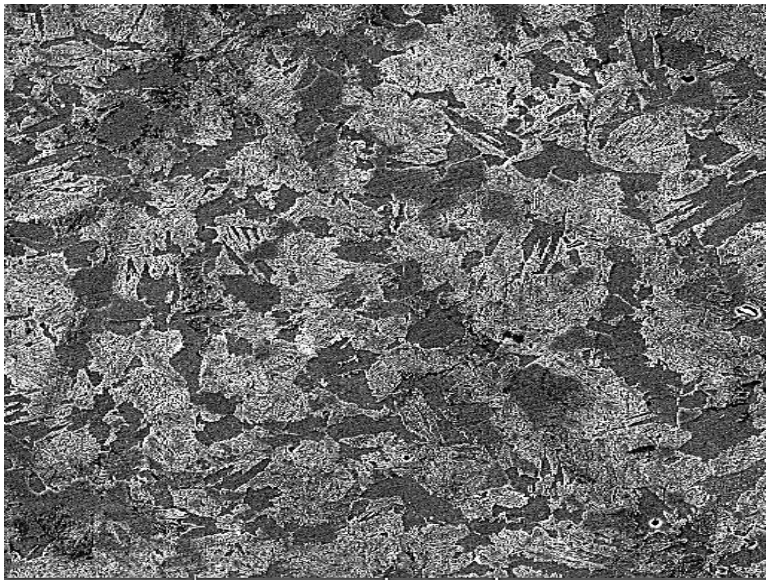

Figure 5.16: SEM image of tempered-martensite at 400^0C for rebar M-1 at 1000x

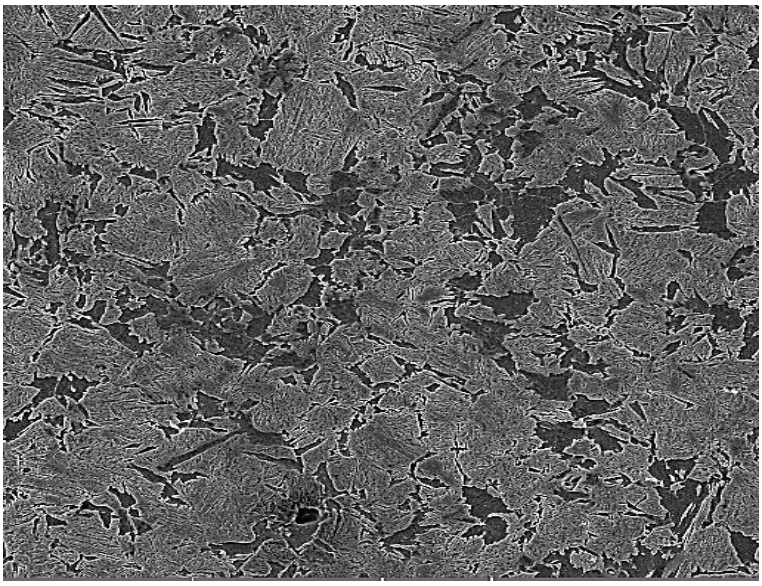

Figure 5.17: SEM image of tempered-martensite at 300^0C for rebar M-2 at 1000x

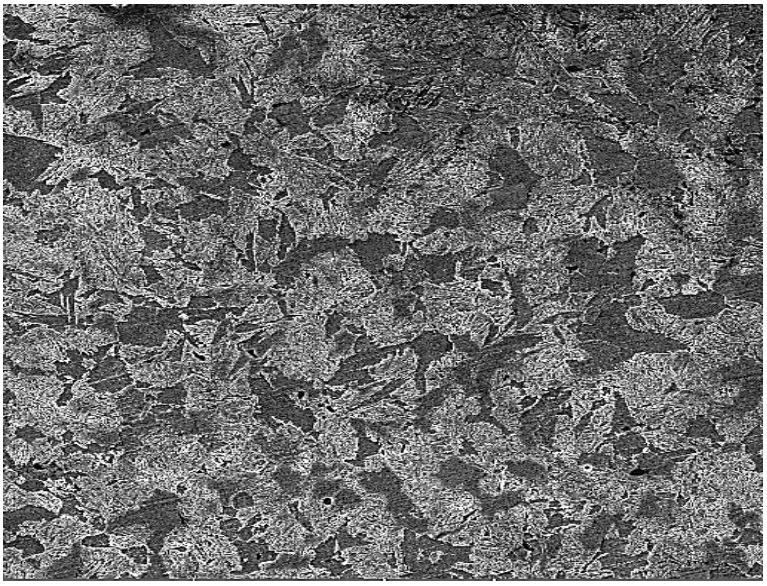

Figure 5.18: SEM image of tempered-martensite 400^0C for rebar M-2 at 1000x

5.4. Electrochemical Testing

Electrochemical testing of both grades of steel rebar was conducted to study the effect of heat treatment and copper composition on the passive layer's composition and resistance in highly alkaline solution (pH>13.5). The pH of the solution prepared with the

described composition in experimental work was noted to be 13.5. All samples were immersed in the alkaline solution for 72 hours and then introduced in the electrochemical cell for conducting electrochemical testing. The composition and pH of the electrolyte used for conducting experiments were set to be the same as used for immersion purpose.

5.4.1. Electrochemical Impedance Spectroscopy for M-1

5.4.1.1. Testing in Alkaline Solution

Firstly, electrochemical impedance spectroscopy (EIS) was conducted on M-1 rebar in pure alkaline solution. All the samples i.e. as-quenched, tempered at 200^0C, 300^0C, 400^0C, 500^0C and 600^0C were tested one by one in order to measure their impedance. The frequency was set from 30KHz to 10mHz.

Nyquist plot in EIS compares the real and imaginary impedance with the change of frequency. However, the change of frequency is invisible in the graph. If we compare the results of each sample, i.e. as quenched, tempered 200^0C, 300^0C, 400^0C, 500^0C and 600^0C, (by Nyquist plots) then it is very clear from the Fig.5.19 that, the sample which was tempered at 400^0C had provided the highest impedance with a value of 10500($\Omega.cm^2$) followed by the samples tempered at 500^0C and 600^0C with a values of 100250 $\Omega.cm^2$ and 10000 ($\Omega.cm^2$), respectively. Overall resultant impedance is the combination of real and imaginary impedance. Though the real impedance value of the tempered 400^0C is better and found more than the rest of the tempered samples, but its imaginary impedance is significantly higher than its two main competitors i.e. tempered 500^0C and 600^0C. However, the impedance of as-quenched, tempered 200^0C and 300^0C samples provided very low electrochemical impedance.

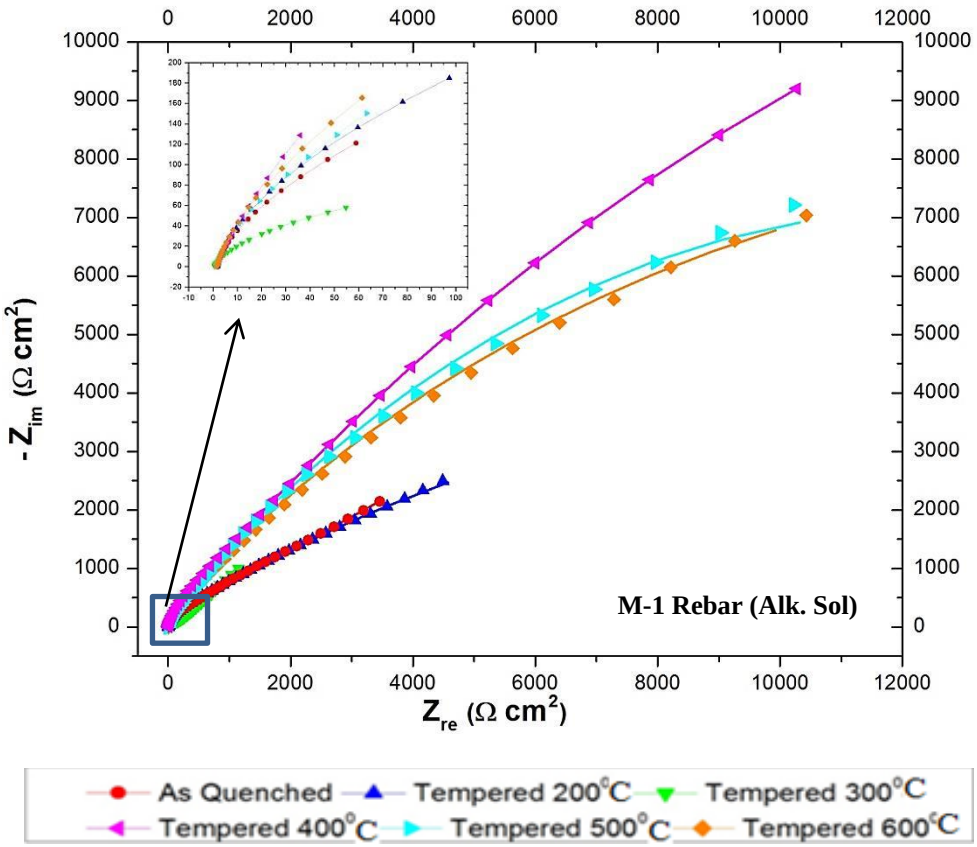

Figure 5.19: Nyquist plot of M-1 rebar tempered at different temperatures in alkaline solution

If we are interested to observe the direct relation of the change of impedance with the change of frequency then Bode plot is the most appropriate one. The resultant impedance in Bode plot for the same tempered sample agrees with Nyquist plot and it can be seen in Fig.5.20. The trend is very obvious and it can be seen that when the frequency was very high then impedance was noted to be very low and vice versa. Initially, downwarding from 30 KHz to 5 KHz, it is cleared that the impedance remained almost constant in this frequency region. This region is at very high frequency and impedance represented by the system at this frequency range is provided only by the solution. However, with the decrease of frequency to 10mHz, the impedance started to increase again which indicates the presence of charge transfer, film resistance and capacitance contribution to the total impedance.

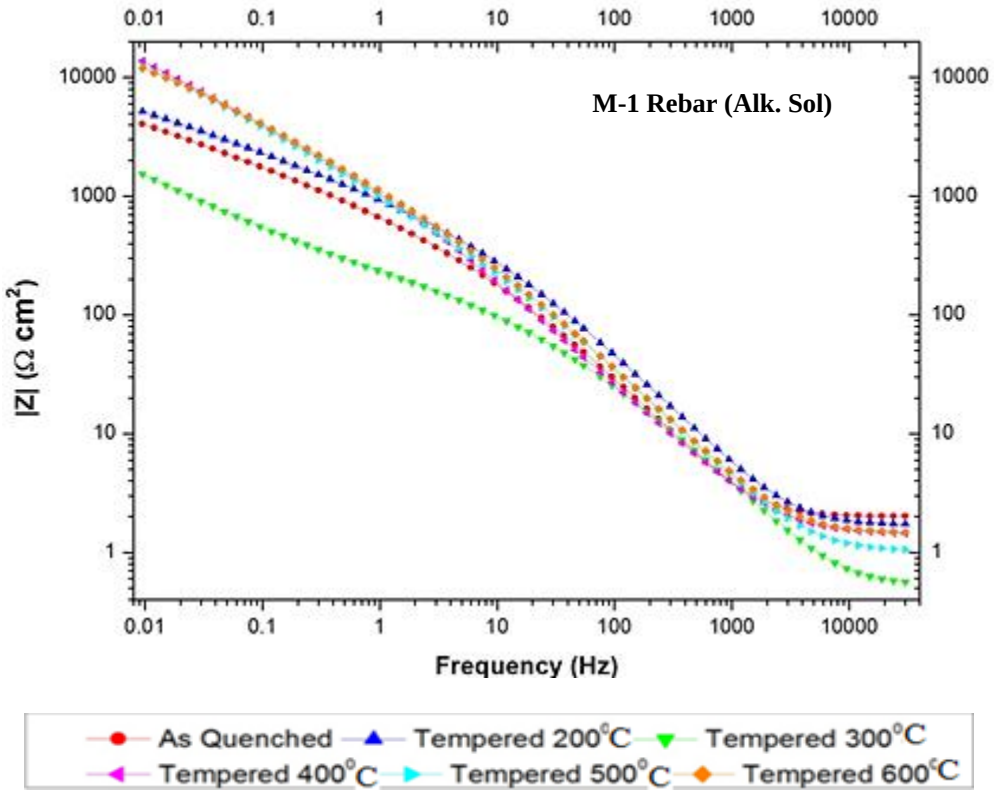

Figure 5.20: Bode plot of M-1 rebar tempered at different temperatures in alkaline solution

Bode plot represents the relationship between change of frequency and phase shift (angle). As the provided voltage is of alternating nature, thus, it reveals great information by shifting its phase shift with the change of frequency. For instance, when frequency was too high then it can be seen that phase shift was noted to be very small or near to zero as shown in Fig.5.21. This reflects that, at very high frequency, the capacitor or constant phase elements are under short circuit and no current is passing through the resistors. That's why there is no chance for the current to shift its phase at very high frequency. However, with lowering of frequency, the change (shift) of phase becomes prominent and it started to increase steeply from 30 KHz to 100 Hz with a mark of 75 degree. This shifting of phase at lower frequency indicates the presence of a passive layer over the surface of steel and this newly formed film is acting as a capacitor or a constant

phase element. So, at lower frequency, the capacitor acts as insulator and provides the infinite resistance to the current. This current then passes through the alternate parallel path occupied by the resistor. Furthermore, when the frequency was more reduced below than 100 Hz then the decrease in phase angle was observed and finally, at 10 mHz, the difference in phase shift was found different against each tempering temperatures.

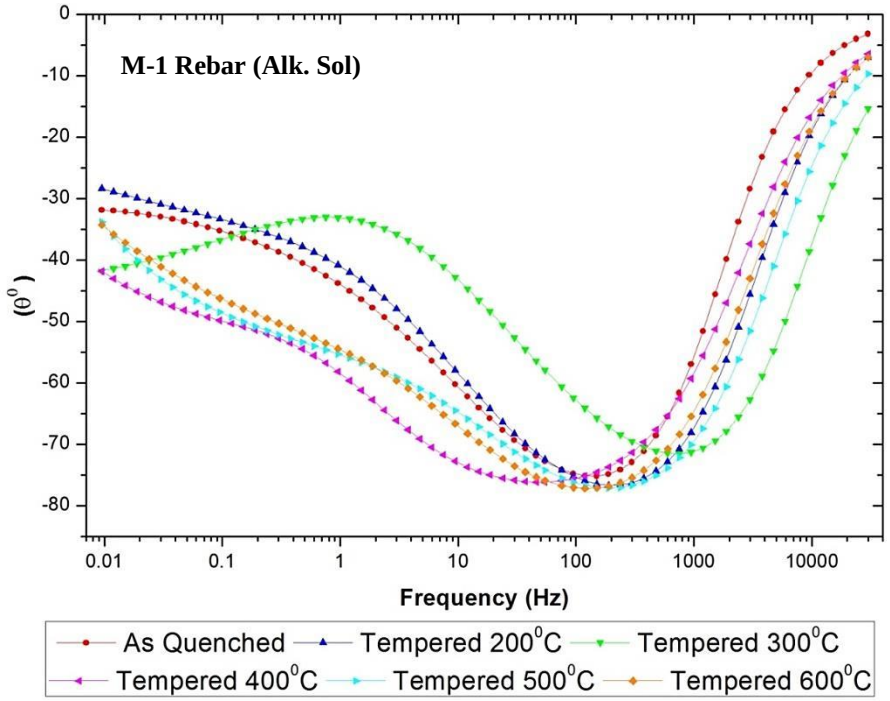

Figure 5.21: Bode plot representing phase shift of M-1 rebar tempered at different temperatures in alkaline solution

5.4.1.2. Equivalent Circuit Model Fitting

Nyquist plot or Bode plot obtained by electrochemical impedance spectroscopy (EIS) gives only the resultant impedance with the change of frequency and they lack the information that how the material was behaving actually at a specific frequency. So the arising questions not answered by Nyquist and Bode plot are:

i- What is the charge transfer resistance (corrosion resistance)?

ii- What is the passive film resistance?

iii- What is the solution resistance?

iv- What is the nature of the passive film?

These are the questions in fact which are not answered by Nyquist and Bode plot. So to know in depth, EIS data was fitted on the proposed model which should be the best representative of the actual physical state at the metal-film interface and at the film-electrolyte interface. But before knowing the actual physical state of the interfaces, we have to know it first that how the passive film is formed when steel rebar is introduced in the environment simulated to concrete system. The general passive film formation mechanism of the tested system, irrespective of copper presence, is stated in equations 5.1-5.6 [101] and the proposed diagram is shown in Fig.5.22

$$Fe + OH^- = [Fe(OH)]_{ads} + e^- \quad (5.1)$$

$$[Fe(OH)]_{ads} = [Fe(OH)]_{ads}^+ + e^- \quad (5.2)$$

$$[Fe(OH)]_{ads}^+ + OH^- = Fe(OH)_2 \quad (5.3)$$

$$3Fe(OH)_2 + 2OH^- = Fe_3O_4 + 4H_2O + 2e^- \quad (5.4)$$

$$Fe_3O_4 + OH^- + H_2O = 3\alpha\text{-}FeOOH + e^- \quad (5.5)$$

$$2Fe_3O_4 + 2OH^- = 3\gamma\text{-}Fe_2O_3 + H_2O + 2e^- \quad (5.6)$$

Initially, the hydroxyl ions (OH^-) from the electrolyte moves towards the surface of the steel rebar and adsorbs over the surface and form $[Fe(OH)]_{ads}$ .This $[Fe(OH)]_{ads}$ then release an electron on the surface of the steel and form a positive charge (Equ.5.2). This formed positive charged $[Fe(OH)]_{ads}^+$ reacts further with the hydroxyl ions (OH^-) coming from the electrolyte and forms $Fe(OH)_2$ which is the first stable compound to be

deposited over the steel surface to form passive layer (Equ.5.3). In the next step, this formed $Fe(OH)_2$ is electro-oxidized and reacts further with the hydroxyl ions (OH^-) (abundantly available in the solution) and forms the magnetite (Fe_3O_4) (Equ.5.4). The newly formed Fe_3O_4 layer is subjected either to further chemical reaction with the hydroxyl ions (OH^-) or there exists structural rearrangements in term of aging for enhanced modification. The transformed product can be either the composite of goethite (α-FeOOH), lepidocrocite (γ-FeOOH), akagonite (β-FeOOH) or it can be γ-Fe_2O_3 [101].

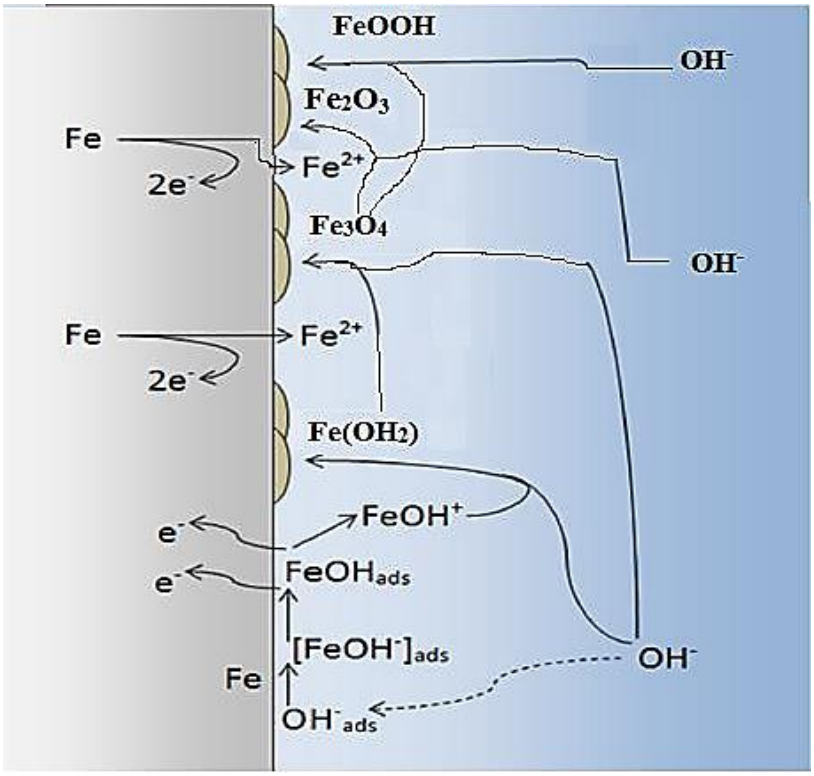

Figure 5.22: Proposed passive film formation mechanism [102]

After understanding this physiochemical interaction in between metal and electrolyte interface, now we can propose the model simulating to concrete environment condition. As the tempering temperature was not fixed so a single model was not fitting the data very accurately. In this scenario, two of proposed models are used to fit the data and both of these models are provided below:

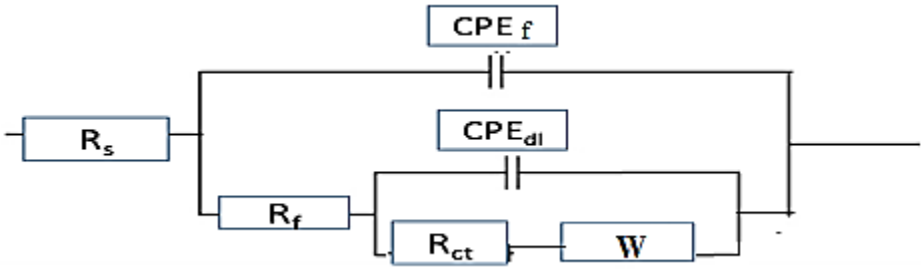

Figure 5.23: **Type A: Equivalent circuit model with two constant phase elements and Warburg element**

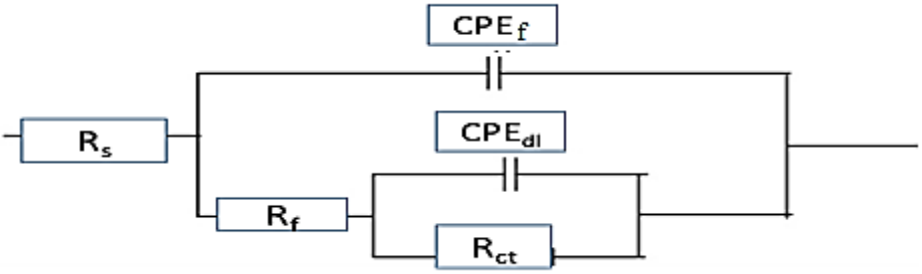

Figure 5.24: Type B: Equivalent circuit model with two constant phase elements

The equivalent circuit used against each heat treatment tempering temperature is provided in Table 5.3. Also when the data from EIS experiments was fitted to these models, the values obtained are shown in Table 5.4.

In Table 5.4, R_s represents the solution (electrolyte) resistance, R_{ct} represents the charge transfer resistance and R_f represents the film resistance due to pores and defects in the developed passive film. Also it can be seen that the two constant phase elements (CPE) were used in equivalent circuits against all tempered temperature.

Table 5.3: Types of equivalent circuit model used against different tempered steel rebar M-1

Alkaline Solution		Alkaline Solution + 0.8M NaCl	
Heat Treatment	**Model Type**	**Heat Treatment**	**Model Type**
As-Quenched	A	As-Quenched	A
Tempered 200^0C	A	Tempered 200^0C	A
Tempered 300^0C	A	Tempered 300^0C	A
Tempered 400^0C	B	Tempered 400^0C	A
Tempered 500^0C	A	Tempered 500^0C	A
Tempered 600^0C	A	Tempered 600^0C	A

Table 5.4: EIS parameters obtained after fitting data on equivalent circuit model for M-1 rebar in alkaline Solution

Specimen	$\mathbf{R_s}$ **(Ωcm^2)**	$\mathbf{R_{ct}}$ **(Ωcm^2)**	$\mathbf{R_f}$ **(Ωcm^2)**	$\mathbf{CPE_{dl}}$ **(S.s^n/cm^2)**	$\mathbf{n_{dl}}$	$\mathbf{CPE_f}$ **(S.s^n/cm^2)**	$\mathbf{n_f}$	**W (S.s$^{1/2}$)**
As-Quenched	1.316	$1.21\text{x}10^4$	$2.64\text{x}10^2$	$5.96\text{x}10^{-4}$	0.80	$5.69\text{x}10^{-5}$	0.93	$7.46\text{x}10^{-3}$
Tempered 200^0C	1.421	$1.57\text{x}10^4$	$1.62\text{x}10^2$	$5.10\text{x}10^{-4}$	0.81	$5.96\text{x}10^{-5}$	0.92	$1.21\text{x}10^{-3}$
Tempered 300^0C	1.501	$2.92\text{x}10^2$	$8.57\text{x}10^1$	$6.62\text{x}10^{-4}$	0.78	$1.39\text{x}10^{-4}$	0.84	$6.67\text{x}10^{-3}$
Tempered 400^0C	1.409	$5.59\text{x}10^4$	$1.41\text{x}10^3$	$2.78\text{x}10^{-4}$	0.87	$3.29\text{x}10^{-5}$	0.95	--
Tempered 500^0C	1.319	$4.43\text{x}10^4$	$2.57\text{x}10^2$	$3.17\text{x}10^{-4}$	0.84	$3.69\text{x}10^{-5}$	0.92	$4.76\text{x}10^{-5}$
Tempered 600^0C	1.454	$3.44\text{x}10^4$	$4.06\text{x}10^2$	$3.6\text{x}10^{-4}$	0.85	$3.50\text{x}10^{-5}$	0.91	$3.3\text{x}10^{-5}$

Capacitive element is used for the uniform or ideal film but in most of the films formation, the layer is heterogeneous or non-ideal due to the surface roughness and that's why capacitive element is replaced with the CPE to get best fit. So one CPE_{dl} is used parallel to charge transfer resistance and second CPE_f is used parallel to the film passive film resistance. Warburg element (W) was used for the diffusion mechanism.

It can be seen that the charge transfer resistance (R_{ct}) and film resistance of the sample tempered at 400^0C were the highest and found to be $5.59x10^4$ (Ωcm^2) and $1.41 x10^3$ (Ωcm^2), respectively. Fig. 5.25 depicts the simulated model representing the physical state of metal-layer and film-electrolyte interface with the superimposed equivalent circuit.

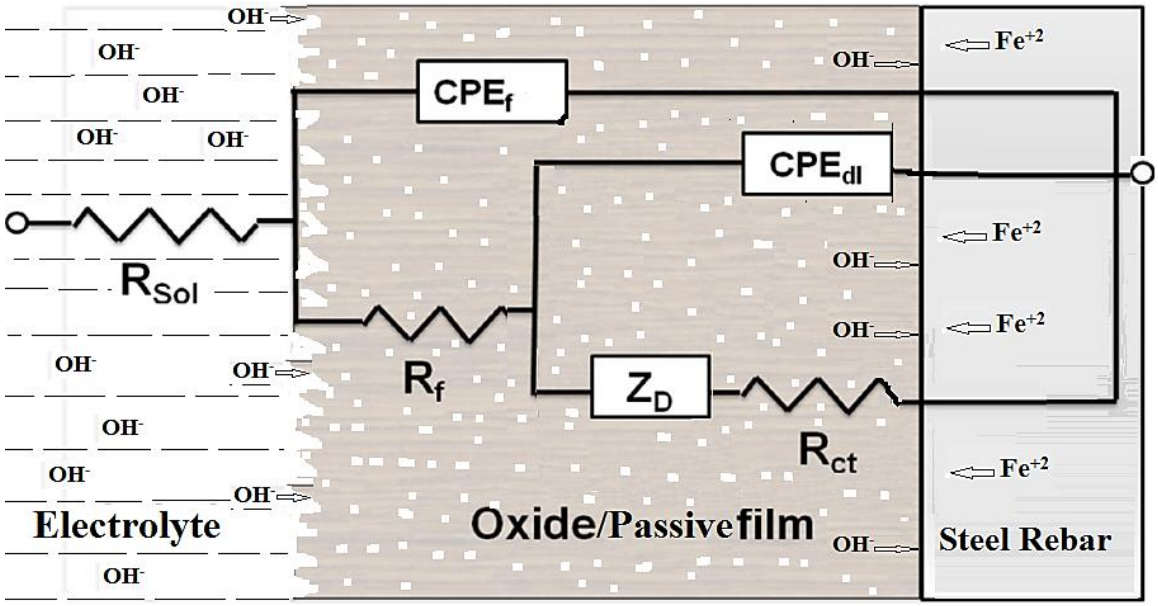

Figure 5.25: Proposed model representing the physical nature of metal-layer and film-electrolyte interfaces by superimposing the equivalent circuit model A.

On the other side, except 400^0C, other equivalent circuit used for different tempering temperatures i.e. as-quenched, 200^0C, 500^0C and 600^0C samples were under diffusion mechanism at lower frequency. This represents that, at lower frequency, chargers are still being transferred across the double layer. It can also be observed that, with the increase of tempering temperature, both film resistance and charge transfer resistance started to decrease.

5.4.1.3. Testing in Alkaline Solution + 0.8M NaCl

In the previous section, electrochemical impedance spectroscopy (EIS) was used for measurement in alkaline solution free of chlorides. However, in true concrete environment, chlorides are always present as they come with the sand which is a necessary constituent for making the concrete mixture.

Chlorides were introduced in the alkaline solution by adding sodium chloride (NaCl) in the test solution. The concentration of sodium chloride was used 0.8M/lit to ensure the ratio of $[(Cl^-)/(OH^-)]$ to1[76-77].

The EIS experiment was conducted by using the same parameter i.e. from 30 kHz to 10 mHz frequency of the applied volt which was set to 10mV. The obtained EIS graphs of different samples are shown in Fig 5.26.

The Nyquist plot shows that the trend of the tested samples with the addition of chlorides in the alkaline solution is very similar with the trend of those samples which were tested in alkaline solution. Nevertheless, it can be seen that, even with the presence chlorides in the test solution, 400^0C is still the leading sample with highest impedance followed by 500^0C and 600^0C tempering temperature.

Bode plot (Fig.5.27) also agrees with the Nyquist plot and again it is cleare that the highest impedance was shown by tempered 400^0C rebar sample followed by 500^0C and 600^0C tempering temperature. Bode plot in Fig. 5.28 shows the phase shift with change of frequency.

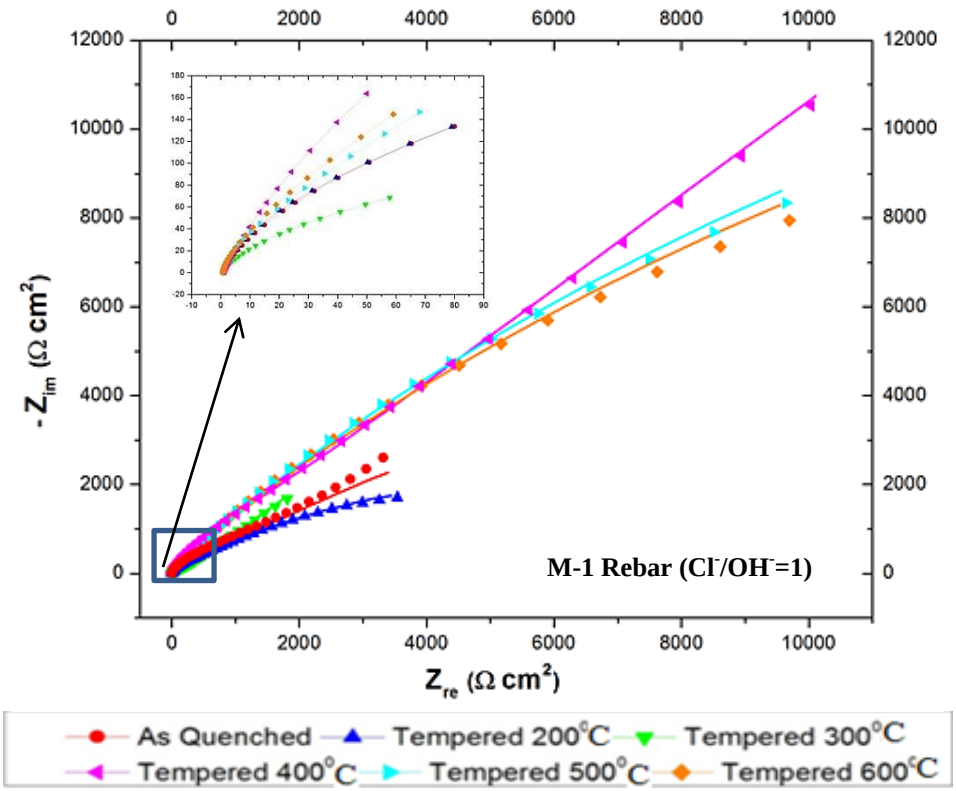

Figure 5.26: Nyquist plot of M-1 Rebar tempered at different temperatures in alkaline+0.8M NaCl solution

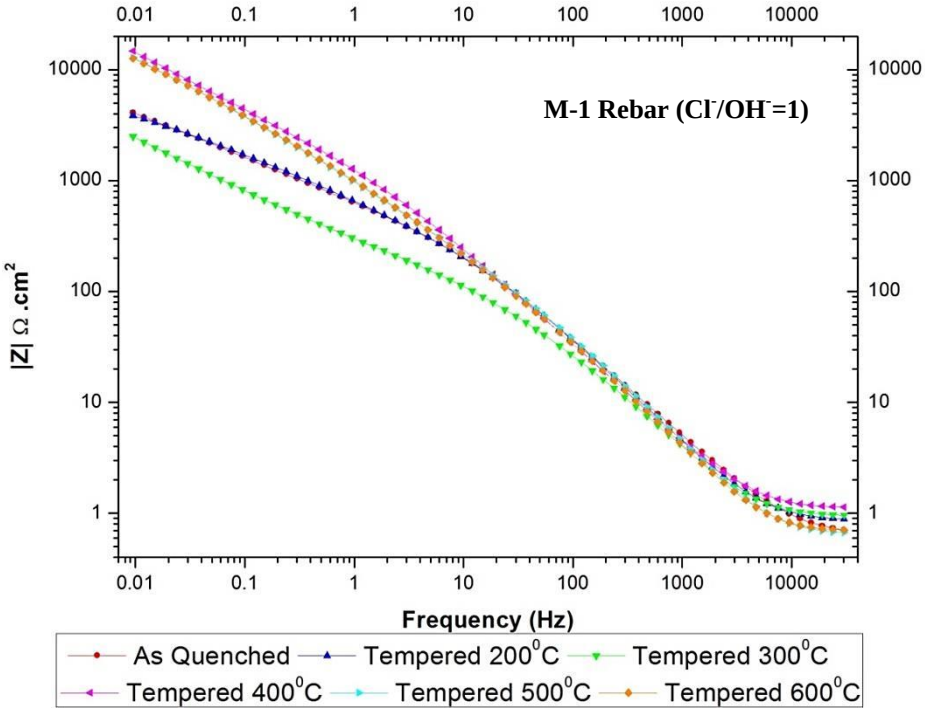

Figure 5.27: Bode Plot of M-1 rebar tempered at different temperatures in alkaline+0.8M NaCl Solution

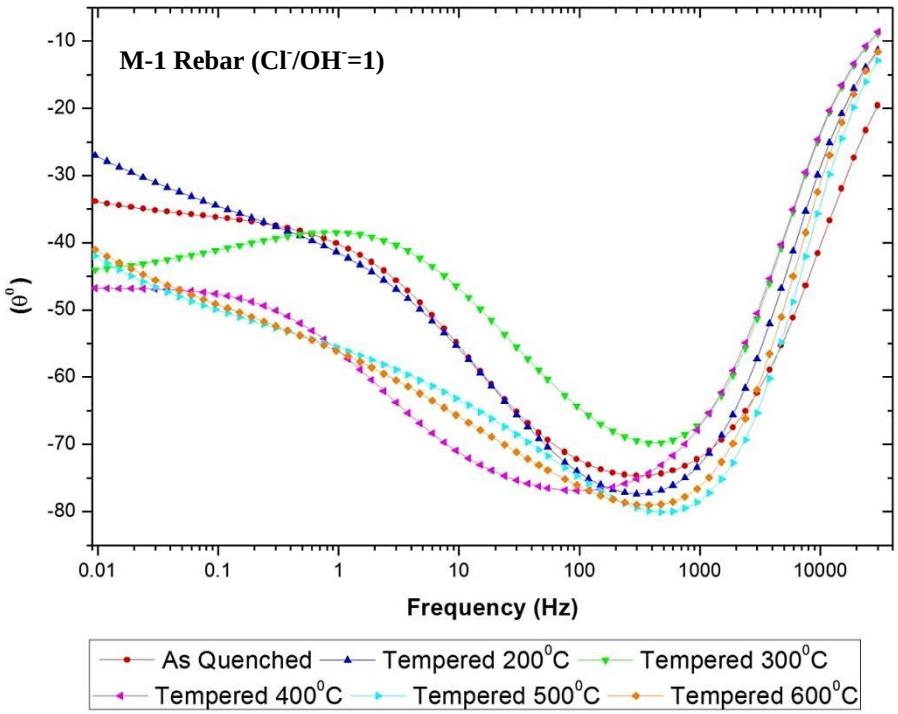

Figure 5.28: Bode plot representing phase shift of M-1 rebar tempered at different temperatures in alkaline + 0.8M NaCl solution

5.4.1.4. Equivalent Circuit Model Fitting

Table 5.5 shows the EIS parameters obtained after fitting the experimental data on the proposed equivalent circuit provided in Fig.5.23**.** Type of equivalent circuit used against each tempering temperature is provided in Table 5.3.

It is clear from the parameters extracted by fitting the data on equivalent circuit that, under the presence of chlorides, the charge transfer resistance and film resistance of the tempered steel rebar were reduced remarkably. Though, the charge transfer resistance and film resistance of the tempered 400^0C steel rebar are still better compared to the rebars tempered at other temperatures, but, overall decrease in film resistance and charge transfer resistance was observed. The passive film may damage by chlorides and hence its efficiency to protect the surface of the metal is reduced.

Table 5.5: EIS parameters obtained after fitting data on equivalent circuit for M-1 Rebar in alkaline + 0.8M NaCl solution

Specimen	R_s ($\Omega.cm^2$)	R_{ct} ($\Omega.cm^2$)	R_f ($\Omega.cm^2$)	CPE_{dl} ($S.s^n/cm^2$)	n_{dl}	CPE_f ($S.s^n/cm^2$)	n_f	W ($S.s^{1/2}$)
As-Quenched	0.62	$8.42x10^3$	$1.15x10^2$	$7.04x10^{-4}$	0.83	$8.72x10^{-5}$	0.92	$8.85x10^{-3}$
Tempered 200^0C	0.85	$1.55x10^3$	$1.10x10^2$	$7.46x10^{-4}$	0.81	$8.79x10^{-5}$	0.91	$3.77x10^{-3}$
Tempered 300^0C	0.90	$8.61x10^1$	4.5410^1	$7.84x10^{-4}$	0.82	$2.39x10^{-4}$	0.81	$8.67x10^{-3}$
Tempered 400^0C	0.70	$1.785x10^4$	$6.55x10^2$	$5.43x10^{-4}$	0.83	$5.68x10^{-5}$	0.93	$2.47x10^{-4}$
Tempered 500^0C	0.65	$6.29x10^3$	$5.57x10^1$	$6.15x10^{-4}$	0.80	$6.54x10^{-5}$	0.96	$5.39x10^{-4}$
Tempered 600^0C	0.69	$6.35x10^3$	$3.53x10^1$	$6.03x10^{-4}$	0.81	$6.98x10^{-5}$	0.94	$4.2x10^{-4}$

5.4.2. Electrochemical Impedance Spectroscopy (EIS) for M-2

5.4.2.1. Testing in Alkaline Solution

EIS experiments were conducted on heat treated steel rebars, i.e. on as-quenched and tempered at 200^0C, 300^0C, 400^0C, 500^0C and 600^0C in alkaline solution. The obtained EIS spectra are shown in Nyquist plot (Fig.5.29).

Bode plot (Fig. 5.30) is in agreement with the Nyquist plot, and it can be seen that 400^0C is the tempering temperature over which most promising electrochemical properties were achieved followed by 200^0C tempered rebar. However, it can be observed that, with the presence of copper as an alloying element, higher tempering temperatures i.e. 500^0C and 600^0C provided lower impedances than tempered 400^0C and 200^0C. It can be said that higher tempering temperature is found detrimental if tested in pure alkaline solution of high pH.

Bode plot in Fig.5.31 represents the change of phase shift with the frequency.

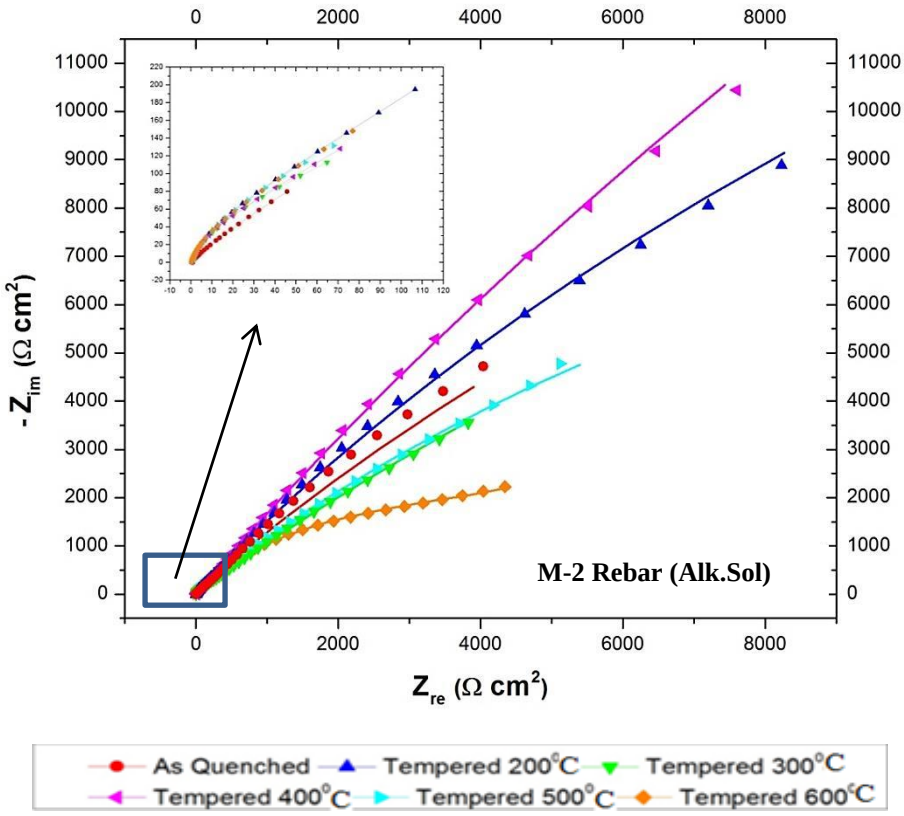

Figure 5.29: Nyquist plot of M-2 rebar tempered at different temperatures in alkaline solution

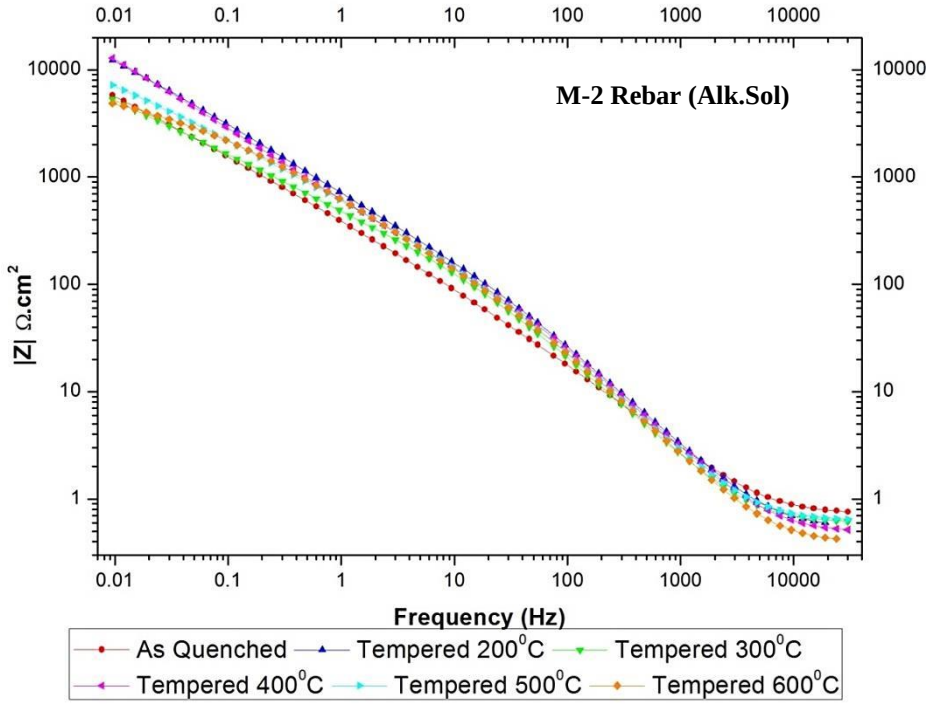

Figure 5.30: Bode plot of M-2 rebar tempered at different temperatures in alkaline solution

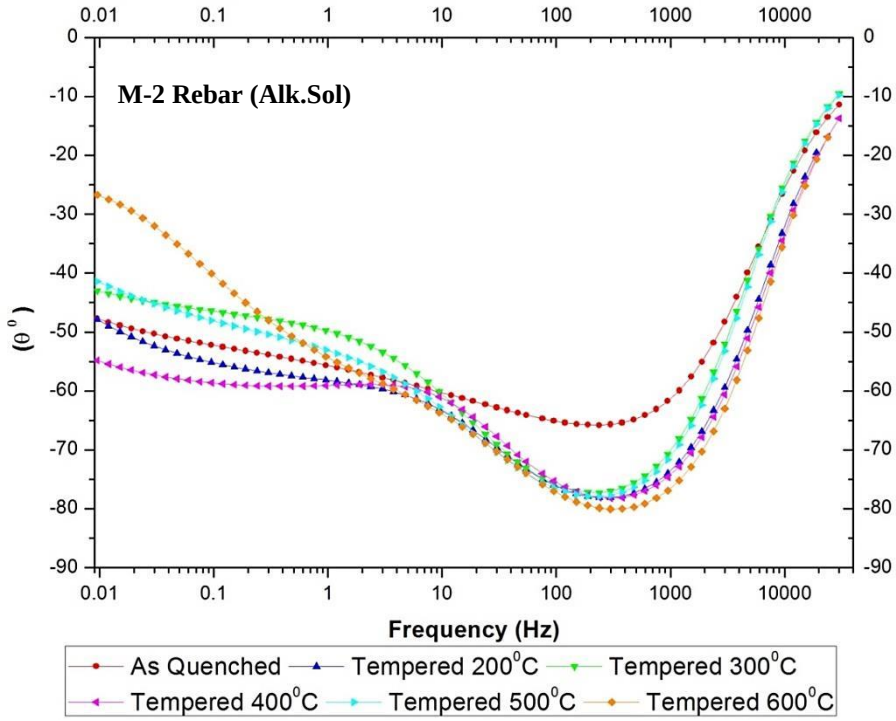

Figure 5.31: Bode plot representing phase shift of M-2 rebar tempered at different temperatures in alkaline solution

5.4.2.2. Equivalent Circuit Model Fitting

The proposed equivalent circuits are presented in Fig.5.23 and Fig.5.24. The type of equivalent circuit used against each heat treatment is provided in Table 5.6 and the extracted parameters after fitting EIS data on the equivalent circuit models are provided in Table.5.7.

From Table 5.7, it can be seen that for M-2, the charge transfer resistances of all samples are way higher than the rebar in M-1. This increase in charge transfer resistance is attributed to the presence of copper in the steel rebar. It is worth noting that even tempered 300^0C steel rebar which has provided lowest charge transfer resistance in M-2 (5.77×10^4 Ω.cm^2) is still competing the charge transfer resistance of the best standing tempered 400^0C steel rebar from M-1 which provided R_{ct} of 1.64×10^5 Ω.cm^2. Tempered

400^0C sample provided the highest charge transfer resistance which is noted to be 1.64 $x10^5$ $\Omega.cm^2$ followed by tempered 200^0C rebar (7.35 $x10^4$ $\Omega.cm^2$).

Table 5.6: Types of equivalent circuits used against each tempering temperature condition for M-2 rebar

Alkaline Solution		**Alkaline Solution + 0.8M NaCl**	
Heat Treatment	**Model Type**	**Heat Treatment**	**Model Type**
As-Quenched	B	As-Quenched	B
Tempered 200^0C	B	Tempered 200^0C	B
Tempered 300^0C	B	Tempered 300^0C	B
Tempered 400^0C	B	Tempered 400^0C	A
Tempered 500^0C	B	Tempered 500^0C	A
Tempered 600^0C	A	Tempered 600^0C	B

Table 5.7: EIS parameters obtained after fitting data on equivalent circuit for M-2 rebar in alkaline solution

Specimen	**R_s ($\Omega.cm^2$)**	**R_{ct} ($\Omega.cm^2$)**	**R_f ($\Omega.cm^2$)**	**CPE_{dl} ($S.s^n/cm^2$)**	**n_{dl}**	**CPE_f ($S.s^n/cm^2$)**	**n_f**	**W ($S.s^{1/2}$)**
As-Quenched	1.6	$5.94x10^4$	$2.17x10^2$	$6.39x10^{-4}$	0.83	$7.76x10^{-5}$	0.93	---
Tempered 200^0C	1.5	$7.35x10^4$	$1.69x10^2$	$5.66x10^{-4}$	0.81	$7.87x10^{-5}$	0.91	---
Tempered 300^0C	1.7	$5.77x10^4$	$1.27x10^2$	$6.57x10^{-4}$	0.80	$7.98x10^{-5}$	0.92	---
Tempered 400^0C	1.5	$1.64x10^5$	$1.48x10^2$	$4.08x10^{-5}$	0.94	$7.75x10^{-5}$	0.94	---
Tempered 500^0C	1.4	$4.14x10^4$	$1.37x10^2$	$7.28x10^{-4}$	0.84	$7.81x10^{-5}$	0.95	---
Tempered 600^0C	1.6	$3.64x10^4$	$1.08x10^2$	$7.77x10^{-4}$	0.82	$8.0x10^{-5}$	0.93	$2.14x10^{-3}$

Compared to M-1, film resistance is noted to be reduced on all tempering temperatures in M-2 rebar. Highest film resistance of 1.48 $x10^2$ $\Omega.cm^2$ is noted against

400^0C tempering temperature which is ten times less than M-1 rebar ($1.41x10^3$ $\Omega.cm^2$) at the same tempering temperature.

5.4.2.3. Testing in Alkaline Sol. + 0.8M NaCl

For steel rebar M-2, EIS was conducted by adding 0.8M NaCl in the alkaline solution and the spectra obtained are provided in Fig.5.32.

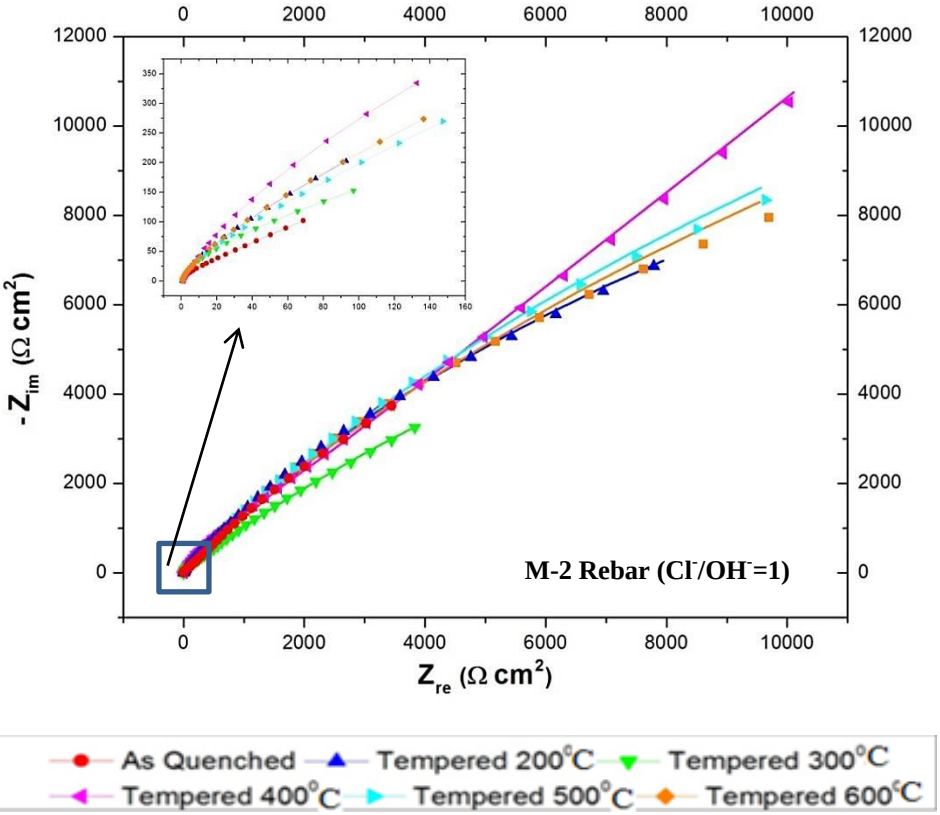

Figure 5.32: Nyquist plot of M-2 rebar tempered at different temperatures in alkaline + 0.8M NaCl solution

Nyquist plot (Fig.5.32) and Bode plot (Fig.5.33) are in agreement with each other and explain that impedance is improved of higher tempered temperature steel rebars under the presence of chlorides. For instance, the impedance value increased for tempered 400^0C, 500^0C and 600^0C under chlorides presence compared to environment

when they were tested in pure alkaline solution (free chloride solution). However, the impedance of as-quenched 200^0C and 300^0C tempered samples remained unchanged. Tempered 400^0C is still the leading sample in term of impedance.

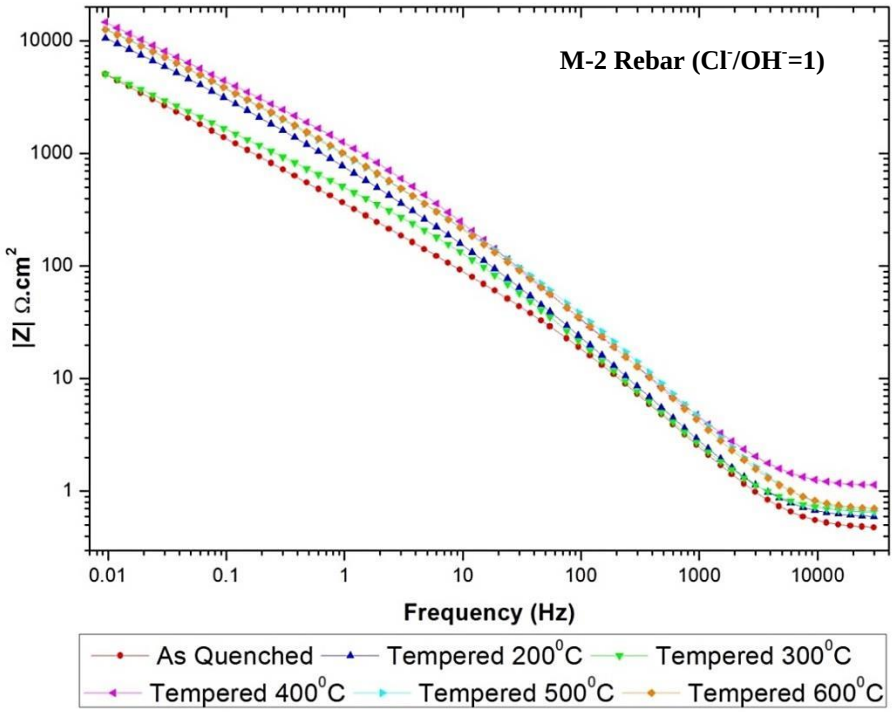

Figure 5.33: Bode plot of M-2 rebar tempered at different temperatures in alkaline solution + 0.8M NaCl

5.4.2.4. Equivalent Circuit Model Fitting

After fitting the data obtained by EIS experiments on equivalent circuit, it can be seen that the EIS parameters obtained after adding NaCl in concrete simulated solution changed as compared to the parameters obtained in the absence of NaCl. It is clear from Table 5.8 that the charge transfer resistance decreased under the presence of chlorides for all sample and the film resistance improved for every tempered sample (except as-quenced) under the same environment.

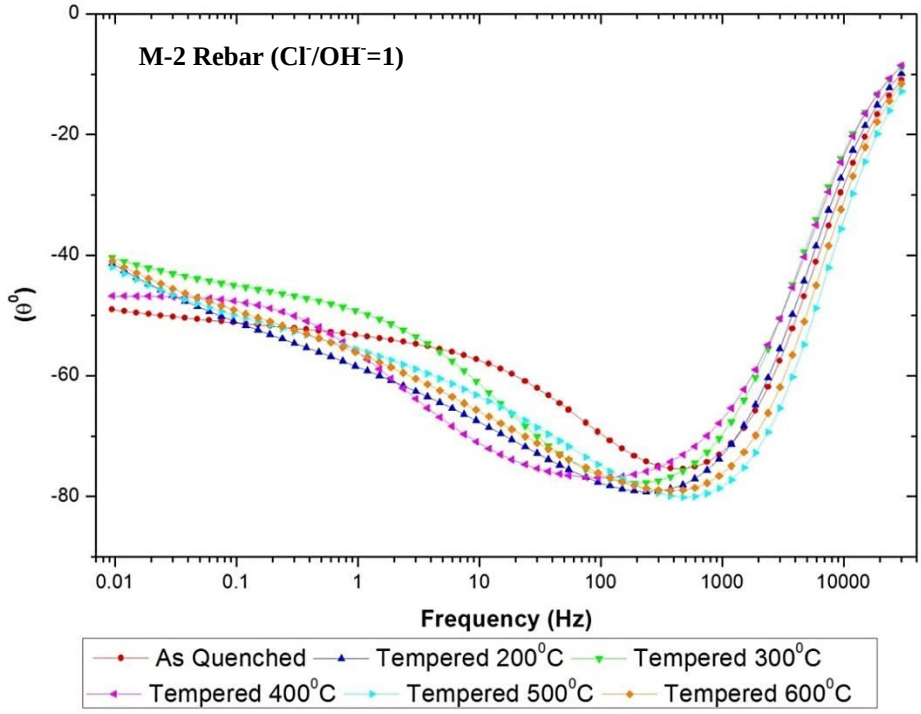

Figure 5.34: Bode plot representing phase shift of M-2 rebar tempered at different temperatures in alkaline + 0.8M NaCl solution

The EIS parameters obtained from Table 5.8 revealed that chlorides played an adverse role when they were introduced in the alkaline solution for carbon steel alloyed with 0.2% copper. Charge transfer resistance is reduced due to chloride ingression and, as a result, freely moved Fe^{+2} ions migrate towards metal-film interface. These migrated Fe^{+2} ions participate in film transformation mechanism and might be the cause of increased passive film resistance. So, it can be assumed that reduced charge transfer resistance in copper alloyed steel under the chlorides attack might be assisting to improve passive film resistance.

Table 5.8: EIS parameters obtained after fitting data on equivalent circuit for M-2 rebar in alkaline + 0.8M NaCl solution

Specimen	R_s ($\Omega.cm^2$)	R_{ct} ($\Omega.cm^2$)	R_f ($\Omega.cm^2$)	CPE_{dl} ($S.s^n/cm^2$)	n_{dl}	CPE_f ($S.s^n/cm^2$)	n_f	W ($S.s^{1/2}$)
As-Quenched	0.46	$1.32x10^4$	$3.56x10^1$	$8.99x10^{-4}$	0.83	$6.99x10^{-5}$	0.93	---
Tempered 200^0C	0.58	$4.10x10^4$	$1.89x10^2$	$6.57x10^{-4}$	0.80	$8.18x10^{-5}$	0.94	---
Tempered 300^0C	0.63	$3.81x10^4$	$1.35x10^2$	$7.24x10^{-4}$	0.84	$4.78x10^{-4}$	0.91	---
Tempered 400^0C	0.41	$9.89x10^4$	$6.40x10^2$	$6.19x10^{-5}$	0.94	$5.81x10^{-5}$	0.96	$2.48x10^{-4}$
Tempered 500^0C	0.65	$2.35x10^4$	$5.58x10^2$	$7.55x10^{-4}$	0.81	$5.39x10^{-5}$	0.90	$5.39x10^{-1}$
Tempered 600^0C	0.68	$1.29x10^4$	$4.53x10^2$	$8.03x10^{-4}$	0.83	$4.06x10^{-5}$	0.92	---

5.4.3. Linear Polarization Resistance

5.4.3.1. Linear Polarization Resistance of M-1

The linear polarization resistance (LPR) was conducted for M-1 in a pure concrete simulated solution free of chloride. The corrosion rates are shown in Table 5.9 and graphically can be seen in Fig.5.35

It can be observed that when there was no corrosive media in the test electrolyte then corrosion rate was noted to be low. The lowest corrosion rate was found for tempered 400^0C tempered rebar with a value of 0.5 mpy and the highest rate was for the tempered 300^0C with 2.8 mpy. However, with the addition of chlorides, the corrosion rate increased notably.

Table 5.9: LPR corrosion rates of M-1 steel rebar tempered at different temperatures with and without chlorides in alkaline test solution

Specimen	Alk. Sol		Alk. Sol. +0.8M NaCl	
	Polarization Resistance (Rp) ($K\Omega.cm^2$)	Corrosion Rate (mpy)	Polarization Resistance (Rp) ($K\Omega.cm^2$)	Corrosion Rate (mpy)
As Quenched	5.1	1.3	4.5	1.8
Tempered 200^0C	6.5	1.0	5.3	1.4
Tempered 300^0C	2.4	2.8	1.9	3.3
Tempered 400^0C	10.5	0.5	9	0.8
Tempered 500^0C	10	0.8	8.5	1.1
Tempered 600^0C	8.7	0.9	7.6	1.2

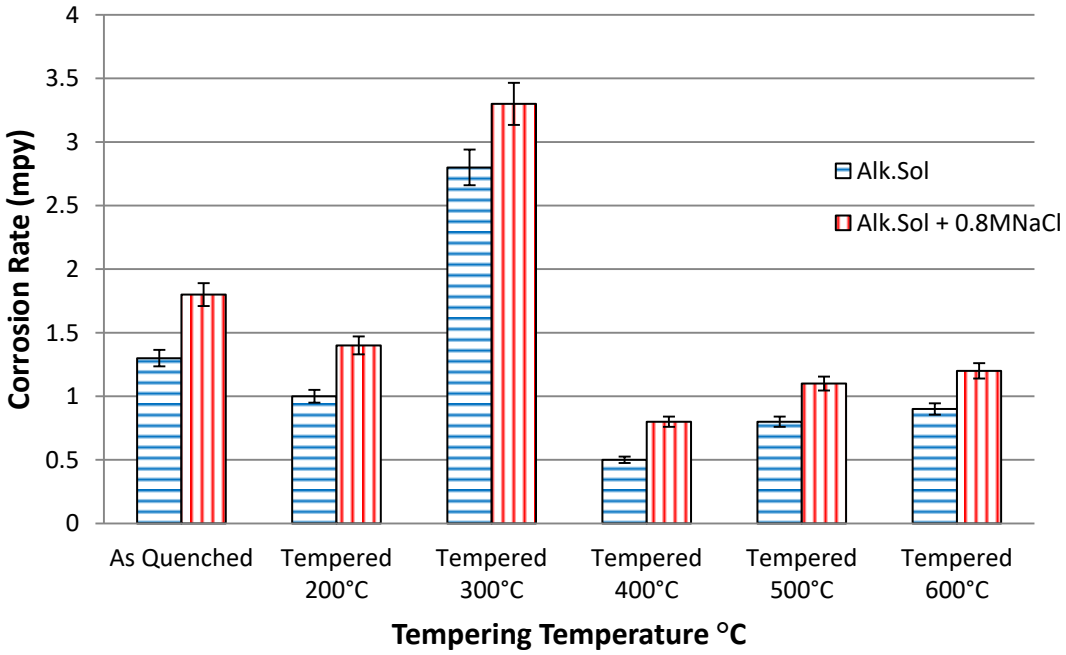

Figure 5.35: Effect of tempering on corrosion rate in steel rebar M-1

Moreover, if we compare the corrosion rate of M-1rebar, obtained by LPR, with the charge transfer resistance (R_{ct}) of M-1 then it becomes clear that both are consistent. For instance, tempered 400^0C provided the highest R_{ct} with and without the presence of chlorides and tempered 300^0C was on the lowest side with poor charge transfer resistance. Similarly, for the same steel rebar, tempered 400^0C and tempered 300^0C are the best and worst, respectively, in term of corrosion rate (obtained by LPR) with and without the presence of corrosive media.

5.4.3.2. Linear Polarization Resistance of M-2

Corrosion rates measured by LPR for the different tempered rebar in M-2 can be seen in Table 5.10 and Figure 5.36. It can be seen through the table that the corrosion rate was low when the test experiment was conducted in just concrete simulated solution. The lowest corrosion rate was noted again at 400^0C tempered sample and again the worst corrosion rate was found to be for 300^0C tempered sample.

Table 5.10: LPR corrosion rate of M-2 steel rebar tempered at different temperatures with and without chlorides in alkaline test solution

Specimen	Alk. Sol		Alk. Sol. +0.8M NaCl	
	Polarization Resistance (Rp) (KΩ)	Corrosion Rate (mpy)	Polarization Resistance (Rp) (KΩ)	Corrosion Rate (mpy)
As Quenched	8.9	0.7	7.0	0.9
Tempered 200^0C	16.6	0.4	12.9	0.6
Tempered 300^0C	7.3	1.1	6.26	1.6
Tempered 400^0C	19.2	0.3	13.9	0.5
Tempered 500^0C	9.7	0.7	12.8	0.6
Tempered 600^0C	6.2	1	11.9	0.8

However, when 0.8M NaCl solution was added in the alkaline solution, the corrosion rate increased slightly. It is obvious that M-2 rebar provided the lower corrosion rate at the optimized tempering temperature, i.e. at 400^0C, compared to the rebar M-1 at the same tempering temperature. This is already explained from EIS parameters and can be attributed due to the higher charge transfer resistance.

However, at higher tempering temperature, i.e. 500^0C and 600^0C, it can be seen that pure alkaline solution of very high pH was found detrimental by providing higher corrosion rate compared to the environment when 0.8M NaCl was added in the test solution. It can be seen in Table 5.10 that under the presence of chlorides, the polarization resistance (R_p) increased and the corrosion rate reduced for both of the discussed tempering temperature. This behavior of the material at higher tempering temperature agrees with the EIS parameters where film resistance (R_f) was noted to be improved at the expense of charge transfer resistance (R_{ct}) with the addition of chlorides and the reason already has been defined in EIS discussion. Fig. 5.37 provides the comparison of corrosion rate for both steel rebar M-1 and M-2.

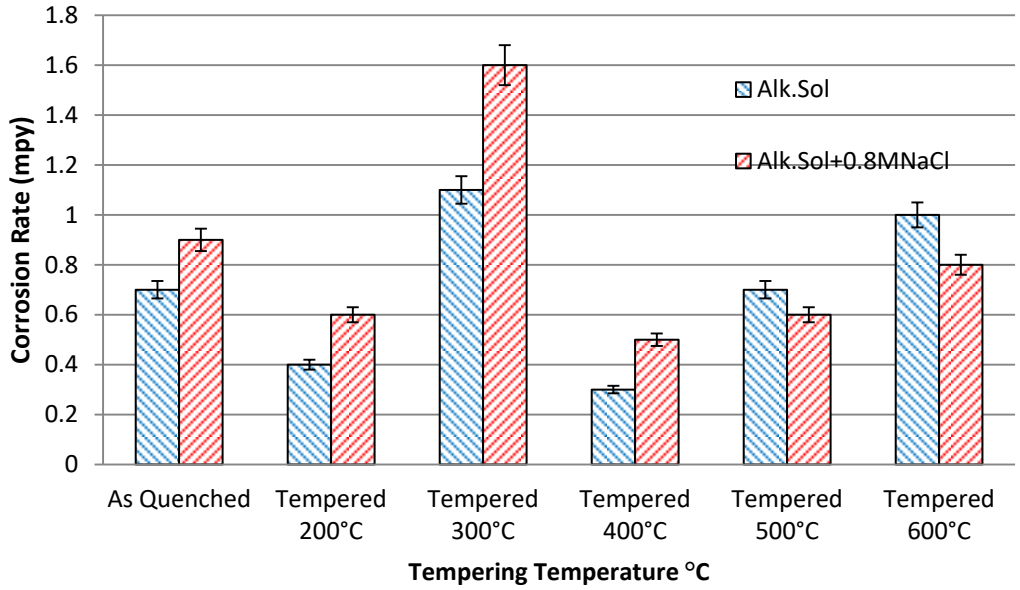

Figure 5.36: Effect of tempering on LPR corrosion rates in M-2 steel rebar

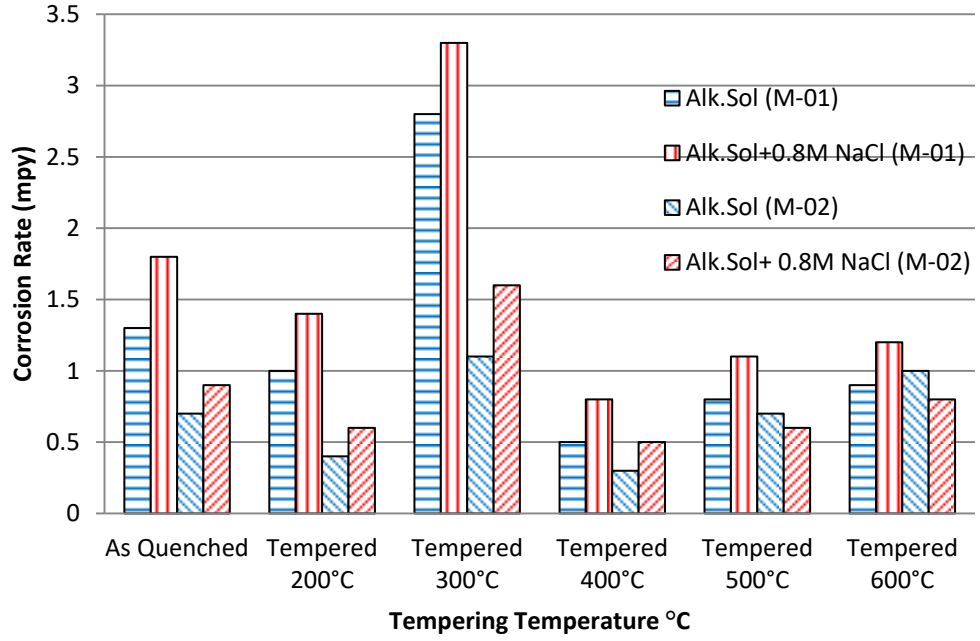

Figure 5.37: Comparison of LPR corrosion rates with the change of tempering temperature in rebar M-1 and M-2

5.4.4. Potentiodynamic Polarization (PDP) for M-1

5.4.4.1. Testing in Alkaline Solution

Potentiodynamic polarization (PDP) tests were conducted firstly for the M-1 in alkaline solution representing true concrete mixture. PDP graphs obtained at different temperatures are shown in Fig.5.38.

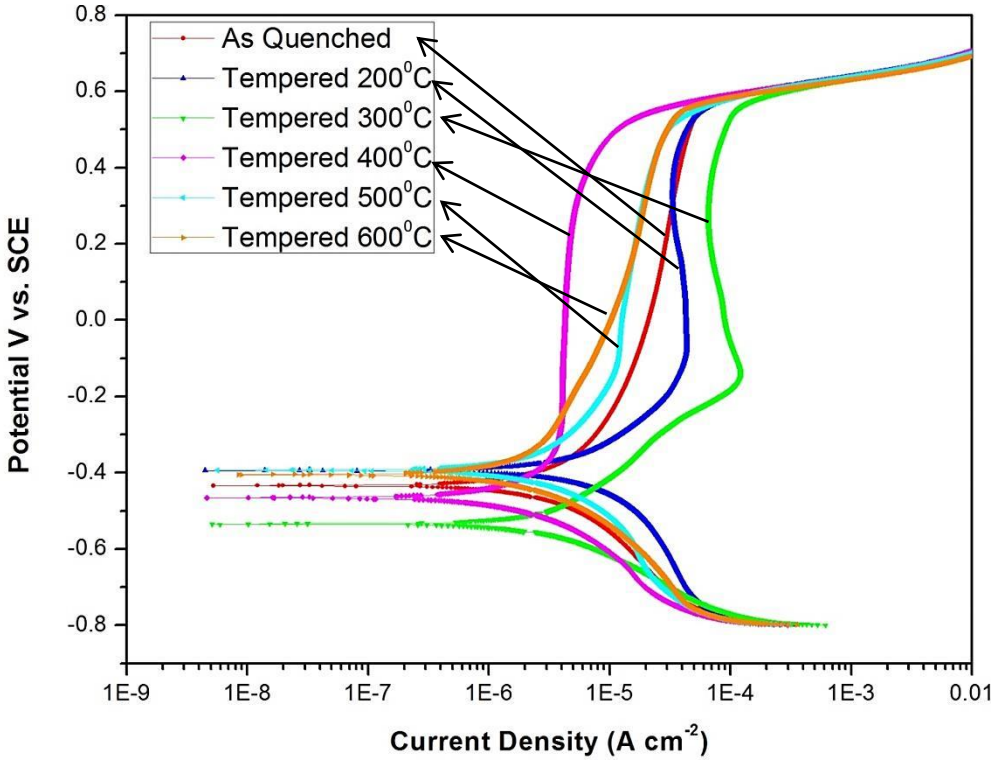

Figure 5.38: Potentiodynamic polarization (PDP) of M-1 rebar tempered at different temperatures in alkaline solution

It can be seen through the PDP graphs that tempered 400^0C rebar provided lowest passive film current density with a constant resistance to depassivation for over a long range of change in the potential. For example, the passive film current density (i_{pass}) noted $4x10^{-6}A/cm^2$ and it remained constant for the change of potential (V_{SCE}) range from -0.48V to 0.4V. However, upward to that potential, de-passivation started to occur with the active transition.

It can be seen in Fig. 5.38 that different tempering temperatures on rebar M-1 did not alter the pitting potential and pitting started when potential was increased to 0.5V.

For as-quenched and tempered 600^0C, it can be seen that they did not provide the passive film with a constant resisting nature and, in fact, they were quite active. On the other side, tempered 500^0C acted actively in the start but it started to passivate itself when potential (V_{SCE}) reached to -0.1 but, unlike 400^0C, the current density (i_{pass}) of the passive film was noted higher and varied with the applied potential. Tempered 200^0C and 300^0C samples were also linear in the start but they started to achieve the re-passivation after crossing $-0.2V_{SCE}$ at very high current density. However, it can be seen that pitting started at all tempering temperatures once the voltage exceeded beyond $0.5V_{SCE}$.

If we compare the obtained EIS parameters with the PDP, then it is in agreement that tempered 400^0C sample provided lowest corrosion rate with highest passive film resistance.

5.4.4.2. Testing in Alkaline Solution + 0.8M NaCl

After the addition of 0.8M NaCl in the alkaline environment, the PDP experiment was again conducted on rebar (M-1) and it can be seen in the Fig.5.39 that the presence of chlorides disturbed the passive state of the film and constant current density was not observed at any tempering temperature. Though, every tempered sample maintained its trend just like the same way as it was achieved in chlorides free environment, but the physical state of the film was not stable. It can also be seen that, in the presence of chlorides, the current density of all the samples increased and, for tempered 400^0C rebar, it increased from $4x10^{-6}A/cm^2$ to $6x10^{-6}A/cm^2$.

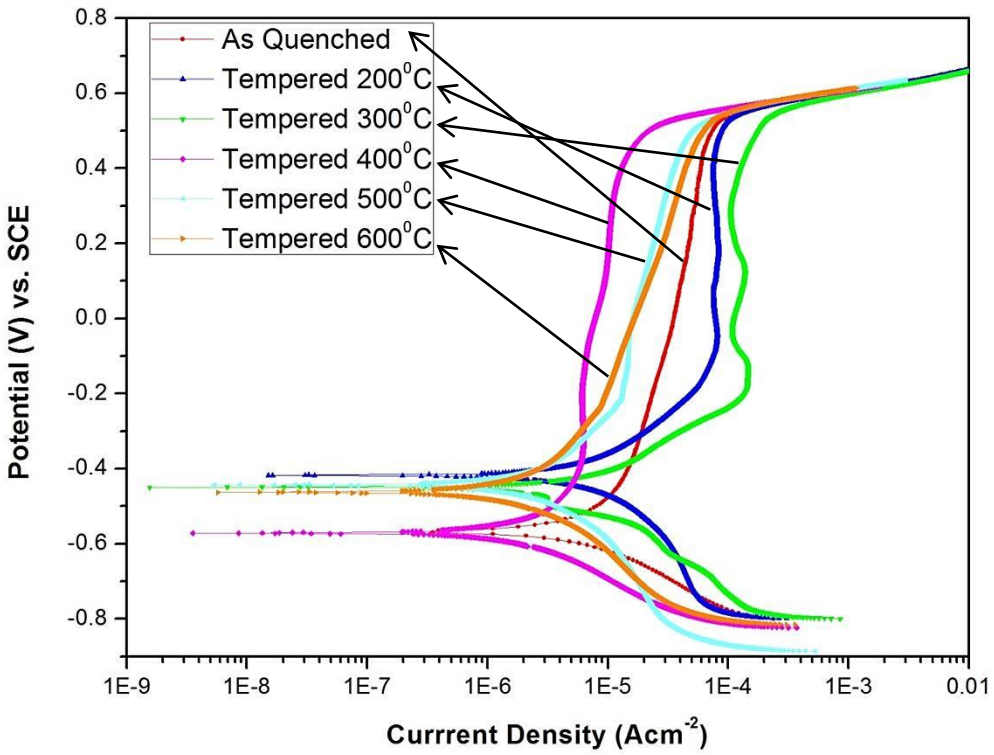

Figure 5.39: Potentiodynamic polarization (PDP) of M-1 rebar tempered at different temperatures in alkaline + 0.8M NaCl solution

5.4.5. Potentiodynamic Polarization (PDP) for M-2

5.4.5.1. Testing in Alkaline Solution

Potentiodynamic polarization (PDP) experiment was also evaluated for rebar M-2 to study the nature of passive film with and without the presence of chlorides.

The test was conducted for M-2 in alkaline solution and the PDP graphs are shown in Fig.5.40. It is clear from the PDP graphs that, though, the tempered 200^{0}C started the passivation at a lower i_{pass} with a current density of $4x10^{-6}$ Acm^{-2} than 400^{0}C tempered rebar ($1x10^{-5}$ Acm^{-2}) but after a very little change of potential, the current density started to increase continuously. On the other side, tempered 400^{0}C was noticed active up to -0.3V but when the potential was increased from -0.3V to -0.2V then it

started to passivate. The constant passive current density ($7x10^{-6}Acm^{-2}$) was achieved when the potential was increased from -0.2V to 0V.

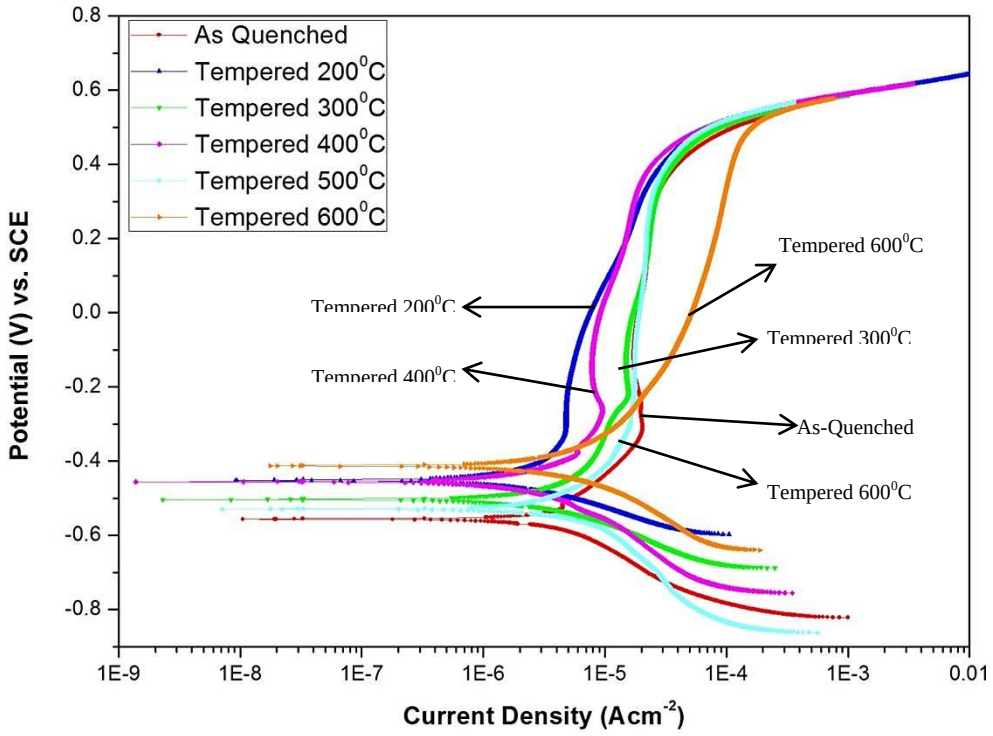

Figure 5.40: Potentiodynamic polarization (PDP) of M-2 rebar tempered at different temperatures in alkaline solution

It is notable that the presence of copper in M-2 rebar did not provide the film formation tendency to that extent as M-1 provided. In addition to 400^0C, as-quenched, tempered 300^0C and tempered 500^0C also provided passivation but their re-passivation was achieved at very high current density. On contrary, tempered 600^0C and 200^0C were lacking the re-passivation tendency and remained active just like the same way as it was observed in rebar free of copper (M-1).

5.4.5.2. Testing in Alkaline Solution + 0.8M NaCl

In order to study the effect of chlorides, 0.8M NaCl solution was added in the alkaline solution. Potentiodynamic polarization (PDP) tests were conducted for the same

range of voltage and the graphs obtained for each tempering temperature are provided in Fig.5.41.

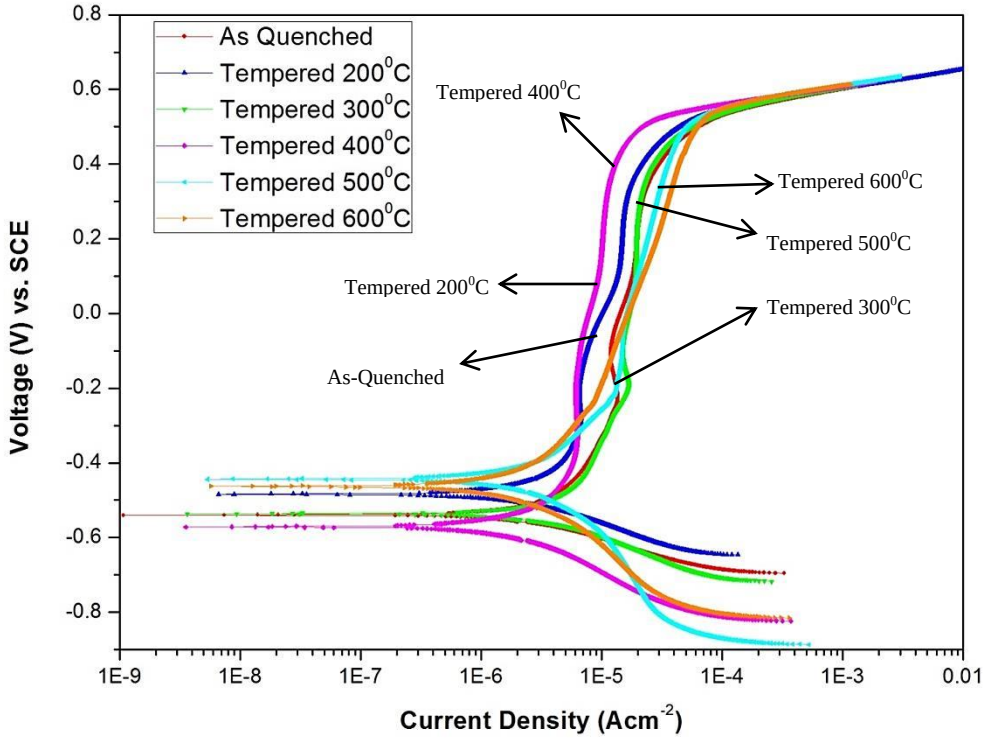

Figure 5.41: Potentiodynamic polarization (PDP) of M-2 rebar tempered at different temperatures in alkaline + 0.8M NaCl solution

It can be seen that the presence of chlorides affected the passive behavior. For example, PDP of tempered 400^{0}C indicates that passive film resistance improved in the presence of chlorides. It can be seen that, from the very start, a constant current density was achieved of 7x10^{-6} Acm^{-2} when the potential was changed from -0.5V to -0.1V. This constant current density in fact represents the passive film resistance for tempered 400^{0}C. But, with the change of potential from -0.1V to 0.1V, the current density increased to 1x10^{-5} Acm^{-2} due to chlorides ingression. However, it regained the constant current density behavior at 1x10^{-5} Acm^{-2} when potential was increased from 0.1V to 0.4V.

However, for all other tempering temperatures samples, no constant current density was achieved for any other temperature against the change of voltage. Instead of getting perpendicular linearity with the change of potential at a constant current density, the trends were found active for tempered 600^0C. Though, as-quenched and tempered 300^0C provided the re-passivation tendency but their i_{pass} was observed very high.

5.5. X-Ray Photoelectron Spectroscopy

X-Ray Photoelectron Spectroscopy (XPS) was used to characterize the nature and chemical composition of the passive film developed on the surface of steel rebar in the concrete simulated mixture for both grades (M-1 and M-2) against the selective tempered temperatures. The XPS spectra of selective samples are shown from Fig.5.42 to Fig.5.48.

5.5.1. XPS for M-1

The de-convolution of the XPS spectra helps us to understand the chemistry of the passive film. The formation of the passive film has already been described in section 5.4.21.2.

From the XPS spectra of tempered 400^0C steel rebar in M-1, it can be seen in Fig. 5.42 that the final film composition is composed of FeO, Fe_3O_4 and γ-Fe_2O_3. Initially, after the formation of $Fe(OH)_2$, the first developed oxide was FeO which, on further oxidation with OH^-, turned into Fe_3O_4. The FeO/Fe_3O_4 transformation is a complex mechanism and, on the final stage, a lamellar oxide layer of FeO/Fe_3O_4 is formed and in detail it can be seen somewhere else [110].

FeO and Fe_3O_4 are defect free oxide layers and that's why their presence as a major constituents increased the overall film resistance of the passive film in tempered 400^0C

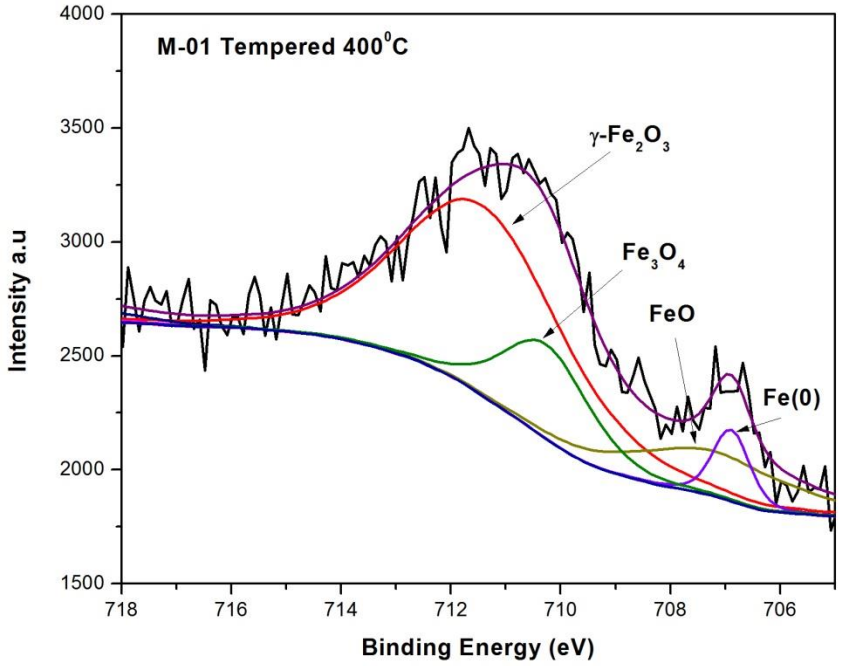

Figure 5.42: XPS spectra representing chemical composition of passive film developed on M-1 rebar tempered at 400^{0}C in alkaline solution

steel rebar. However, when the outer exposed surface of Fe_3O_4 is further oxidized in the presence of OH^- then Fe_2O_3 is formed which is considered a defective oxide layer. Fe_2O_3 has the same spinal structure like Fe_3O_4 and that's why it is also called cation-deficient Fe_3O_4. So the presence of Fe_2O_3 actually compromises the performance of the film resistance and film resistance decreases with the increased number of cation vacancies.

Similarly, from the XPS spectra of tempered 300^{0}C in Fig. 5.43, it can be observed that significant amount of Fe_3O_4 was transformed into α-FeOOH or γ-Fe_2O_3. Both of these transformed oxides (α-FeOOH or γ-Fe_2O_3) reduce the film resistance because of larger number of defects and cation vacancies. So, despite of the formation of multi oxide layer, the poor film resistance (R_f) and higher current density (i_{pass}) in tempered 300^{0}C rebar is most probably due to the larger proportion of these defective oxides layers in the developed passive film. So, these defective oxides layers are directly exposed to the

electrolyte and continuous oxidation with OH^- makes them full of flaws. In addition to these, another reason behind poor film resistance in tempered 300^0C can be because of the multilayer oxide structure. Since the most outer exposed oxide layers are very defective and they are not resisting the OH^- to diffuse, so they increase the susceptibility of oxidation to the inner oxides layer at Fe_2O_3/Fe_3O_4 and Fe_3O_4/FeO interfaces. The results indicates that the presence of FeO and Fe_3O_4 has a remarkable impact in providing most resistant film with higher film resistance (R_f) and lower current density (i_{pass}). Also, the increased ratio of FeOOH to Fe_2O_3 affects the film properties adversely.

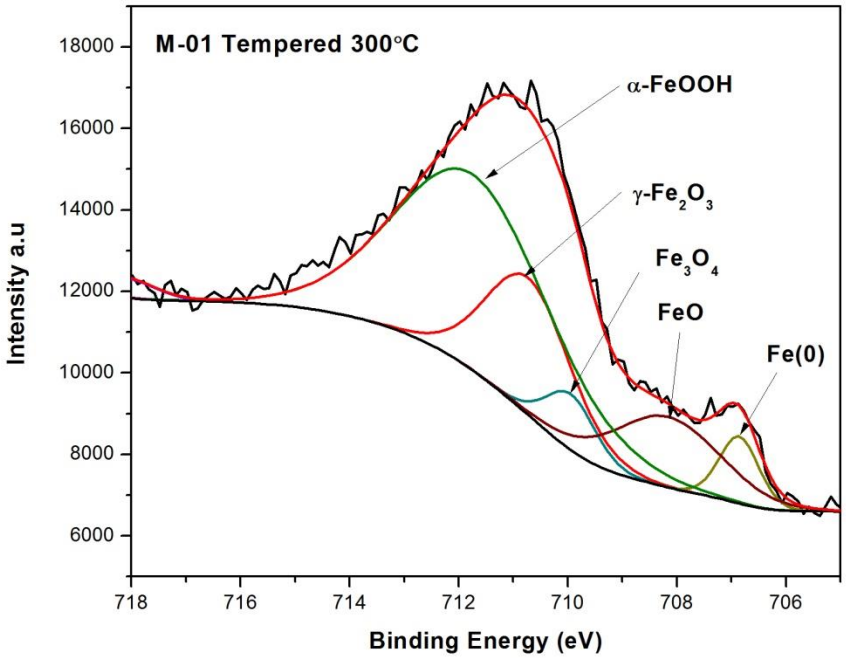

Figure 5.43: XPS spectra representing chemical composition of passive film developed on M-1 rebar tempered at 300^0C in alkaline solution

5.5.2. XPS for M-2

The de-convolution of the XPS spectra reveals the information about the chemistry of the developed passive film on the surface of steel rebar M-2 (0.2%Cu) in concrete simulated environment. The graphs are shown in Fig.5.44-5.47.

It can be seen that for the tempered 400^0C rebar in Fig. 5.44, the oxides layer are composed of α-FeOOH and γ-Fe_2O_3 with the absence of FeO and Fe_3O_4 unlike in M-1 at the same tempering temperature. In other words, both FeO and Fe_3O_4 were fully transformed into α-FeOOH or in γ-Fe_2O_3. It is also visible that the area under the curve of transformed α-FeOOH is very less compared to γ-Fe_2O_3 and hence it reduced the ratio of FeOOH/Fe_2O_3 which has increased the overall resistance of the tempered 400^0C in M-2 since FeOOH is very defective than Fe_2O_3. It was noted while analyzing the EIS spectra that the charge transfer resistance (R_{ct}) increased considerably due to the presence of copper and hence the film resistance (R_f) reduced due to the unavailability of the iron ions for further transformation. That is why, in the start, Fe_3O_4 layer was formed easily because of the availability of iron ions on the surface of the steel. Once this layer was fully transformed to α-FeOOH and γ-Fe_2O_3 because of the oxidation of OH^- ions then, due to the very high charge transfer resistance, material resisted to provide more Fe^{+2} ions to develop new oxide layer of FeO and Fe_3O_4. This is the reason that the passive film formed in the presence of copper had a less film resistance (R_f) and current density (i_{pass}) compared to the material with negligible copper (M-1). So, from the XPS analysis, it can be proposed that, the lower film resistance in M-2 is due to the full transformation of FeO and Fe_3O_4 into α-FeOOH and γ-Fe_2O_3.

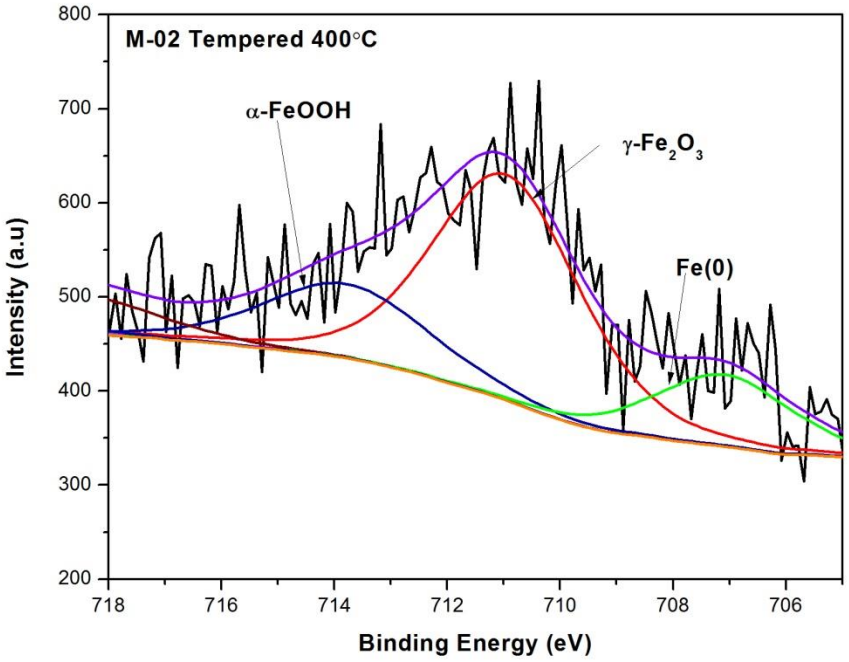

Figure 5.44: XPS spectra representing chemical composition of passive film developed on M-2 rebar tempered at 400^0C in alkaline solution

The de-convolution of XPS spectra for copper oxides, it is cleared in Fig.5.45 that the passive film on copper alloyed carbon steel was free of any oxide of copper.

On the other side, for the tempered 300^0C sample of M-2, it can be seen (Fig.5.46) that again the oxide film composition was a composite of all oxides i.e. FeO, Fe_3O_4, γ-Fe_2O_3 and α-FeOOH just like the same way as it was in M-1at the same tempering temperature. So the film resistance and electrochemical properties were found to be decreased again with the increased ratio of FeOOH/Fe_2O_3. In addition to this, it can be seen that the bare metal representing very high area under the peak Fe(0). It is true clarification that the complete developed oxide layer is very highly defective.

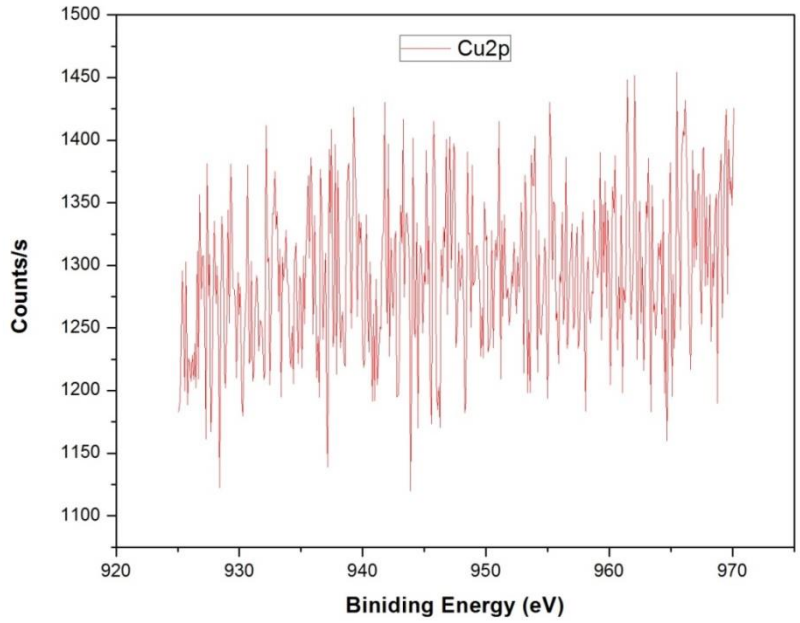

Figure 5.45: XPS spectra representing chemical composition of copper in passive film developed on M-2 rebar tempered at 400^0C in alkaline solution

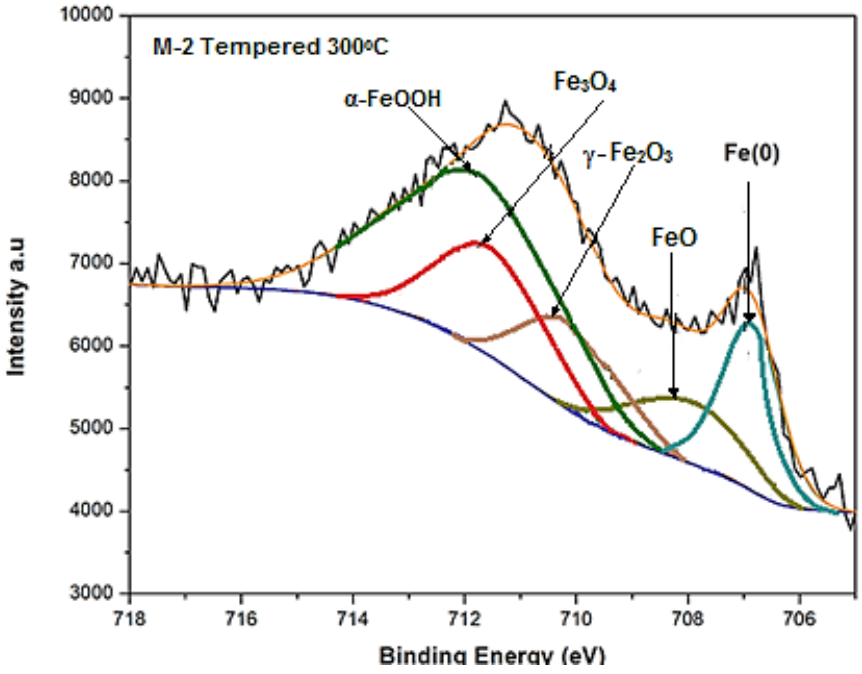

Figure 5.46: XPS spectra representing chemical composition of passive film developed on M-2 rebar tempered at 300^0C in alkaline solution

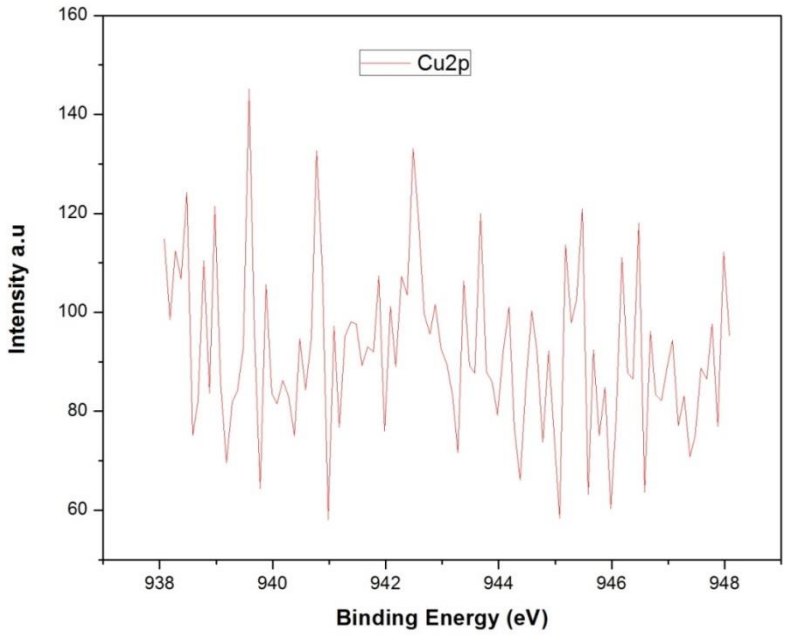

Figure 5.47: XPS spectra representing chemical composition of copper in passive film developed on M-2 rebar tempered at 300^0C in alkaline solution

Again, the de-convoluted spectra of XPS for the passive film presented in Fig.5.47 show that the passive film formed on copper alloyed tempered 300^0C rebar is free of copper oxides.

CHAPTER 6: Discussion

6.1. Effect of Tempering Temperature

Steel rebar develops an oxide layer over its surface when it is introduced in highly alkaline solution of very high pH (>13.5). However, when the steel rebar tempered at different temperatures is introduced in highly alkaline solution then the composition of the passive film seems to be dependent on the underlying microstructure and morphology of the steel rebar. When tempered steel is immersed in alkaline solution, then OH^- ions are adsorbed on highly active regions such as laths interfaces. Generally, in the presence of electrolyte, OH^- ions attack on the interfaces around the martensitic laths [98]. As a result, due to the number of reactions involved (5.1-5.6), OH^- ions start developing the passive oxide film over the surface of steel rebar in alkaline solution.

Tempering does not alter the basic grain boundaries but it changes the morphology of the laths. In addition to morphology, the ferrite recovery is also attributed to the change of tempering temperature. For instance, at 300^0C tempering temperature, little amount of ferrite can be seen in the microstructure (Fig.6.1a). This ferrite formed due to the transformation of austenite during the quenching mechanism. However, when tempering temperature was increased to 400^0C, then recovery of the ferrite was achieved due to the decomposition of martensite and it can be seen in (Fig.6.1b).

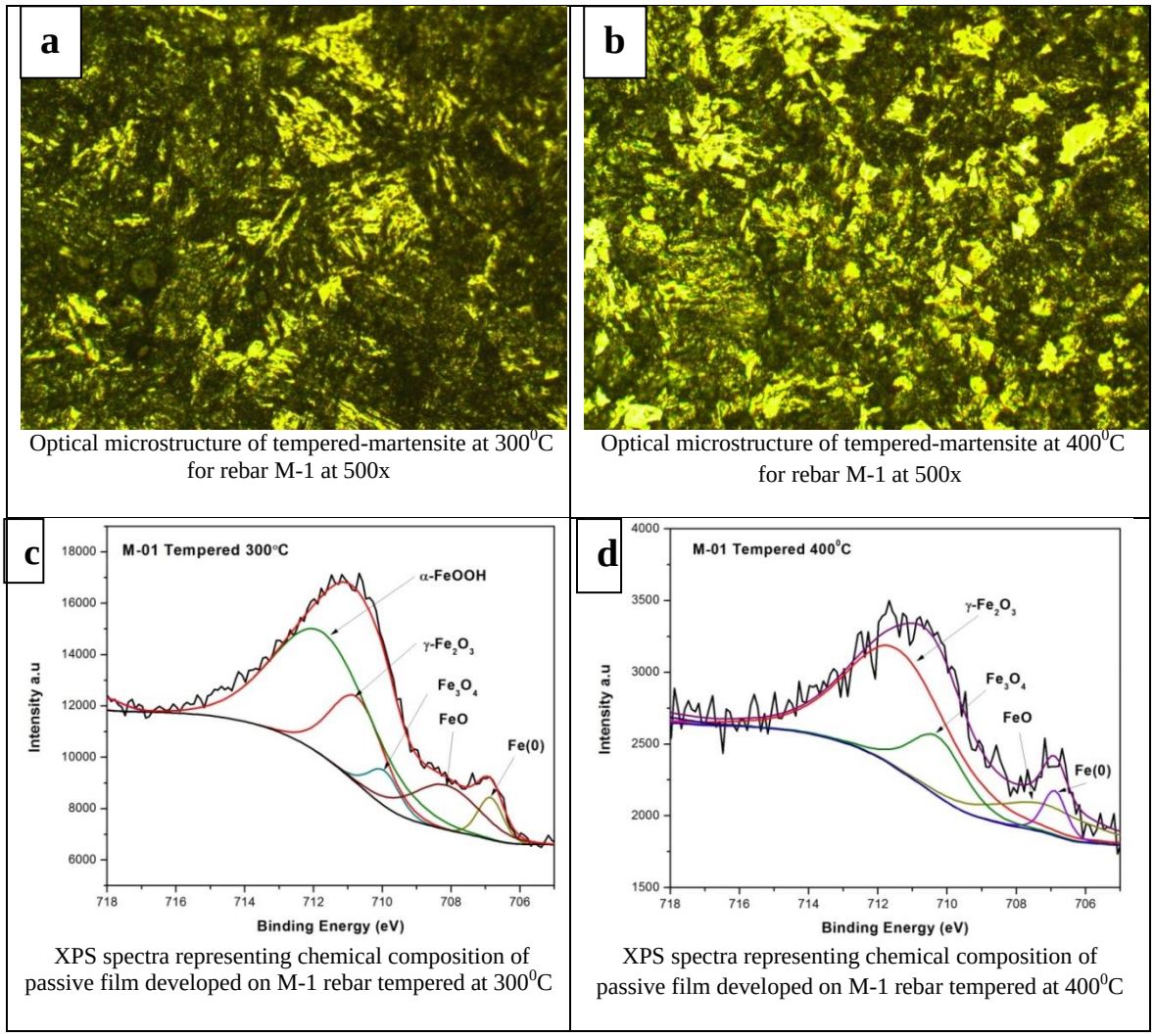

Optical microstructure of tempered-martensite at 300^0C for rebar M-1 at 500x

Optical microstructure of tempered-martensite at 400^0C for rebar M-1 at 500x

XPS spectra representing chemical composition of passive film developed on M-1 rebar tempered at 300^0C

XPS spectra representing chemical composition of passive film developed on M-1 rebar tempered at 400^0C

Figure 6.1: Effect of tempering temperature on the composition of passive film in M-1 rebar

It can be seen in Fig.6.1 (a) and Fig.6.2 (a) that when tempering temperature was set to 300^0C then little ferrite amount was formed and major portion of the structure consisted of tempered martensite matrix. From Fig.6.1 (c) and Fig.6.2 (c), it can be seen that, at 300^0C tempering temperature, the passive film chemistry developed on rebar surface was a composite oxides i.e. FeO, γ-Fe_2O_3, Fe_3O_4 and α-FeOOH. It reflects that martensite laths matrix providing high surface to volume ratio and, perhaps, larger numbers of lath carbides are, subsequently, providing larger number of anchoring sites for the growth of oxide film at the interfaces [119].

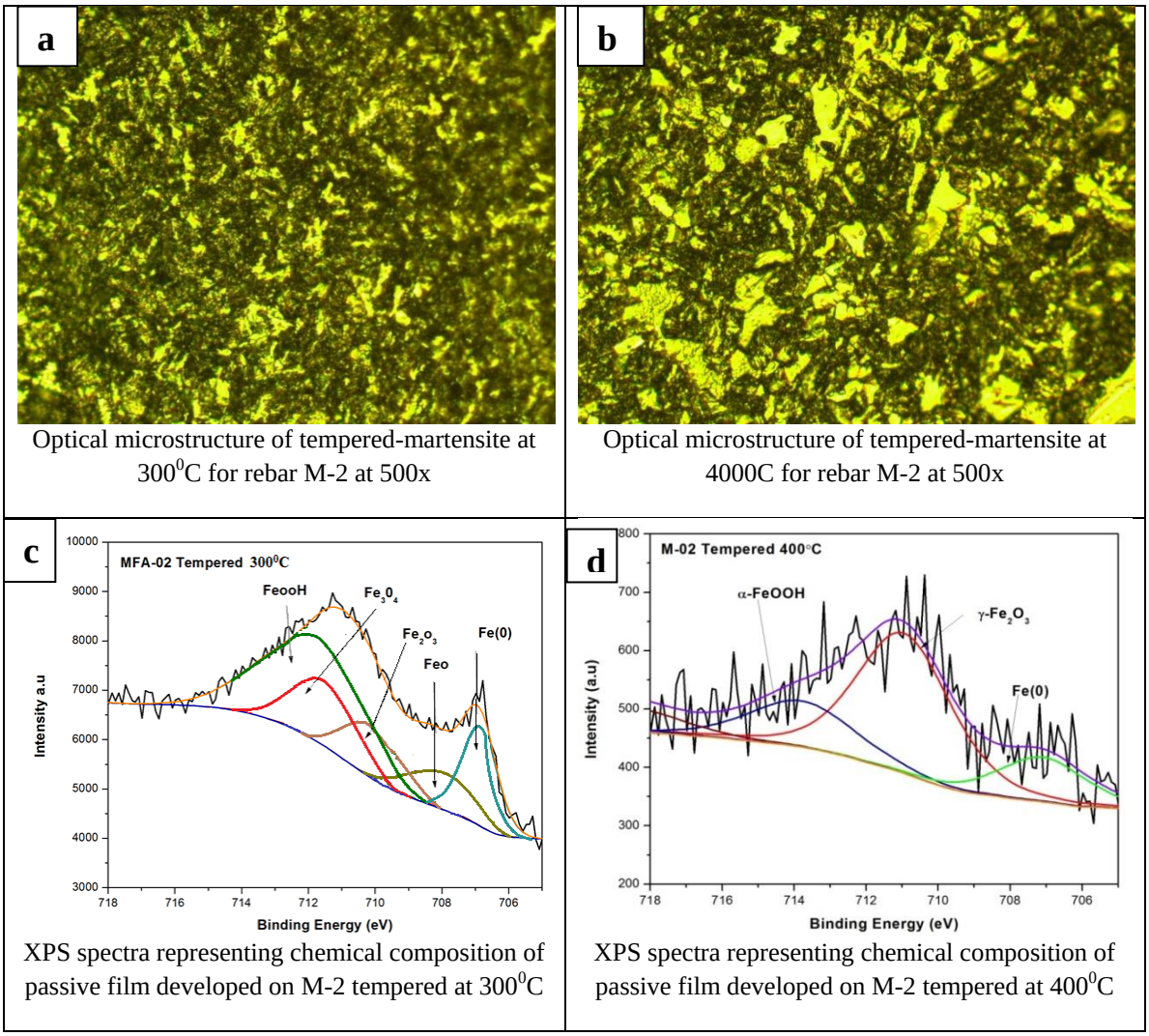

Optical microstructure of tempered-martensite at 300^0C for rebar M-2 at 500x

Optical microstructure of tempered-martensite at 4000C for rebar M-2 at 500x

XPS spectra representing chemical composition of passive film developed on M-2 tempered at 300^0C

XPS spectra representing chemical composition of passive film developed on M-2 tempered at 400^0C

Figure 6.2: Effect of tempering temperature on the composition of passive film in M-2 rebar

On contrary, when tempering was done at 400^0C temperature then higher amount of ferrite can be seen in both steel rebar regardless of the copper presence. The microstructures Fig.6.1 (b) and Fig.6.2 (b) show that considerable amount of ferrite was recovered at 400^0C tempering temperature. The lowest corrosion rate at this tempering temperature revealed that increased amount of ferrite is balancing the martensitic matrix and, hence, corrosion rate was lower than the rest of tempering temperatures. It can be seen in Fig.6.1 (d) the composition of the passive oxide film for M-1 rebar was mainly composed of γ-Fe_2O_3 and Fe_3O_4, and partially of FeO. On the other side, for M-2 rebar, it

can be seen from Fig.6.2 (d) that the film chemistry was mainly composed of γ-Fe_2O_3 and partially of α-FeOOH.

The chemistry of the passive film for tempered 300^0C steel rebar exposed that the increased ratio of α-FeOOH/γ-Fe_2O_3 in steel rebar, regardless of the copper presence, decreased the film resistance of steel rebar in alkaline solution. On the contrary, for tempered 400^0C steel rebar, the increased ratio of Fe_3O_4/Fe_2O_3 in the film increased the passive film resistance. From this, it can be easily extracted that the transformation of the Fe_3O_4 either into γ-Fe_2O_3 or α-FeOOH made the film defective and its resistance reduced. So, the basic theme can be understood from the model given in Fig.6.3 that how the change of tempering temperature affected the nature of passive film.

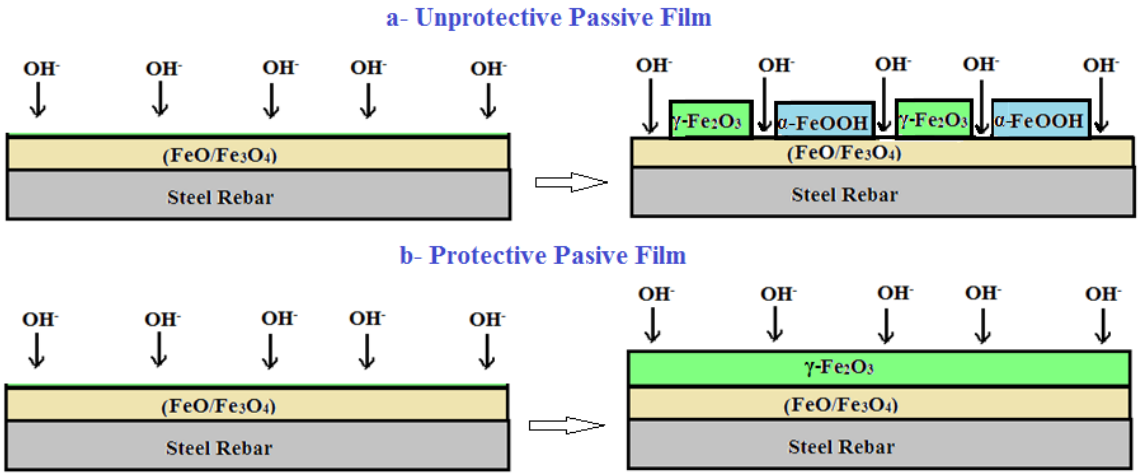

Figure 6.3: Model illustrating the effect of tempering temperature on the composition of passive film developed on steel rebar in alkaline solution (a)-Tempered 300^0C, (b)-Tempered 400^0C [111]

The effect of tempering temperature on the composition of passive film is not understood clearly but the change of open circuit potential (OCP) with tempering temperature might explain this dependence. It can be seen from the Table.6.1 that open circuit potential of tempered 300^0C rebar was found more negative than the rebar which was tempered at

400^0C. The more negative OCP at 300^0C tempering temperature seems to favor the tendency for the formation of α-FeOOH.

Table 6.1: Open circuit potential of rebars M-1 and M-2 measured in concrete simulated solution: (pH=13.5) at room temperature.

Specimen	Open circuit potential (mV)	
	Rebar M-1	Rebar M-2
Tempered 300^0C	-390	-387
Tempered 400^0C	-284	-255

6.2. Effect of Copper

6.2.1. Passivity in Alkaline Solution

From Table 6.2, it can be seen that in pure alkaline solution, the steel rebar having no copper (M-1) provided higher film resistance of $1.41x10^3$ ($\Omega.cm^2$) than the copper alloyed rebar M-2 ($1.48x10^2$ $\Omega.cm^2$) at 400^0C (Fig.6.4). But at the same tempering temperature, M-2 steel rebar provided higher charge transfer resistance of $1.64x10^5$ ($\Omega.cm^2$) than M-1 rebar ($5.59x10^4$ $\Omega.cm^2$) and can be seen in Fig.6.5. It supports the fact that, tempering at 400^0C of the rebar M-2, exposed to concrete environment enhanced the charge transfer resistance to very high extent than the rebar M-1 at the same condition. As a whole, film resistances of both rebars were found to be much less than the charge transfer resistances. Compared to M-2 rebar, lower charge transfer resistance and higher film resistance in M-1 rebar can be because of the increased charge transfer mechanism. If more Fe^{2+} leaves the surface of steel, because of less charge transfer resistance, more they will contribute to the mechanism of passive film formation and transformation. Moreover, polarization also helps us to understand the effect of copper on the passivation tendency in concrete pore solution. From Table (6.2), higher polarization resistance (R_p)

of $1.92x10^4$ ($\Omega.cm^2$) in M-2 rebar, at 400^0C, states that the presence of copper improved the polarization resistance in concrete pore solution. However, tempering at 300^0C for both M-1 and M-2 provided lowest film resistance as well as charge transfer resistance.

Table 6.2: Comparison of charge transfers resistance, film resistance and polarization resistance (LPR) with and without chlorides presence in alkaline solution

Specimen	Rebar	Alkaline Sol.			Alkaline Sol.+ 0.8MNaCl		
		R_{ct} ($\Omega.cm^2$)	R_f ($\Omega.cm^2$)	R_p ($\Omega.cm^2$)	R_{ct} ($\Omega.cm^2$)	R_f ($\Omega.cm^2$)	R_p ($\Omega.cm^2$)
Tempered 300^0C	M-1	$2.92x10^2$	$8.57x10^1$	$2.4x10^3$	$8.61x10^1$	4.5410^1	$1.9\ x10^3$
Tempered 300^0C	M-2	$5.77x10^4$	$1.27x10^2$	$6.3x10^3$	$3.81x10^4$	$1.35x10^2$	$6.26\ x10^3$
Tempered 400^0C	M-1	$5.59x10^4$	$1.41x10^3$	$1.05x10^4$	$1.785x10^4$	$6.55x10^2$	$9\ x10^3$
Tempered 400^0C	M-2	$1.64x10^5$	$1.48x10^2$	$1.92x10^4$	$9.89x10^4$	$7.51x10^2$	$1.39\ x10^4$

If we compare the passive film chemistry of both the grades at 400^0C temperature, then it is very clear from Fig.6.6 that the oxide layer in M-2 is mainly composed of γ-Fe_2O_3 and, partially, of α-FeOOH. It appears that initial formed Fe_3O_4 was fully transformed into α-FeOOH and γ-Fe_2O_3. The reason behind lower film resistance of copper alloyed steel rebar can be due to the absence of FeO and Fe_3O_4. On contrary, steel rebar having negligible amount of copper (M-1) provided higher passive film resistance because of the presence of FeO and Fe_3O_4 or due to the absence of α-FeOOH which is considered defective in its nature.

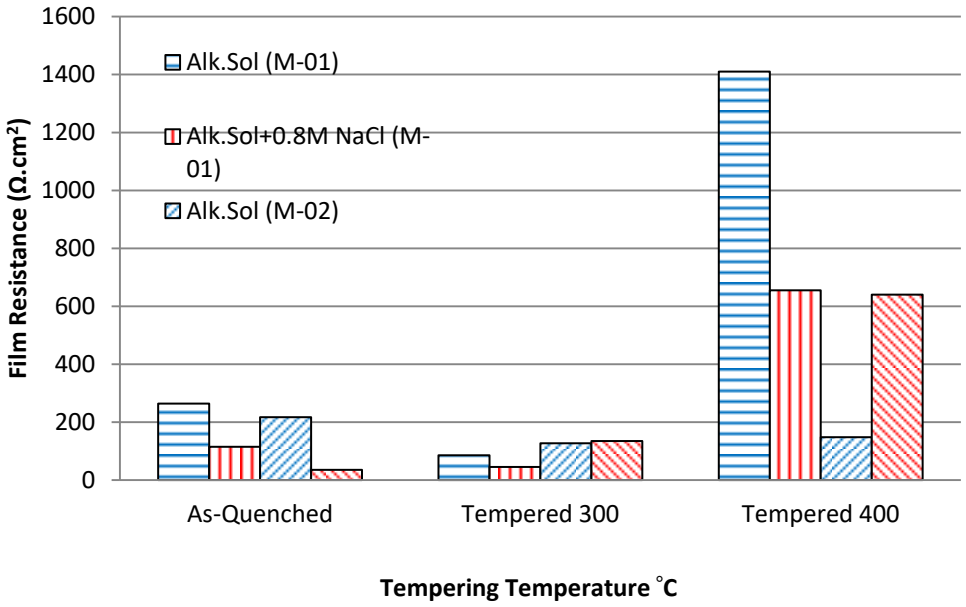

Figure 6.4: Effect of tempering temperature on film resistance in M-1 and M-2 steel rebar

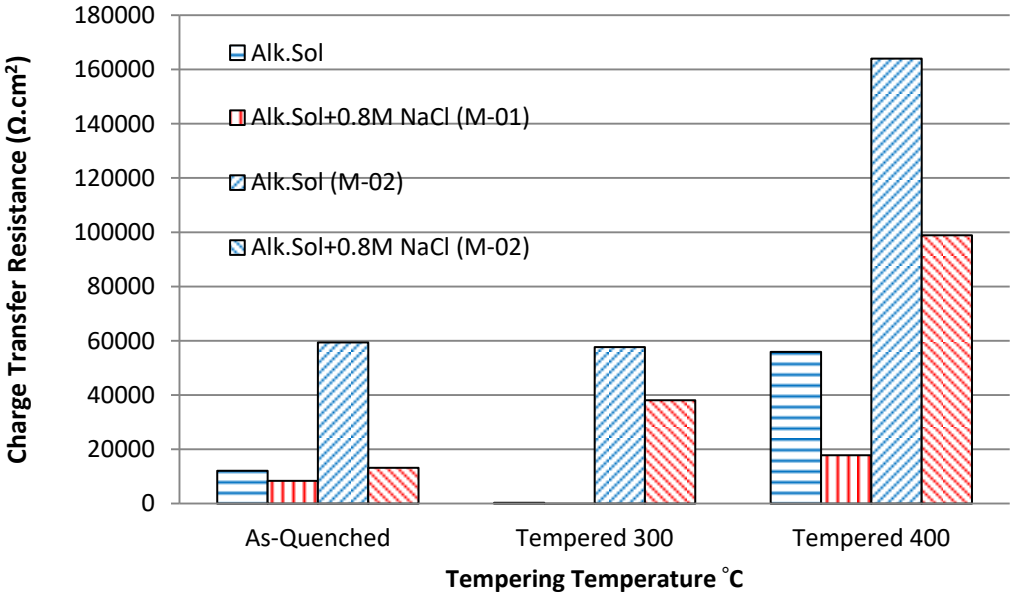

Figure 6.5: Effect of tempering temperature on charge transfer resistance in M-1 and M-2 steel rebar

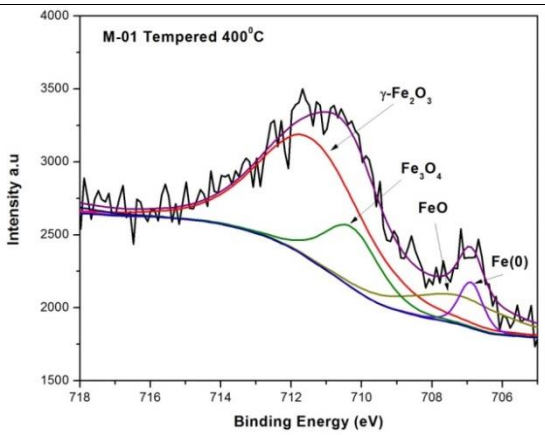

XPS spectra representing chemical composition of passive film developed on M-1 rebar tempered at 400^0C

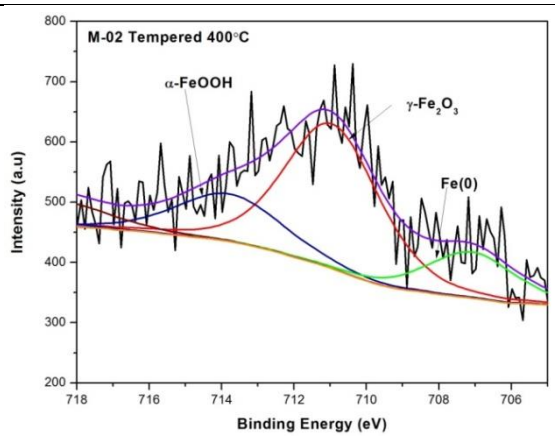

XPS spectra representing chemical composition of passive film developed on M-2 rebar tempered at 400^0C

Figure 6.6: Comparison of the passive film chemistry with and without copper in steel rebar under concrete pore solution

From the potentiodynamic polarization (PDP) graphs, the nature of the passive film and its current density can be analyzed. For instance, from the Fig.6.7, it can be seen that, at 400^0C, a constant passive film of lowest current density ($4x10^{-6}Acm^{-2}$) was achieved for M-1 rebar. The developed passive film was so resistant that even the change of potential from -0.3V to +0.3V could not alter the current density. On the other side, passive film developed over the surface of steel rebar M-2 was higher in current density ($8x10^{-6}Acm^{-2}$) and the film was not resistant to the change of potential and its current density kept on varying with the change of potential.

Fig.6.7 shows that copper has adverse effect on the pitting potential. It can be seen that, steel rebar without copper (M-1) provided higher pitting resistance than the rebar with copper M-2.

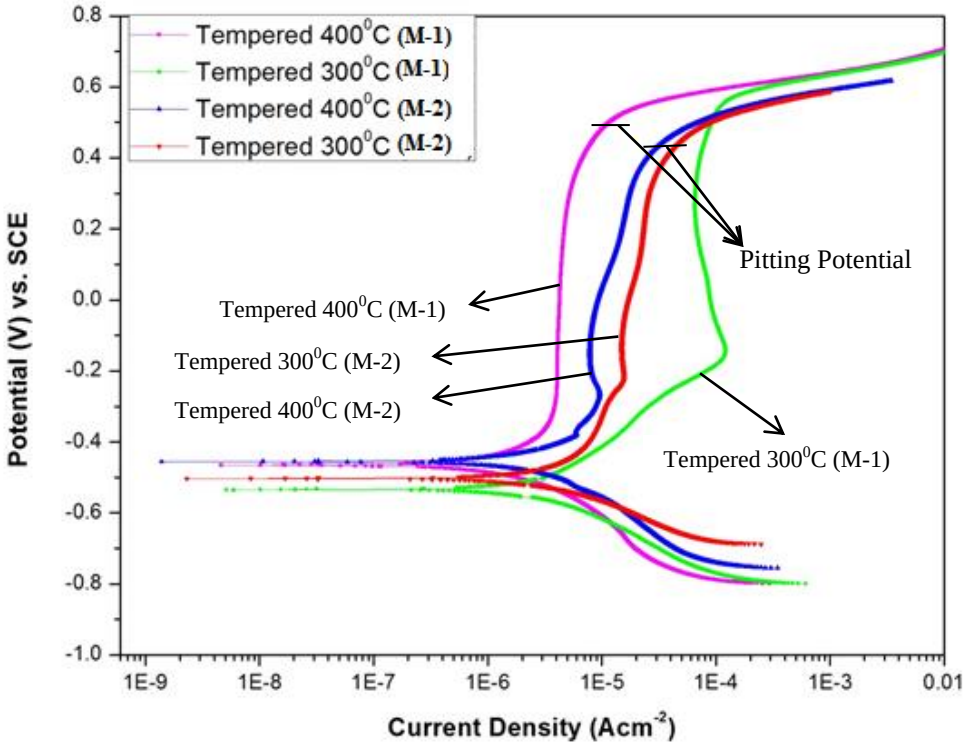

Figure 6.7: Comparison of PDP graphs for M-1 and M-2 rebar tempered at 300^{0}C and 400^{0}C temperatures and tested in alkaline solution

6.2.2. Alkaline Solution+0.8MNaCl

Recalling Table 6.2, it can be seen that the addition of 0.8M NaCl reduced the charge transfer resistance, film resistance and polarization resistance of steel rebar M-1. Reduction in all of these resistances reflects that chlorides play an adverse role by attacking the passive film. However, regardless of copper presence, tempering 400^{0}C was found the temperature where highest charge transfer resistance and constant current passive film with lowest current density was achieved. For instance, at 400^{0}C tempering temperature, charge transfer resistance of M-2 rebar reduced from $1.64x10^5$ ($\Omega.cm^2$) to $9.89x10^4$ ($\Omega.cm^2$) when chlorides were introduced in concrete pore solution. The decrease in charge transfer resistance might have helped in film transformation and, hence, film resistance increased from $1.48x10^2$ ($\Omega.cm^2$) to $7.51x10^2$ ($\Omega.cm^2$). So, from this behavior, it can be assumed that, at 400^{0}C tempering temperature, copper increased the passive film

resistance at the expense of charge transfer resistance. For M-1 rebar, when chlorides were introduced in the alkaline solution, the charge transfer resistance (Table.6.2) decreased from $5.59x10^4(\Omega.cm^2)$ to $1.785x10^4(\Omega.cm^2)$ but, unlike M-2, film resistance also decreased.

Tempering 300^0C remained still the worst tempering temperature with lowest charge transfer resistance and film resistance.

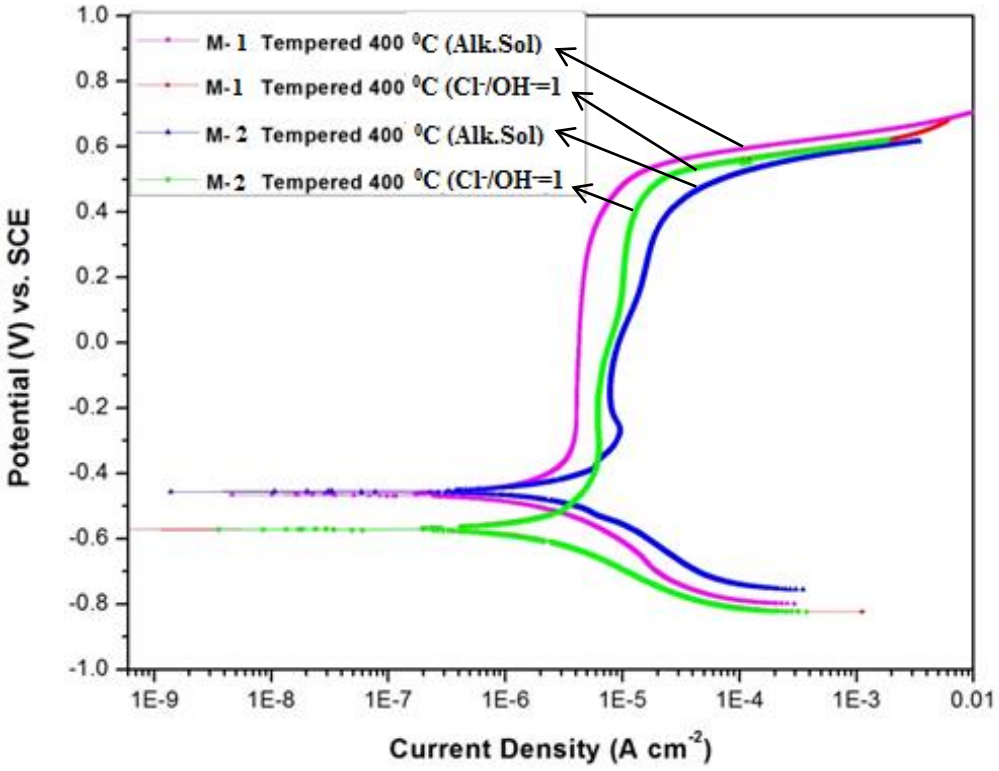

Figure 6.8: Comparison of PDP graphs for M-1 and M-2 rebar tempered at 400^0C with and without the presence of chlorides

From Fig.6.8, the effect of copper can be examined in both grades of steel rebar with the help of PDP curves. It can be seen that M-1 steel rebar (with no copper) in alkaline solution developed a passive film with lowest current density while M-2 rebar developed

a passive film with higher and varying current density. However, with the addition of chlorides, it can be seen that both M-1 and M-2 rebars are overlaying on each other. It reflects that, under the chlorides attack, current density of M-1 rebar increased while it reduced for copper alloyed steel (M-2). This trend is in agreement with EIS parameters and reflects that, under the presence of chlorides, passive film resistance of copper alloyed rebar improved by the self defense mechanism provided by the synergistic effect of copper and true (400^0C) tempering temperature. In other words, it can be assumed that, tempering of copper alloyed steels is found detrimental when they are exposed to pure alkaline environment of very high pH.

CHAPTER 7: Conclusions and Recommendations for Future

7.1. Conclusions

Two commercial grades of carbon steel with different copper content were used to investigate the effect of heat treatment on the corrosion resistance of rebars in concrete simulated environment. Both steel grades were quenched and tempered (Q&T) at 200^0C, 300^0C, 400^0C, 500^0C and 600^0C. Electrochemical testing of heat treated samples were carried out in concrete pore solution with and without chloride addition. The main conclusions of this study are:

- LPR results indicated that Q&T of M-1 and M-2 rebars at 400^0C produced microstructures with highest corrosion resistance in simulated concrete pore environments (pH 13.5) with and without chloride. M-1 and M-2 rebars Q&T at 300°C showed the lowest corrosion resistance.

- M-1 rebar showed the lowest and highest passive current densities for samples Q&T at 400°C and 300°C, respectively.

- EIS data for M-1 (Cu=0.04%) and M-2 (0.2%) rebars exposed to concrete pore solution showed that Q&T samples at 400^0C had the highest charge transfer resistance while samples Q&T at 300^0C had the lowest. M-2 sample Q&T at 400°C showed increased charge transfer resistance ($1.65x10^5\ \Omega.cm^2$) as compared to M-1 rebar ($5.59x10^4\ \Omega.cm^2$) in alkaline solution.

- The presence of copper improved the charge transfer resistance significantly even at 300^0C for M-2 rebar ($5.77x10^4\ \Omega.cm^2$) and it was found much higher than M-

1 rebar ($2.92x10^2\ \Omega.cm^2$) at the same tempering temperature in concrete pore environment.

- PDP results indicated that a constant passive film with lower current density ($4x10^{-6}$ Acm^{-2}) was observed for M-1 rebar and the presence of copper increased the current density to $7x10^{-6}Acm^{-2}$ for M-2 rebar. Pitting resistance was decreased with the presence of copper in M-2.
- When chlorides were introduced in the test solution at a ratio of Cl^-/OH^- to 1 then charge transfer resistance, film resistance and polarization resistance decreased for both tempered 300^0C and 400^0C rebars. PDP curve indicated that the film was disturbed with chlorides by increasing the current density.
- The characterization of the passive film by XPS revealed that, at 400^0C tempering temperature, the film composition for M-1 rebar was mainly composed of Fe_3O_4/FeO in the inner layer and γ-Fe_2O_3 as an outer layer. At 300°C the outer layer was composed a mixed oxides of γ-Fe_2O_3 and α-FeOOH. The presence of α-FeOOH in the passive film might be responsible for reduced passivation resistance.

7.2. Future Work

From the present research work, some questions are raised unanswered yet. There needs to conduct separate research work in future to find their answers. So the recommended research topics are as follows:

1- Optimization of heat treatment and copper composition to study the passivation of steel rebar in concrete simulating solution.
2- Investigation of critical chloride limit against the passivation of steel rebar at optimized tempering temperature and copper composition in concrete simulating environment.
3- The effect of microstructural phases on the passivation tendency of steel rebar in concrete/marine environment

REFERENCES

[1] C.L. Page, V.T. Ngala, M.M. Page, Magazine of Concrete Research 52 (2000) 25

[2] J.M. Gaidis, Cement & Concrete Composites 26 (2004) 181

[3] C.L. Page, V.T. Ngala, M.M. Page, Mag. Concr. Res. 52 (2000) 25

[4] C.M. Hansson, L. Mammoliti, B.B. Hope, Cem. Concr. Res. 28 (1998) 1775

[5] B. Elsener, Corrosion inhibitors for steel in concrete, State of the art report, EFC Publication 35, The Institute of Materials, Maney Publishing, London, 2001

[6] A.M. Rosembreg, J.M. Gaidis, Mater. Performance 18 (1979) 45

[7] J.M. Gaidis, Cem. Concr. Compos. 26 (2004) 181

[8] J.A. Gonz´alez, E. Ram´ırez, A. Bautista, Cem. Concr. Res. 28 (1998) 577

[9] M. Saremi, E. Mahallati, Cem. Concr. Res. 32 (2002) 1915

[10] K.Y. Ann, H.S. Jung, H.S. Kim, S.S. Kim, H.Y. Moon, Cem. Concr. Res. 36 (2006) 530

[11] N.S. Berke, M.C. Hicks, Cem. Concr. Comp. 26 (2004) 191

[12] L. Veleva, M.A. Alpuche-Aviles, M.K. Graves-Brook, D.O. Wipf, J. Electroanal. Chem. 537 (2002) 85

[13] L. Veleva, M.A. Alpuche-Aviles, M.K. Graves-Brook, D.O. Wipf, J. Electroanal. Chem. 578 (2005) 45

[14] S. Go˜ni, C. Andrade, Cem. Concr. Res. 20 (1990) 525

[15] J.A. Gonzalez, E. Ramirez, A. Bautista, S. Feliu, Cem. Concr. Res. 26 (1996) 501

[16] C. Monticelli, A. Frignani, G. Trabanelli, J. Appl. Electrochem. 32 (2002) 527

[17] M.F. Hurley, J.R. Scully, Corrosion (2006) 892

[18] A. Poursaee, C.M. Hansson, Cem. Concr. Res. 37 (2007) 1127

[19] http://www.hsegmbh.de

[20] Selzer Jacob. Quenched and Tempered Bar. A Publication of the Association for Iron and Steel Technology. AIST.org, (2012) 120-126

[21] C.S. Viswanatha, L.N. Prasad, Radhakrishna and H.S. Nataraja. Sub-standard rebars in the Indian market: An insight. The Indian Concrete Journal, 78 (2004) 52-55.

[22] Amret R Tuladhar, e-conference (1), BREINS-Building Research Institute (P) Ltd, (2010)

[23] O.H. Ibrahim: Comparison of Impact Properties for Carbon and Low Alloy SteelsJ. Mater. Sci. Technol., 27 (2011) 931-936

[24] Lundberg Sven-Erik. Quenched and Self-tempered Rebar – Process Overview, Layouts, Operational Parameters and Cost Savings. AISTech Proceedings, 2 (2010) 719-726

[25] JFE Technical Report No. 15 (2010)

[26] M. Durand-Charre, Microstructure of Steels and Cast Irons, Springer, Berlin, (2003)

[27] M. Pourbaix, Lectures on electrochemical corrosion, Plenum Press, New York/London, (1973)

[28] M. Pourbaix, Atlas d'équilibres électrochimiques, Centre Belge d'Etude de la Corrosion CEBELCOR / Gauthier-Villars & Cie, Paris, (1963)

[29] A. Pourbaix, Localized corrosion: behaviour and protection mechanisms, in: A. Turnbull (Ed.), Corrosion Chemistry within Pits, Crevices and Cracks, Teddington, Middlesex, National Physical Laboratory, (1984) 1-15

[30] L.L. Shreir, R.A. Jarman, G.T. Burstein (Eds.), Corrosion, 3rd Ed. 1 (1994) Butterworth Heinemann, Oxford

[31] H.-H. Strehblow, Mechanisms of Pitting Corrosion, in: P. Marcus (Ed.) Corrosion Mechanisms in Theory and Practice, 2nd ed., Marcel Dekker Inc., New York, (2002) 243-285

[32] A. Bäumel, Die Auswirkung von Betonzusatzmitteln auf das Korrosionsverhalten von Stahl in Beton, Zement-Kalk-Gips 7 (1959) 294-305

[33] C.L. Page, Mechanism of corrosion protection in reinforced concrete marine structures, Nature 258 (1975) 514-515

[34] M.N. Al Khalaf, C.L. Page, Steel/mortar interfaces: Microstructural features and mode of failure, Cem. Concr. Res. 9 (1979) 197-207

[35] A.T. Horne, I.G. Richardson, R.M.D. Brydson, Quantitative analysis of the microstructure of interfaces in steel reinforced concrete, Cem. Concr. Res. 37 (2007) 1613-1623

[36] C.L. Page, Initiation of chloride-induced corrosion of steel in concrete: role of the interfacial zone, Mater. Corros. 60 (2009) 586-592

[37] K. Byfors, Influence of silica fume and flyash on chloride diffusion and pH values in cement paste, Cem. Concr. Res. 17 (1987) 115-130

[38] J. Tritthart, Chloride binding in cement. I. Investigations to determine the composition of porewater in hardened cement, Cem. Concr. Res. 19 (1989) 586-594

[39] J. Tritthart, Chloride binding in cement. II. The influence of the hydroxide concentration in the pore solution of hardened cement paste on chloride binding, Cem. Concr. Res. 19 (1989) 683-691

[40] A. Hidalgo, G. De Vera, M.A. Climent, C. Andrade, C. Alonso, Measurements of chloride activity coefficients in real portland cement paste pore solutions, J. Am. Ceram. Soc. 84 (2001) 3008-3012

[41] B. Elsener, L. Zimmermann, H. Böhni, Non destructive determination of the free chloride content in cement based materials, Mater. Corros. 54 (2003) 440-446

[42] C.L. Page, P. Lambert, P.R.W. Vassie, Investigations of reinforcement corrosion. 1. The pore electrolyte phase in chloride-contaminated concrete, Mater. Struct. 24 (1991) 243-252

[43] P. Lambert, C.L. Page, P.R.W. Vassie, Investigations of reinforcement corrosion. 2. Electrochemical monitoring of steel in chloride-contaminated concrete, Mater. Struct. 24 (1991) 351-358

[44] M. Stern, A.L. Geary, Electrochemical polarization. I. A theoretical analysis of the shape of polarization curves, J. Electrochem. Soc. 104 (1957) 56-63

[45] C. Andrade, J.A. González, Quantitative measurements of corrosion rate of reinforcing steels embedded in concrete using polarization resistance measurements, Mater. Corros. 29 (1978) 515-519

[46] W.J. McCarter, R. Brousseau, The a.c. response of hardened cement paste, Cem. Concr. Res. 20 (1990) 891-900

[47] B. Elsener, H. Böhni, Corrosion of steel in mortar studied by impedance measurements, Mater. Sci. Forum 8 (1986) 363-372

[48] B.B. Hope, J.A. Page, A.K.C. Ip, Corrosion rates of steel in concrete, Cem. Concr. Res. 16 (1986) 771-781

[49] W.J. McCarter, G. Starrs, T.M. Chrisp, Electrical monitoring methods in cement science, in: J. Bensted, P. Barnes (Eds.), Structure and Performance of Cements, Spon Press, Taylor & Francis, London, 2 (2002) 442-456

[50] "Corrosion Engineering", Mars G. Fontana and Norbert D. Greene, McGraw-Hill, New York, (1967)

[51] "Electrochemical Polarization. I. A. Theoretical Analysis of the Shape of Polarization curves", M. Stern and A. L. Geary, J. Electrochem. Soc. 104 (1957) 33-63.

[54] Manna, M., "Effect of steel substrate for phosphate treatment: an option to simulate TMT rebar surface", Corrosion Science, 51 (2009) 451-457

[55] Maslehuddin, M., Al-Zahrani, M.M., Al-Dulaijan, S.U., Abdulquddus, R.S. and Ahsan, S.N., "Effect of steel manufacturing process and atmospheric corrosion on the corrosion-resistance of steel bars in concrete", Cement and Concrete Composites, 24 (2002) 151-158

[56] Zaky, A.I., El-Morsy, A. and El-Bitar, T., "Effect of different cooling rates on thermo-mechanically processed high-strength rebar steel", Journal of Materials Processing Technology, 209 (2009) 1565-1569

[57] Zitrou, E., Nikolaou, J., Tsakiridis, P.E. and Papadimitriou, G.D., "Atmospheric corrosion of steel reinforcing bars produced by various manufacturing processes", Construction and Building Materials, 21 (2007) 1161-1169

[58] Wei, J., Dong, J.H. and Ke, W., "The influence of cooling processes on the corrosion performance of the rebar scale", Construction and Building Materials, 24 (2010) 275-282

[59] Wei, J., Dong, J.H. and Ke, W., "Corrosion resistant performance of a chemical quenched rebar in concrete", Construction and Building Materials, 25 (2011)1243-1247

[60] Sun, W.H., Tieu, A.K., Jiang, Z.Y., Lu, C. and Zhu, H.T., “Surface characteristics of oxide scale in hot strip rolling”, Journal of Materials Processing Technology, 140 (2003) 76-83

[61] Burke, D.P. and Higginson, R.L., “Characterization of multi-component scale by electron back scattered diffraction (EBSD)”, Scripta Materialia, 42 (2000) 277-281

[62] Xu, T.Q., Liu, H.W., Yan, C.W., Du, K.L., Zhang, C.R. and Li, Y.F., “Study and application of the rust and protection of the water-cooling bars”, Mater. Protect., 41 (2008) 233-234

[63] Lambert P., Page C., Vassie P., Mater. Struct., 24 (1991) 351-358

[64] Glass G. K., Page C. L., Short N. R., Zhang J. Z., Corros. Sci., 39 (1997) 1657-1663

[65] Cheng Y. F., Luo J. L., Electrochim. Acta, 44 (1999) 2947-2957

[66] Freire L., Nóvoa X. R., Montemor M. F., Carmezim M. J., Mater. Chem. Phys., 114 (2009) 962-972

[67] Hamadou L., Kadri A., Benbrahim N., Appli. Surf. Sci., 252 (2005) 1510-1519

[68] Sanchez M., Gregori J., Alonso M. C., Garcia-Jareno J. J., Vicente F., Electrochim. Acta, 52 (2006) 47-53

[69] Wei, F.Y., Hu, F. and Huang, D.L., “Corrosion performance of rebar quenched in a novel agent”, Transactions of Materials Heat Treatment, 32 (2011) 151-154

[70] Yamashita, M., Miyuki, H., Matsuda, Y., Nagano, H. and Misawa, T., “The long term growth of the protective rust layer formed on weathering steel by atmospheric corrosion during a quarter of a century”, Corrosion Science, 36 (1994) 283-299

[71] Dillmann, Ph., Mazaudier, F. and Hoerle´, S., “Advances in understanding atmospheric corrosion of iron: I. Rust characterisation of ancient ferrous artefacts exposed to indoor atmospheric corrosion”, Corrosion Science, 46 (2004) 1401 1429

[72] Bruno Huet, Val´erie L’Hostis, Fr´ed´eric Miserque, Hassane Idrissi, “Electrochemical behavior of mild steel in concrete:Influence of pH and carbonate content of concrete pore solution”, Electrochimica Acta, 51 (2005) 172–180

[73] M. Moreno, W. Morris, M.G. Alvarez, G.S. Duffo, “Corrosion of reinforcing steel in simulated concrete pore solutions:Effect of carbonation and chloride content”, Corrosion Science 46 (2004) 2681–2699

[74] Jiabin Han, Srdjan Neˇsi ´c, Yang Yang, Bruce N. Brown, “Spontaneous passivation observations during scale formation on mild steel in CO_2 brines”, Electrochimica Acta, 56 (2011) 5396–5404

[75] Karthik Subramanian, John Mickalonis, “Anodic polarization behavior of low-carbon steel in concentrated sodium hydroxide and sodium nitrate solutions”, Electrochimica Acta, 50 (2005) 2685–2691

[76] M.B. Valcarce, M. V´azquez, Electrochimica Acta, 53 (2008) 5007–5015

[77] M.B. Valcarce, M. Vázquez, Materials Chemistry and Physics 115 (2009) 313–321

[78] Enrico Volpi, Andrea Olietti, Matteo Stefanoni, Stefano P. Trasatti, Journal of Electroanalytical Chemistry 736 (2015) 38–46

[79] Kro’likowski, A., Karbownicka, B., and Jaklewicz, O., Electrochim. Acta, 51(2006) 6120

[80] Nam, N.D. and Kim, J.G., Corrosion Sci., 52 (2010) 3377

[81] Ujiro, T., Satoh, S., Staehle, R.W., and Smyrl, W.H., Corrosion Sci., 43 (2001) 2185

[82] Corrosion: Fundamentals, Testing and Protection. ASM Handbook, Cramer, S.D. and Covino, B.S., Ed., ASM International, Materials Park, OH, 13 (2003)

[83] Bardal, E., Corrosion and Protection, London: Springer_Verlag, (2004)

[84] Talbot, D. and Talbot, J., Corrosion Science and Technology, Boca Raton FL: CRS Press, (1998)

[85] Lo'pez, D.A., Schreiner, W.H., de Sa'nchez, S.R., and Simison, S.N., Appl. Surf. Sci., 207 (2003) 69

[86] Gonzalez–Rodriguez, J.G., Bahena_Martinez, G., Salinas_Bravo, V.M., Mater. Lett., 43 (2000) 208

[87] Osarolube, E., Owate, I.O., and Oforka, N.C., Scientific Research and Essay, 3 (2008) 224

[88] Möller, H., Boshoff, E.T., and Froneman, H., Journal of the South African Institute of Mining and Metallurgy, 106 (2006) 585

[89] Ibrahim, M.A.M., Abd El Rehim, S.S., and Hamza, M.M., Mater. Chem. and Phys., 11 (2009) 580

[90] Wang, Z.F., Li, P.H., Guan, Y., et al., Corrosion Sci., 51 (2009) 954

[91] Guo, J., Yang, S., Shang, C., et al., Corrosion Sci., 51 (2008) 242

[92] Zhao, Y.T., Yang, S.W., Shang, C.J., et al., Mater. Sci. and Engineering A, 695 (2007) 454–455

[93] Chen, Y.Y., Tzeng, H.J., Wei, L.I., et al., Corrosion Sci., 47 (2005) 1001

[94] Je-Kyoung Kim, Atsushi Nishikata and Tooru Tsuru, “Influence of Copper on Iron Corrosion in Weakly Alkaline Environment Containing Chloride Ions”, Materials Transactions, 44 (2003) 396-400

[95] alloy addition: Young-Wook Jang, Ji-Hyun Hong, and Jung-Gu Kim, “Effects of Copper on the Corrosion Properties of Low-Alloy Steel in an Acid-Chloride Environment”, Met. Mater. Int., 15 (2009) 623~629

[96] Anna D'Aloya, Aleksandar N. Nikoloski, “The passivation of iron in ammoniacal solutions containing copper (II) ions”, Hydrometallurgy 111-112 (2012) 58–64

[97] Sven-Erik Lundberg, Scandinavian Journal of Metallurgy; 31 (2002) 234–240

[98] S. Hakan Atapeka, eyda Polata, and Sibel Zorb, ISSN 20702051, Protection of Metals and Physical Chemistry of Surfaces, Pleiades Publishing, Ltd., 49 (2013) 240–246

[99] B. Huet, V. L.Hostis, F. Miserque, H. Idrissi, Electrochim. Acta, 51 (2005) 172–180

[100] M. Moreno, W. Morris, M.G. Alvarez, G.S. Duffo, Corros. Sci. 46 (2004) 2681–2699

[101] Enrico volpi, Andrea Olietti, Matteo Stefanoni, Stefano P. Trasatti, “ Electrochemical Characterization of mild steel in alkaline solution simulating concrete environment” journal of electrolytic chemistry 736 (2015) 38-46

[102] Ibrahim M. Gadala, Akram Alfantazi, “A study of X100 pipeline steel passivation in mildly alkalinebicarbonate solutions using electrochemical impedance spectroscopy under potentiodynamic conditions and Mott–Schottky”, Applied Surface Science 357 (2015) 356–368

[103] D. E. Lescanoa, S. P. Silvettib, “Study of microestructure and tempered martensite embrittlement in AISI 15B41 steel”, Procedia Materials Science, 1 (2012) 134 – 140

[104] Semyon Vaynman, Morris E. Fine, “High Performance Copper-Precipitation-Hardened Steel”,

[105] M.E. Fine, D. Isheim, “Origin of copper precipitation strengthening in steel revisited”, Scripta Materialia 53 (2005) 115–118

[106] R. Rana, W. Bleck, S.B. Singh, O.N. Mohanty, “Development of high strength interstitial free steel by copper precipitation hardening”, Materials Letters 61 (2007) 2919–2922

[107] Setuo Takaki, Masaaki Fujioka, Shuji Aihara, Yasunobu Nagataki, Takako Yamashita, Naoyuki Sano, Yoshitaka Adachi, Masahiro Nomura and Hiroshi Yaguchi, “Effect of Copper on Tensile Properties and Grain-Refinement of Steel and its Relation to Precipitation Behavior”, Materials Transactions, 45, (2004) 2239-2244

[108] El Sayed, M.S, Mater. Chem. and Phys., 129 (2011) 961

[109] Arne Dugstad, Hallstein Hemmer, Marion Seiersten, “EFFECT OF STEEL MICROSTRUCTURE UPON CORROSION RATE AND PROTECTIVE IRON CARBONATE FILM FORMATION” Corrosion, paper no. 00024 (2000)

[110] S. Hayashi, K. Mizumoto, S. Yoneda, Y. Kondo, H. Tanei and S. Ukai, Oxidation of Metals, 81 (2013) 371

[111] MacDougall, B., Graham, M.J. (Eds.), “Growth and Stability of Passive Films”, Marcel Dekker, Inc., Paris, France, Chapter 5 (1995)

VITAE

Name :Muhammad Faizan

Nationality :Pakistani

Email :mfaizan693@gmail.com

Address :House no 258-1, street 4, Haider Pura Multan, Pakistan

Academic Background :My BS Engineering was in Metallurgy and Materials Engineering from Univeristy of the Punjab, Lahore, Pakistan. After that, I did approximately two years Job in a multinational French Inspection company-Bureau Veritas. In September 2014, I started my MS in King Fahd University of Petroleum and Minerals, Dhahran, Saudi Arabia. Here my major was Materials Science and Engineering. Here I took a number of courses of materials like, Materials Characterization, Thermodynamics, Materials Structure and Defects, Corrosion in oil and petrochemicals, Fatigue and Fracture, Tribology and Nanomaterials. Nevertheless, my research was strictly restricted to my own area of interest and that is none other than corrosion. My Thesis title was “The Effects of Composition and Heat Treatment on the Passivation of Steel Rebar in Concrete Simulated Environment”.